論文 / 著書情報
Article / Book Information

題目(和文)	
Title(English)	Study on Wear/Deformation and Deposit Formation inside Nozzle of Diesel Fuel Injector
著者(和文)	ブトマラシー アティワット
Author(English)	Athiwat Butmarasri
出典(和文)	学位:博士(工学), 学位授与機関:東京工業大学, 報告番号:甲第12284号, 授与年月日:2022年12月31日, 学位の種別:課程博士, 審査員:小酒 英範,天谷 賢治,花村 克悟,平田 敦,佐藤 進
Citation(English)	Degree:Doctor (Engineering), Conferring organization: Tokyo Institute of Technology, Report number:甲第12284号, Conferred date:2022/12/31, Degree Type:Course doctor, Examiner:,,,,
学位種別(和文)	博士論文
Type(English)	Doctoral Thesis

Study on Wear/Deformation and Deposit Formation inside Nozzle of Diesel Fuel Injector

Athiwat Butmarasri

Advisor: Professor Hidenori Kosaka
Co-advisor: Associate Professor Susumu Sato

Dissertation
submitted in partial fulfillment of the requirements for the degree of
Doctor of Engineering

Department of Systems and Control Engineering
Graduate School of Engineering
Tokyo Institute of Technology

December 2022

ABSTRACT

The improvement of fuel injection common-rail system has become an important issue. With the changes of injection conditions, wear deformation and deposit of the nozzle were found. Wear and deformation occur in the body seat of diesel fuel injector nozzles, thereby affecting fuel spray behaviors and injection characteristics. In this study, the effects of body seat temperature, test duration, temperature increase duration, tempering temperature, and tempering duration on the nozzle body seat are investigated using an injector testing device. Surface roughness measurements using a nano search microscope and hardness measurements of the nozzle body seat are performed to investigate the textural and physical characteristics of the nozzle body seat. In addition, optical measurements via optical microscopy and field emission scanning electron microscopy are performed to investigate the topographical information and microstructure of the nozzle body seat. The results show that the increase in deformation is related to the higher test temperature and duration. Additionally, the tempering technique can suppress the deformation of the nozzle body seat.

The nozzle hole deposit formation is investigated by the test rig in which deposit formation can be accelerated at various injection pressures, injection durations, and nozzle tip temperatures. The rotational speeds of the fuel supply pump are varied to obtain the different times between injections. The Bosch method and the constant volume chamber with a high-speed video camera are used to investigate the effects of deposit in the nozzle hole on injection rate and spray characteristics. The results show the longer time between injections promotes the nozzle hole deposit and affects both the fuel injection and the spray characteristics.

ACKNOWLEDGEMENTS

The study is a scholarship provided by Japanese government (MEXT) in Department of Systems and Control Engineering under the Sustainable Engineering Program, Tokyo Institute of Technology. This study has been conducted as a part of a research project in Wear group, Kosaka-Sato Laboratory.

I would like to express, first and foremost, my heartfelt gratitude to my supervisor Professor Hidenori KOSAKA, my main advisor and Associate Professor Susumu SATO for an opportunity to work and study under their extensive supervision, guidance and Assistant Professor Tsuyoshi Nagasawa, for their encouragement and support throughout my thesis. I wish to express and gratefully acknowledge the cooperation of experimental work from Mr.Kou SATAKE, Mr.Shuntaro TEZUKA, Mr.Yuki SUGO, and Mr. Mizuki YABE who are members in Wear group, Mr.Pop-Paul Ewphun and Mr.Dittapoom Shinabuth. The study may not be successful without the generous support from DENSO Corp., Japan for providing sincere advice and technical support.

Last but not least, I'd want to dedicate this accomplishment to my family and friends, who have always been by my side, supported me, and had complete faith in my research work throughout the years

Athiwat Butmarasri

December 2022

CONTENTS

CHAPTER 1
INTRODUCTION

1.1 Background

The use of fossil fuels as transportation fuel has been a concern in recent years. According to reports from the IEA (International Energy Agency) [1], the global energy demand has risen steadily over the past decade. The projections for energy demand in 2030 indicate that oil consumption will increase significantly, particularly in the transportation sector. The annual growth rate is approximately 1.7%. In addition, emissions from the vehicle or transportation sector will increase during the same time period as the use of fossil fuels. Despite the availability of excellent combustion technology, the use of this fossil fuel cannot reduce complete combustion, greenhouse gas, or carbon dioxide emissions. Therefore, for long-term energy use, it is necessary to seek out energy-saving techniques and employ them intelligently. In Japan, it was reported that 94.9% of the carbon dioxide emitted from energy sources was responsible for global warming, with the remaining 18.5% coming from the transportation sector, which includes automobiles and ships [2]. One of these characteristics is engine efficiency. It has been reported that, among internal combustion engines (ICEs), diesel engines have the highest thermal efficiency. Increasing the use of diesel engines is the means by which liquid fossil fuel efficiency can be improved. Most diesel vehicles are used for public transportation, commercial delivery, and utility purposes. Consideration is given to the fuel injection system, high-pressure fuel injection, multi-stage fuel injection, reformation, and reduction of sulfur content in fuel components in order to enhance the performance of a diesel engine. Many diesel engine fuel injection systems utilize a common rail fuel injection system. Common rail fuel injection apparatus, to store boosted fuel to reach the necessary injection pressure by the high-pressure pump to the accumulator called a "common rail," is opened and closed by energization of a solenoid valve, which is equipped with a needle in the injector, the start of injection, and it is designed to control the stop. Thus, the fuel injection pressure and fuel injection timing have the advantage that the fuel injection period can be set independently, thereby enhancing the diesel engine's efficiency and exhaust emissions. In order to increase combustion efficiency and

conform to the new emission regulation standard, the injection system has been modified in response to the continuously tightening emission regulations. Therefore, the nozzle hole was made smaller and the fuel injection pressure was increased in order to improve combustion efficiency [3].

However, this development worsens the wear characteristics of the injection system's components [4-6]. There is a problem that accelerates nozzle seat portion wear and deformation. When the shape of the nozzle is altered, not only the combustion but also the exhaust characteristics are affected. Changes in injection conditions were found to promote and affect the injector's wear and deformation mechanisms. This is especially true for the injector's nozzle. The fuel injection is controlled by opening and closing the needle valve, which results in the deformation of the nozzle's body seat in a diesel fuel injector due to the collision and impact of the needle on the body seat in the nozzle, which may affect the spray behaviors and injection characteristics of the fuel.

Recently, DLC (diamond-like carbon) nozzles have been widely used to protect the body seat, which is softer at high temperatures than the needle, from wear. The DLC coating on the needle reduces wear on the body seat due to its smooth surface, low coefficient of friction, and low opponent aggression [7-9]. However, deformation still exists because the DLC needle is harder than the body seat.

In addition, it has been discovered that the small size of the injector hole and the high fuel temperature at high injection pressure result in the coking of the nozzle hole by the injector nozzle hole deposit [10-17]. In diesel applications, injector deposits in high pressure common rail fuel injection systems are a relatively new problem [18-19]. These deposits are produced within the nozzle and can be viewed as distinct aging from the wear and deformation of the nozzle. Deposits formation have been generated by the use of diesel engines for a very long time. There are numerous factors that influence the generation of deposits and lead to variations in locations, compositions, and mechanisms. These factors result in the alteration of the injector nozzle's internal shape, which influences the injection characteristics. [20-31]. In order to realize and comprehend the mechanism of wear/deformation and deposit formation inside the nozzle, a review of prior literature is required. This contribution may result in enhanced diesel engine fuel and combustion efficiency, emission characteristics, and durability.

1.2 Literature Reviews

This section reviews a variety of experimental data and innovative phenomena from published literature. It presents an introduction to diesel engines, followed by a study of wear and deformation in both automotive and industrial applications as well as the formation of deposits in the engine's fuel injection system.

1.2.1 Diesel Engine

Diesel engines are internal combustion devices that initiate the combustion using the heat from compression inside the combustion chamber. During the last stages of the compression stroke, fuel was injected into the combustion chamber. It was created in 1897 by Rudolf Diesel based on Sardis Sardi Carnot's invention, the Carnot cycle. Diesel engines are distinct from gasoline engines, which ignited using spark plugs. Under high pressure and temperature, compressed air and fuel ignite diesel engines [32].

1.2.1.1 Diesel Engine Operation

The diesel engine works on the principle of compressing air to a higher temperature before injecting fuel. Pressure and temperature rose quickly under compression without any heat loss (Adiabatic compression). After being injected into the combustion chamber, the fuel vaporizes, igniting the mixture on its own. Combustion pressure rises transfer to the piston and connecting rod caused crack shaft rotation.

Diesel engines are two- or four-stroke compression ignition engines. However, diesel engines used in automobiles are four-stroke models. The cycles of four-cycle engine are: intake, compression, power, and exhaust.

-Intake stroke: During intake valve opening and exhaust valve closing, the piston descends from top dead center (TDC) to bottom dead center (BDC). The cylinder draws in fresh air.

-Compression stroke: Piston rises from BDC during the compression stroke. Both the intake and exhaust valves are close together in this timing. With compression, the cylinder's pressure and temperature rise.

-Power stroke: The piston nearly reaches TDC. Fuel is injected into the combustion chamber at the end of the compression stroke. Both the intake and exhaust valves are close together in this timing. Through the piston and crankshaft, the

combustion-induced increase in cylinder pressure is transformed into mechanical energy.

-Exhaust stroke: As the exhaust valve opens and the intake valve closes, the piston rises from BDC to TDC. Exhaust is forced out of the cylinder.

1.2.1.2 Diesel Engine Characteristics

The thermal efficiency of diesel engines is higher than that of other internal combustion engines. Diesel engines are broadly used in commercial and heavy-duty applications. The ability to operate on a variety of fuels is another benefit of diesel engines. However, the configuration of standard diesel engines takes into account the use of diesel fuel made from crude oil. Understanding the characteristics of diesel engines is crucial for the development of new fuel technologies that are compatible with them. These characteristics can be broadly categorized into six groups by the following terms: fuel injection characteristic, fuel spray characteristic, combustion characteristic, engine performance characteristic, ecology characteristic, and economy characteristic [33].

The relationship between the various characteristics of diesel engines is explained. It has been demonstrated that the characteristics of fuel injection and fuel spray have an impact on engine performance, ecology, and economy. All of these characteristics are influenced by fundamental variables such as the type of fuel or injection system, as well as by different process behaviors like the injection process, fuel spray development, atomization, mixture formation, ignition, and combustion. The fuel injection system's mechanical or electronic control of various geometrical and setup parameters may have an impact on the diesel engine's characteristics. In addition, engine combustion performance, emission, and economic characteristics are strongly influenced by injection, spray, and combustion characteristics.

1.2.1.3 Fuel Injection System

For modern diesel engines, the common rail system has been developed. The common rail, which is equipped with pressure sensors, is supplied with high pressure fuel by the supply pump. Fuel pressure inside the common rail is controlled by a pressure sensor to match engine operating conditions. Based on data from various sensors, including the crankshaft positioning sensor, throttle positioning sensor, and intake temperature, the electronic control unit (ECU) controls how the common rail system

operates. The Electric Driver Unit (EDU) uses information from the ECU to control the load and speed of the injector. In order to coordinate with engine operation, the ECU also controls the suction control valve of supply pumps. As a result, the engine can inject fuel unevenly into each cylinder. Improved engine performance, reduced vibration, long life, low maintenance costs, and low exhaust emissions result from this.

1.2.2 Wear and Deformation

Wear and deformation have been widely described in the literature and reported in various perspectives regarding the injector nozzle. The up and down movement of the needle in order to control the injection of the diesel fuel injection system leads to wear and deformation at the nozzle body seat, affecting the injection characteristics. The deformation of the nozzle body seat can be addressed due to repeated collisions of the needle and nozzle body seat. A schematic diagram of the injector and nozzle is shown in Fig. 1.1.

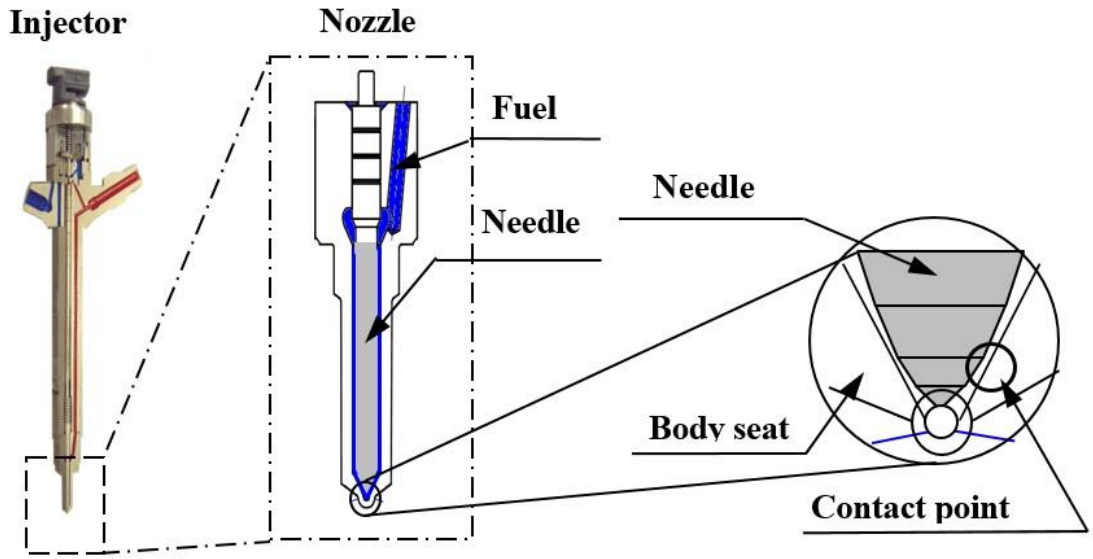

Fig. 1.1 Schematic diagram of diesel injector nozzle.

As studies such as wear and deformation of the internal nozzle, such plastic deformation was investigated for its influence on the operating state or the exhaust of the engine. R. Caprotti et al. [34] explored that the problem of electronically governed unit injectors has been reported when introduced to the field. These involved changes in fuel

flow, fuel rate, and power, resulting in increased exhaust-out smoke emissions. The investigation concluded that they were associated with injector tip erosion/corrosion. Such an erosion/corrosion process seemed to be particularly severe when low temperatures were experienced in the injector sac/tip area. Such a low temperature can lead to corrosive attack from the exhaust gases, leading to a fuel flow increase.

A study was performed by Su T. et al. [35] to correlate the Sauter Mean Diameter (SMD), NOx and particulate emissions of a direct injection diesel engine with various injection pressures and different nozzle geometry. Experimental results showed that for higher injection pressures, a smaller SMD was observed, i.e., a finer spray was obtained. In this case, higher NOx and lower particulate emissions resulted. For different nozzle geometries with the same injection duration and injection delivery, a rounded inlet nozzle gave a larger SMD than a sharp-edged inlet nozzle. The change in SMD between the two tips with injection pressure became smaller as the injection pressure increased. Also, a smaller hole size nozzle produced smaller droplet sizes and a smaller amount of particulate, but the trend of NOx depended on the injection pressure. A double injection strategy gave decreased SMD, reduced NOx, and lower particulate at the same time. It has been reported to greatly influence the amount of NOx emissions and PM by varying spray characteristics such as injection pressure and the internal shape of the injector at the same time Since it was reported to affect the spray characteristics, the effect of changes in the internal shape due to wear or plastic deformation on the exhaust gas is considered non-negligible. However, studies on the wear of the body seat have not been done enough yet. There are many approaches to the friction characteristics and wear mechanism in wear tests of a general metal. These were reported as follows by the literature study. R. Chen and colleagues [36] Experimentally, investigate the effect of atmospheric pressure on the sliding wear by using a non-lubricated reciprocating tester of ball-on-disk type. The amount of wear at a certain critical pressure or more is increased. The maximum wear shown occurs below 103Pa rather than atmospheric pressure. The SEM image observation and EDX analysis of the worn surface were performed to observe the adhesion of the oxide particles at the surface under atmospheric pressure. The reduced pressure indicated that adhesion of the metal particles was confirmed.

Cimenoglu, H et al. [37] studied the sliding contact of the metal, which is accompanied by plastic deformation in the sliding test of the metal, its plastic deformation rate. The worn surface of the ductile material is large. The wear resistance indicates that there is a relationship between surface hardness. The plastic deformation of the surface along with the wear was checked by abrading with abrasive particles of low carbon steel that has been subjected to heat treatment. The work hardening of the subsurface indicates that it is possible to suppress the plastic deformation. Under both dry and lubricated conditions, Pradeep L et al. [38] discovered that the magnitude of the plastic strain gradient and the depth of the highly deformed zone correlate with the coefficient of friction, which is dependent on the surface texture of the harder counter face. It was also observed that the gradient of equivalent strain, as it approaches the worn surface, was higher under dry conditions when compared to that under lubricated conditions. A.T. Alpas et al. [39] observed that both the magnitude of plastic strain (and stress) gradients and the depth of highly deformed layers increased with the sliding distance. Wear proceeds mainly by a mechanism of delamination via subsurface crack growth. It is proposed that the competition between the plastic strain which enhances void growth and the hydrostatic pressure which suppresses it is responsible for the generation of a damage gradient so that the delamination takes place at a certain depth where the damage accumulation rate is maximum. In addition, N. Khanafi-Benghalem et al. [40] studied in more detail the process of plastic deformation and the wear rate of this steel in lubricated sliding against cemented tungsten carbide. All the test conditions generate a significant plastic deformation of the sample steel, even in the quenched and tempered state: it produces a marked increase in the surface hardness. The work hardened layer is much finer for the quenched and tempered state (15 μm) than for the normalized state (40 μm at 20°C). For temperatures $T \leq 100°C$ in a normalized state, the wear follows Archard's law with an increasing rate with temperature. For $T \geq 120°C$, the wear rate decreases during the test, with the global volume of wear being a decreasing function of T. For the quenched and tempered states, the wear rate decreases with the increase of the normal force. This decrease is less than 30% of the normalized state value. The material heating during the wear tests is well correlated with the friction dissipated power but remains small, except in extreme cases (maximum sliding velocity, great friction at high temperatures). These results suggest the existence of two wear mechanisms: abrasion by

sample debris and burr emission by plastic flow. Abrasion is probably the dominating mechanism for the tests carried out at the lowest temperatures. The plastic flow becomes a significant component at the highest temperatures.

A. K. Gondol et al. [41] reported on a radionuclide-based wear investigation of an injector nozzle. The injector nozzle needle, which undergoes continuous hammering with the nozzle seat and sliding motion with the nozzle body, is most susceptible to wear. The important factors affecting wear are the material, heat treatment, clearances, and the type of fuel used. The properties of the diesel fuel which may affect needle wear are its viscosity and sulphur content. They found that the running-in period for injector nozzle needles is up to 30–40 h of operation. High wear rates and low injector overflow are observed during this period. The fuel injector nozzle wear is 30%–40%. The increased wear is attributed mainly to the very low viscosity of the fuel. Needle wear rates for the diesel fuels indicate that higher sulphur content and viscosity reduce the wear. The decrease in wear with high sulfur fuel may be due to the extreme pressure (e.p.) lubricant action of sulfur compounds presents in the diesel fuel.

The suitability of diamond-like carbon (DLC) coatings for the reduction of friction and wear in spark-ignited, direct-injected fuel systems has been investigated by J. Hershberger et al. [42]. Three commercially available DLC coatings have been compared to near-frictionless carbon (NFC) coatings and to uncoated metal in standardized lubricity tests and custom wear tests intended to simulate the fuel system environment. The coatings were applied to both laboratory balls and flats and to production fuel injector tips. When compared to uncoated surfaces, these coatings made friction and wear less of a problem. NFC coatings made the most difference.

Moreover, J. Hershberger et al. [43] also studied the friction and wear behavior of near-frictionless carbon coatings in formulated gasoline. Million-cycle reciprocating wear tests have been carried out to determine the ultimate wear lifetime of near-frictionless carbon (NFC) coatings applied to production fuel-injector tips. Wear tests were performed on existing and reformulated gasoline as part of a study to improve fuel systems for spark-ignited, direct-injected (SIDI) engines. Ball-on-three-disc (BOTD) tests were performed to determine the lubricity of the gasoline, and the wear surfaces were analyzed using Raman spectroscopy. NFC coatings reduced friction and total wear by up to 48% and 39%, respectively. No evidence was seen of coating graphitization, the

formation of transfer films from the coatings, or the presence of chemical protective films originating from the gasoline.

1.2.3 Deposits

The mechanism of deposit formation in the diesel injector is quite complex. Many factors, such as the types of fuel and lubricating oil, in-cylinder gas type, temperature and pressure, injection pressure, and duration, govern the formation of deposits. The literature reviews are required in order to find out the dominant factors that affect deposit formation. There are many researchers' studies in the area of deposit formation in injectors. The results of their studies have been summarized as follows:

Jim Barker et al. [44] proposed a novel technique for investigating the nature and origins of deposits formed in high-pressure fuel injector equipment using the application of the combination of hydro-pyrolysis, gas chromatography, and mass spectrometry in order to analyze the characteristics of fuel injection equipment deposits. The techniques have indicated that the filter deposits are a complex mixture of graphitic carbon, poly-aromatics, cycloalkanes, aromatics, straight-chain and substituted alkanes, acids, and inorganics. Also, it is known that the aromatic and poly-aromatic series are intermediate stages towards the formation of graphitic carbon.

A.M. Liaquat et al. [45] investigated the impact of using the balm biodiesel fuel samples after a 250-h endurance test. Visual inspection of the injector nozzle was carried out by taking photographs at 0 h (new), 60 h, 125 h, 180 h, and 250 h, respectively. Based on visual inspection, photographic views of injectors running on all fuels showed some deposit accumulation. However, the injector running with biodiesel fuel was found to be dirtier than the injector running with DF. Deposits on the injector nozzle running with DF were observed to be oily/greasy, whereas dry deposits were observed when the engine was fueled with biodiesel fuel. At the end of the endurance test, SEM and EDX analysis showed that injector deposits when the engine was run with DF were substantially less than when it was run with both JB20 and PB20. The depositions didn't present a uniformly thick layer of carbon. Moreover, deposits on and around the injector tip didn't interfere significantly with the nozzle holes. When the engine was fueled with JB20, SEM and EDX analysis showed dry, dark deposits on and around the injector tip area and its nozzle holes were nearly covered or otherwise obstructed by the same deposits. A higher

carbon content was observed in the dark areas. In the case of an engine fueled with PB20 blend, it showed relatively thick and overlapping deposits at the tip and around the injection hole exit, along with shrinkage in the diameter of the injector nozzle hole. Moreover, some injector holes are completely closed by the same deposits. All locations of the deposited layer showed a higher concentration of carbon.

Deaen et al. [46] analyzed the tip deposits using a combination of SEM-EDS, FTIR Microscopy, TD-GCMS, and an Alicona Infinite Focus 3D micro-coordinate system to access the chemical composition and topography of deposits, leading to insights into their formation mechanisms. To comprehensively understand the composition and location of the external and internal injector deposits and thoroughly understand the formation mechanism, which leads to mitigation and solution options from the perspective of engine hardware design and fuel blending. The SEM and Alicona testing results showed that different levels of deposits were formed across the injector (on the ball and seat surfaces, in the internal and external nozzle holes, and on the tip outer surface of the injectors). Specifically, film-like deposits with a crystalline structure were observed on the needle ball surface. Similar crystalline deposits were observed on the seat surface. Extensive deposits were observed in both internal and external injector holes, and the external-hole deposits were radially distributed and collected in the shoulder, while the internal aperture deposits were axially distributed and tended to increase in density along one side of the hole. On the outer tip surface, two kinds of deposits can be seen with both a rough and smooth surface. The EDS analysis shows that the deposits in different locations consist of different levels of typical fuel and lubricant elements, such as C, O, Ma, Mg, Si, P, S, K, Ca, and Zn. Four dominating elements (C, S, Ca, and O) were identified for the injector. The percentages of C are shown to increase while the percentages of S and Ca decrease as the regions selected are located closer to the combustion chamber. However, no obvious regularity can be found between the percentages of O and the positions of deposits. Mixtures of carbon soot (C only) and sulfates (S, O, and Ca) may explain this.

Quigley et al. [47] studied the effects of the internal diesel injector deposit phenomenon to analyze fuel injectors and filter deposits from IDID affected engines using advanced techniques for possible insights into the deposit formation mechanism. SEM/EDS and ESI-MS analyses of failed injectors recovered from field use showed that

calcium and/or sodium were present in all of the sticking injectors, with high levels of sulfur and chlorine found in some cases. Dodecanoyl and hexadecenoyl succinic acids were found in most of the residues from sticking injectors. No single molecular fragment was found in all of the sticking injectors that were looked at.

To define the potential range of fuel components, contaminants, or additives that may be responsible for deposits was investigated by P. Lacey et al. [48]. The study can be summarized as IID formation increases rapidly above a critical temperature. All pure hydrocarbon fuels evaluated to date require a very high temperature to initiate IID formation. Reactive fuel components and contaminants effectively reduce the reaction temperature to a point where deposits occur during engine operation. IID were not observed at normal test temperatures with pure additive-free diesel or the same fuel containing up to 30% high quality FAME meeting EN 14214. At normal test temperatures, the addition of sodium to high quality additive-free diesel fuel did not result in IIDs. The addition of sodium to the high quality B10 biodiesel does result in sodium soap deposits, indicating residual acids present even in high quality biodiesel are sufficient to generate soap-based deposits. Poor quality biodiesel with a high sodium concentration and poor stability caused the most severe IID formation. With this fuel, a sodium concentration of 0.1 mg/kg or more was enough to cause deposits to build up.

Scott D et al. [49] studied Internal Injector Deposits in High-Pressure Common Rail Diesel Engines to identify alternate corrosion inhibitor and detergent chemistries that significantly reduce the propensity to build sticking deposits in low clearance areas inside high-pressure diesel injectors. Several methods were used to analyze deposits, such as SEM/EDS, FTIR, MS, LC/MS, and MS/MS. The study concluded that a number of HPCR injectors showing symptoms of needle and/or command plunger sticking were obtained from the field or from OEM test stands. The internal parts of these injectors are generally coated with a light-colored deposit visible to the naked eye. Using several analytical techniques, it was determined that the bulk of these deposits were comprised of sodium salts of alkenyl (hexadecenoyl or dodecanoyl) succinic acids. Sodium can enter the fuel distribution system from salt driers and caustic water used at refineries, storage tank water bottoms, and seawater used as ship ballast. Alkenyl succinic acids are widely used as pipeline corrosion inhibitors and in additive packages. Once formed, these salts are insoluble in ULSD fuel and can exist as very fine particulates that can pass through

vehicle fuel filters, eventually depositing on the internal surfaces of an injector. Because HPCR injectors have tight tolerances, they can get stuck with very little deposit.

An engine test was developed that reproduced the behavior and the chemical makeup of the sticking deposits observed on injectors from OEM test stands and field returns. This test was also used to investigate the effects of diesel fuel detergents on injector sticking. Even when sodium salts of alkenyl succinic acids are present, a new detergent was made and showed to keep deposits from forming on clean injectors and get stuck injectors to work normally again.

Allen A. Aradi et al. [50] looked at how the type of fuel and how the engine works affects the plugging and depositing of high-pressure, direct injection gasoline (DIG) injectors. Injector tips were photographed and external deposits scraped off and collected together as one for each fuel, then analyzed by SEM and IR. External injector deposits appear to be primarily fuel-derived but also contain crankcase lubricant elements. Internal injector deposits are only fuel-derived. The effect of fuel composition on deposit formation and injector plugging showed that injector tip temperature had a big effect on how much flow was lost during injection.

Shun Kumagai et al. [51] investigated the effect of zinc contamination on injector performance using a 4,000 cc, 4-cylinder common-rail direct injection diesel engine with cooled EGR and Variable Geometry Turbo system. The researcher tried to put as much thermal stress on the fuel as possible. The test fuel is specified to contain 1 ppm of Zn because one of the factors of the nozzle deposit is regarded as metal in fuel. On the other hand, regarding sticky deposits inside injectors, the engine test protocols reported so far are limited to the use of pro-fouling agents like NaOH and a certain type (experimental but not market-representative) of Polyisobutylene Succinimides (PIBSI). The test procedure was designed to construct a severe thermal condition for fuel in a relatively long time. Results from the study found that, in the injector deposit formation test, the engine torque started to decrease linearly, and torque reduction reached 9% after 300 hours of operation. The investigation into the dismantled injector after the injector deposit formation test revealed that the reason for the torque drop was a nozzle hole deposit, and no sticky deposits on the sliding parts were found. Therefore, it was concluded that the test conditions were effective.

The torque drop ratio was reduced to 5%/300 hours, and unlike the zinc-containing fuel, some recoveries in engine torque were found. It was confirmed that the torque was dropped by the formation of the nozzle hole deposit, not by the sticky deposit. However, the morphology of the nozzle deposit was more brittle. The impact on loss of fuel injection quantity is limited, but some deposits and power loss were demonstrated in a Zn-free fuel. Therefore, it was concluded that the test procedure is sufficiently severe to produce nozzle deposits and power loss using fuels with and without a zinc contaminant. Having such a test provides increased confidence that in further tests, the fuel/additive benefits shown will work in vehicles on the road.

Ramya Venkataraman et al. [52] investigated the solid deposition from commercially available high-pressure diesel fuel injectors during engine operation. The structural and chemical properties of injector deposits were compared to the formed form by the thermal oxidative stressing of a diesel fuel range compound, n-hexadecane. Results from the study showed that the chemical and morphological properties of HPDI deposits showed similarities in structure properties to those formed from the thermal oxidative degradation of a model compound, n-hexadecane, in short-duration experiments. These results suggest that the deposits formed at the tip of the diesel injector were also formed by oxidative degradation of diesel fuel under similar temperature-pressure conditions. Both kinds of deposits consist of polycondensed aromatic hydrocarbons arranged with varying degrees of structural order in the solid carbon. Both deposits also contained oxygenated functional groups.

1.3 Conditional Strategy

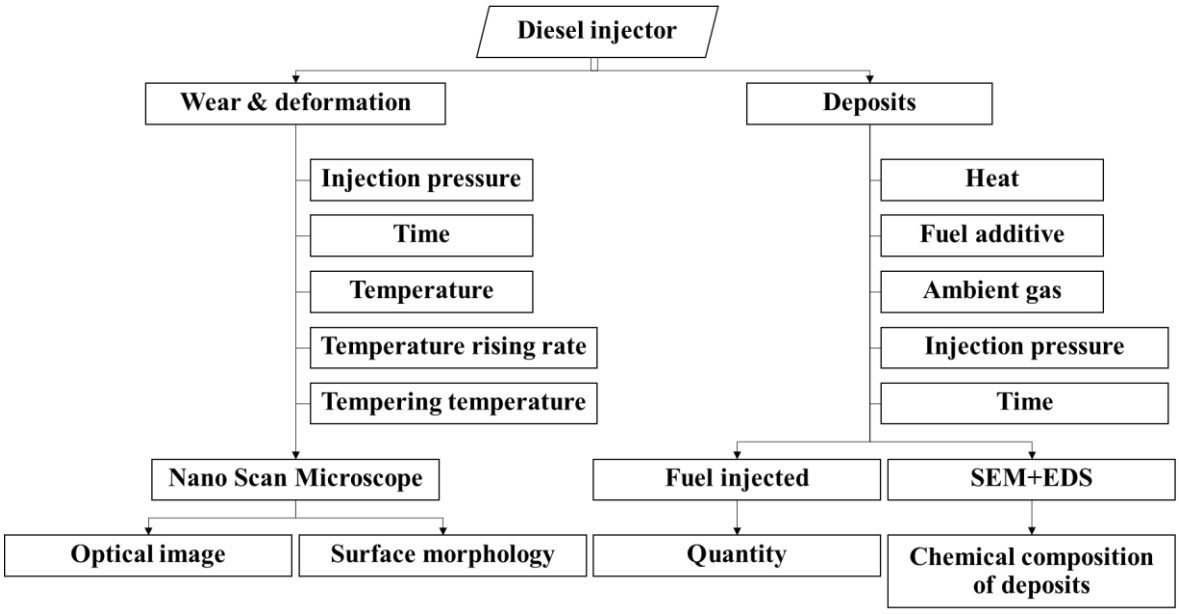

Fig. 1.2 Schematic diagram of condition strategy.

From the literature reviews which are already explained in the previous topic, the study of wear, deformation, and deposits has been proposed by many researchers in various ways and applications. The dominant factors that affect wear, deformation, and deposit formation have been summarized as shown in Fig. 1.2. In the case of wear and deformation, it has been reported that wear and deformation mechanisms are strongly affected by not only external force but also temperature. In spite of how much wear and deformation research data is available, there are only a few authors who have implemented the topic in internal combustion engine components. Due to a lack of information, the wear and deformation of diesel injector nozzles have not been clarified yet.

On the other hand, deposits in diesel injectors are also important to be concerned about in order to minimize diesel engine emissions and maximize combustion efficiency. The deposit formation mechanisms in diesel injectors, which include conventional and internal diesel injector deposit types, show that the process is strongly related to variations in fuel composition, temperature, and emission gases inside the combustion chamber. Although mainly studied and focused on internal diesel injector deposits only, the

conventional deposits inside the nozzle hole, which involve injection characteristics, are important as well. Based on a non-combustion test machine, the nozzle temperature and ambient gas were subjected to imitate the actual engine operating condition.

As described above, it would be better to clarify the mechanism of wear and deformation with the critical operating conditions at high temperature and length. Moreover, the deposit formation mechanism of the diesel injector nozzle hole needs to be elucidated.

1.4 Objectives

The study in this thesis consists of two parts which are deformation mechanism at injector nozzle body seat and deposit formation mechanism of injector nozzle hole. The objectives of this study are listed as follows:

-To clarify the effect of temperature and test duration on deformation mechanism of diesel injector nozzle body seat.

-To study the effect of heat treatment on nozzle material characteristics and deformation mechanism of body seat.

-To study the effect of fuel additive and ambient gas on injection characteristics of diesel fuel injector and deposits formation mechanism of diesel injector nozzle hole under non-combustion test condition.

-To investigate the effects of time between injections on nozzle hole deposit formation mechanism, fuel injection and spray characteristics.

1.5 Outline of the Thesis

Generally, this thesis includes two research activities, The first part is a study of body seat deformation mechanism, and the second part is a study of nozzle hole deposit formation mechanism including its effects on injection and spray characteristics which both experiments were carried out at the same facilities.

In chapter 1, the recent trend for wear/deformation and deposit formation in diesel engine was reviewed, including the fundamental of diesel combustion process and fuel injection system. The research objective and outline of the thesis were introduced in this chapter.

In chapter 2, the specification and principle of the test rig and test equipment developed specifically to simulate the operation of the actual engine were described. The imaging techniques used to observe the nozzle's surface morphology and characteristics were described. The surface morphology of the nozzle body seat was analyzed using a nano search microscope. Furthermore, Auger electron microscopy was utilized to investigate the material properties of the nozzle. To study the deposit formation inside the nozzle hole, scanning electron microscopy, energy dispersive X-ray spectroscopy, and attenuated total reflection-FTIR were introduced. For the investigation of fuel injection and spray characterization, the Bosch measurement method and shadowgraph technique were depicted.

In chapter 3, the mechanism of deformation on the nozzle body seat was emphasized. Temperature and test duration were intensively studied for their effects. In addition, the pre-heat treatment was considered in order to find a way to prevent the deformation of the nozzle body seat. Finally, the proposed mechanism related to deformation was presented.

In chapter 4, the mechanism of deposit formation under varying time between injections and its effects on injection and spray characteristics were analyzed. In the final section of the chapter, the mechanism for deposit formation inside the nozzle hole was described.

In chapter 5, summarization of all the research works undertaken including the key findings were presented. Future research developments and recommendations were given as well.

Bibliography

[1] Oil, coal, natural gas seen as fuels of the future, http://www.sae.org/mags/aei/4429.

[2] Greenhouse Gas Inventory Office of Japan (GIO). (2016). http://www-gio.nies.go.jp/aboutghg/nir/2016/NIR-JPN-2016-v3.0_rev_web.pdf

[3] Lazarev, V. E., Lazarev, E. A., Lomakin, G. V. and Wloka, J. (2014). Injection Nozzle Design for Longer Life at Higher Injection Pressures. MTZ industrial, 4, 64–69.

[4] Tuteja, A. D. (1966). Wear rate of injector nozzle while using different fuels. IIP Report. 44/212.

[5] Pielecha, I., Skowron, M. and Mazanek, A. (2018). Evaluation of the injectors operational wear process based on optical fuel spray analysis. Maintenance and Reliability, 20, 1, 83-89.
[6] Sachdev, K., Sharma, R. K. and Kumar, V. (1967). Study of injector nozzle wear while using different fuels by radiotracer technique. IIP Report. 44/256.
[7] Y. Liu, A. Erdemir, E.I. Meletis, "A Study of The Wear Mechanism of Diamond-Like Carbon Films," Surface and Coatings Technology, pp. 48-56, July 1996.
[8] Liu, Y., Erdemir, A. and Meletis, E. I. (1996). An investigation of the relationship between graphitization and frictional behavior of DLC coatings. Surface and Coatings Technology, 86-87, 564-568.
[9] R. P. C. Costa, D. A. L. Oliveira, F. R. Marciano, V. J. T. Airoldi., "Tribological behavior of DLC films in space and automotive oil under boundary lubrication.", Journal of Aerospace Engineering, Sciences and Applications, Jan. - Mar. 2012, Vol. IV, No 1.
[10] Behrendt, C. and Smith, A., "A Study of Diesel Fuel Injector Deposit Effects on Power and Fuel Economy Performance," SAE Technical Paper 2017-01-0803, 2017, https://doi.org/10.4271/2017-01-0803.
[11] Ikemoto, M., Omae, K., Nakai, K., Ueda, R. et al., "Injection Nozzle Coking Mechanism in Common-rail Diesel Engine," SAE Int. J. Fuels Lubr. 5(1):78-87, 2012, https://doi.org/10.4271/2011-01-1818.
[12] Smith, A. and Williams, R., "Linking the Physical Manifestation and Performance Effects of Injector Nozzle Deposits in Modern Diesel Engines," SAE Int. J. Fuels Lubr. 8(2):344-357, 2015, https://doi.org/10.4271/2015-01-0892.
[13] Tang, J., Pischinger, S., Lamping, M., Korfer, T., Tatur, M., and Tomazic, D., 2009, "Coking Phenomena in Nozzle Orifices of DI-Diesel Engines," SAE Paper No. 2009-01-0837.
[14] Song, H., Xiao, J., Chen, Y., and Huang, Z., "The Effects of Deposits on Spray Behaviors of a Gasoline Direct Injector," Fuel, Volume 180, 2016, Pages 506-513, ISSN 0016-2361, https://doi.org/10.1016/j.fuel.2016.04.067.
[15] Pos, R., Cracknell, R., and Ganippa, L., "Transient characteristics of diesel sprays from a deposit rich injector," Fuel, Volume 153, 2015, Pages 183-191, ISSN 0016-2361, https://doi.org/10.1016/j.fuel.2015.02.114.
[16] Caprotti, R., Breakspear, A., Graupner, O., Klaua, T., Schik, A., and Rouff, C., 2005,

"Injector Deposit Test for Modern Diesel Engines," Proceedings of the TAE Symposium 2005, Esslingen, Germany.

[17] Caprotti, R., Bhatti, N., and Balfour, G., 2010, "Deposit Control in Modern Diesel Fuel Injection Systems," SAE Paper No. 2010-01-2250.

[18] Caprotti, R., Breakspear, A., Graupner, O., and Klaua, T., 2005, "Detergency Requirements of Future Diesel Injection Systems," SAE Paper No. 2005-01-3901.

[19] Caprotti, R., Leedham, A., Graupner, O., and Klaua, T., 2004, "Impact of Fuel Additives on Diesel Injector Deposits," SAE Paper No. 2004-01-2935.

[20] Caprotti, R., Graham, B., Ullmann, J., Geduldig, M., and Stutzenberger, H. A., 2008, "Investigation on the Formation and Prevention of Internal Diesel Injector Deposits," SAE Paper No. 2008-01-0926.

[21] Lepperhoff, G., and Houben, M., 1993, "Mechanisms of Deposit Formation in Internal Combustion Engines and Heat Exchangers," SAE Paper No. 931032.

[22] Hoffmann, H., Koch, W., and Lucka, K. (2015). "A Novel Injector Deposit Fuel Test Method: ENIAK," Proceedings of the European Combustion Meeting 2015.

[23] Mancaruso, E., Sequino, L., Vaglieco, B., and Ciaravino, C., "Coking Effect of Different FN Nozzles on Injection and Combustion in an Optically Accessible Diesel Engine," SAE Technical Paper 2013-24-0039, 2013, https://doi.org/10.4271/2013-24-0039.

[24] Som, S., Ramirez, A. I., Longman, D. E., and Aggarwal, D. E., "Effect of Nozzle Orifice Geometry on Spray, Combustion, and Emission Characteristics under Diesel Engine Conditions," Fuel 90 (2011) 1267–1276. doi: 10.1016/j.fuel.2010.10.048.

[25] D'Ambrosio, S., and Ferrari, A. (April 12, 2012). "Diesel Injector Coking: Optical-Chemical Analysis of Deposits and Influence on Injected Flow-Rate, Fuel Spray and Engine Performance," ASME. J. Eng. Gas Turbines Power. June 2012; 134(6): 062801. https://doi.org/10.1115/1.4005991.

[26] Pham, V., V., and Nguyen, D., (2020). "A Brief Review of Formation Mechanisms, Properties and Affecting Factors of Combustion Chamber Deposits in Diesel Engines using Biodiesel," AIP Conference Proceedings. 2292. 040011. 10.1063/5.0030964.

[27] Tang, J., Pischinger, S., Grutering, U., and Keck, J., "Influences on the Formation of Deposits on Injection Nozzles in Direct-Injection Diesel Engines," MTZ 0912008 Volume 69.

[28] Montanaro, A. and Allocca, L., “Impact of the Nozzle Coking on Spray Formation for Diesel Injectors,” SAE Technical Paper 2013-01-2546, 2013, https://doi.org/10.4271/2013-01-2546.

[29] Birgel, A., Ladommatos, N., Aleiferis, P., Zülch, S. et al., “Deposit Formation in the Holes of Diesel Injector Nozzles: A Critical Review,” SAE Technical Paper 2008-01-2383, 2008, https://doi.org/10.4271/2008-01-2383.

[30] Hoang, A.T., Le, V.V., Pham, V.V., and Tham, B.C., 2019. “An Investigation of Deposit Formation in the Injector, Spray Characteristics, and Performance of a Diesel Engine Fueled with Preheated Vegetable Oil and Diesel Fuel,” Energy Sources, Part A Recover. Util. Environ. Eff., pp. 1–13. https://doi.org/10.1080/15567036.2019.1582731.

[31] Cracknell, R., Wardle, R., Pos, R.,and Ganippa, L., (2016). “Effect of diesel injector tip deposits on transient spray behavior,” https://doi.org/10.1007/978-3-658-12918-7_13.

[32] Pulkrabek, W. W. (2014). Engineering fundamentals of the internal combustion engine. 2nd edn. Pearson education limited. London.

[33] Kegl B., Kegl M. and Pehan H. (2013). Green diesel engines. 1st edn.Springer. London.

[34] R. Caprotti, W. J. Fowler、G. Lepperhoff、and M. Houben., “Diesel Additive Technology Effects on Injector Hole Erosion/Corrosion Injector Fouling and Particulate Traps”, SAE paper 932739.

[35] T. F. Su、C. T. Chang、R. D. Reitz、P. V. Farrel、A. D. Pierpont、and T. C. Tow. “Effects of Injection Pressure and Nozzle Geometry on Spray SMD and D.I. Emissions” 、SAE paper 952360.

[36] R.Chen、A.Iwabuchi、T.Shimizu.“Effects of ambient pressure on fretting friction and wear behavior between SUS304 steels”、Wear 249 (2001) 379-388.

[37] Cimenoglu H., “Subsurface characteristics of an abraded low carbon steel”, Elsevier Science S.A., Wear 210 (1997) 204-210.

[38] Pradeep L. Menezesa、Kishorea、Satish V. Kailas., “Role of surface texture of harder surface on subsurface deformation”, Wear 266 (2009) 103-109.

[39] A. T. Alpas、H. Hu and J. Zhang., “Plastic deformation and damage accumulation below the worn surfaces”, Wear 162-164 (1993) 188-195.

[40] N. Khanafi-Benghalema、 E. Felderb、 K. Loucif、 P. Montmitonnet., “Plastic deformation of 25CrMo4 steel during wear: Effect of the temperature、 the normal force、 the sliding velocity and the structural state”, Wear 268 (2010) 23-40.
[41] A. K. Gondol and P. C. Nautiyal., “Wear investigation of injector nozzle using radionuclide technique”, Wear, 147 (1991) 375-384.
[42] J. Hershberger*, O. O¨ ztu¨rk1, O.O. Ajayi, J.B. Woodford, A. Erdemir, R.A. Erck, G.R. Fenske., “Evaluation of DLC coatings for spark-ignited, direct-injected fuel systems”, Surface and Coatings Technology 179 (2004) 237–244.
[43] J. Hershberger*, J.B. Woodford, A. Erdemir, G.R. Fenske., “Friction and wear behavior of near-frictionless carbon coatings in formulated gasolines”, Surface and Coatings Technology 183 (2004) 111–117.
[44] Jim Barker, Paul Richards, Colin Snape and Will Meredith., “A Novel Technique for Investigating the Nature and Origins of Deposits Formed in High Pressure Fuel Injector Equipment”, SAE 2009-01-2637.
[45] A.M. Liaquat, H.H. Masjuki, M.A. Kalam and I.M. Rizwanul Fattah., “Impact of palm biodiesel blend on injector deposit formation”, Applied Energy 111 (2013) 882–893.
[46] K. Deaen, J. Hu, H. Ding, H. Xu1, A. Weall, P. Kirkby, B. Cooper, I. Edington and J.K. Venus., “An Investigation into the Characteristics of DISI Injector Deposits Using Advanced Analytical Methods”, SAE 2014-01-2722.
[47] R. Quigley1, R. Barbour1, E. Fahey1, D.C. Arters2, W. Wetzel2 and J. Ray., “A Study of the Internal Diesel Injector Deposit Phenomenon”, Lubrizol.
[48] P. Lacey, S. Gail, J.M. Kientz, N. Milovanovic and C. Gris., “Reviewed: Internal Fuel Injector Deposits”, SAE 2011-01-1925.
[49] Scott D. Schwab, Joshua J. Bennett, Steven J. Dell, Julie M. Galante-Fox, Alexander M. Kulinowski and Keith T. Miller., “Reviewed: Internal Injector Deposits in High-Pressure Common Rail Diesel Engines”, SAE International 2010-01-2242.
[50] Allen A. Aradi, Bill Imoehl, Noyes L. Avery, Paul P. Wells and Richard W. Grosser., “The Effect of Fuel Composition and Engine Operating Parameters on Injector Deposits in a High-Pressure Direct Injection Gasoline (DIG) Research Engine”, SAE 1999-01-3690.

[51] Shun Kumagai1, Ayumi Takahashi1, Hiroyuki Nagato2 and Richard Stardling., “Reviewed: Development of an Injector Deposit Formation Test Method for a Medium-duty Diesel Engine”, JSAE 20159029, SAE 2015-01-1914.
[52] Ramya Venkataraman1 and Semih Eser., “Characterization of deposits formed on diesel injectors in field test and from thermal oxidative degradation on n-hexadecane in a laboratory reactor”, Chem Cent J. 2008 Dec 17;2:25.

CHAPTER 2
DEVELOPMENT OF DIESEL FUEL INJECTION TEST RIG AND METHODOLOGY

2.1 Basic Specifications

2.1.1 The Fuel Injection Device of Diesel Engine

Many of the fuel injection system of a diesel engine (Also referred to as injector) employs a common rail fuel injection system. Common rail fuel injection apparatus, stored in the fuel boosted to necessary injection pressure by the high-pressure pump to the accumulator called a common rail, is opened and closed by energization of a solenoid valve which is provided with needle in the injector, the start of injection and it is intended to control the stop. Thus, the fuel injection pressure, fuel injection timing, has the advantage that the fuel injection period can be set independently, that improves fuel efficiency and exhaust emissions of diesel engine.

2.1.2 Injector Nozzle

The body seat refers to a portion provided in contact of the needle with inner wall of the nozzle. It is considered as wear and plastic deformation occurs when there is the overlapping when the valves open and close. On the other hand, the needle seat refers to the portion provided in contact of the inner wall of the nozzle with needle. It is considered as wear and deformation caused by contact with the body seat at its shoulder portion.

The material of the body seat is carburizing treatment, quenching, sub-zero treatment, a chromium-molybdenum steel which has been subjected to heat treatment such as tempering, more than 90% is a martensitic structure. Vickers hardness of the body seat is a 720Hv as body seat temperature at 120℃, drops to 680HVv at 240℃.

For the ferrite and cementite in the hardening does not change by quenching, performed from the state it was sufficiently changed to austenite structure immediately prior to hardening. Very hard martensitic structure by quenching is formed, organizations that do not change in the martensite is soft retained austenite. In order to further transformation to fully martensite austenite, carry out the sub-zero treatment. Sub-zero treatment is what was once hardening from the austenite region, it is a method to promote

the martensitic transformation immediately kept at a low temperature of 0℃ or less. Then, the martensite is stronger and hard, the toughness is lowered. In order to improve this, perform tempering by heating to remove the internal strain caused by quenching, to soften the tissue, to improve the ductility. Therefore, the body seat portion combines appropriate strength and ductility of steel is obtained.

On the other hand, the material of the needle is a high-speed tool steel, Vickers hardness is constant at 745Hv in the range of seat temperature 120℃ ~ 240℃. An injector and its nozzle are shown in Fig. 2.1-2.2. Fig. 2.3 shows the position of the nozzle body seat and cross-sectional view a body seat.

Fig. 2.1 G3S injector.

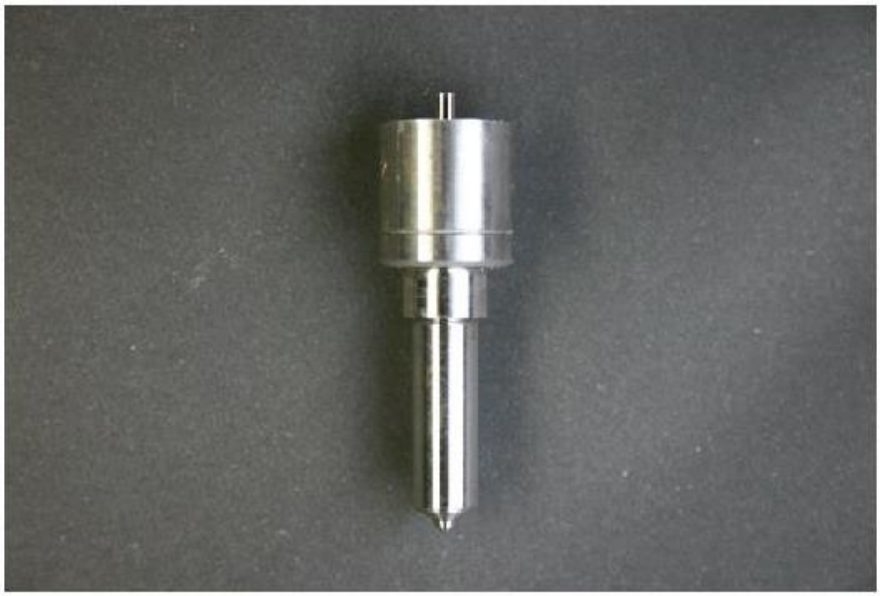

Fig. 2.2 Diesel injector nozzle.

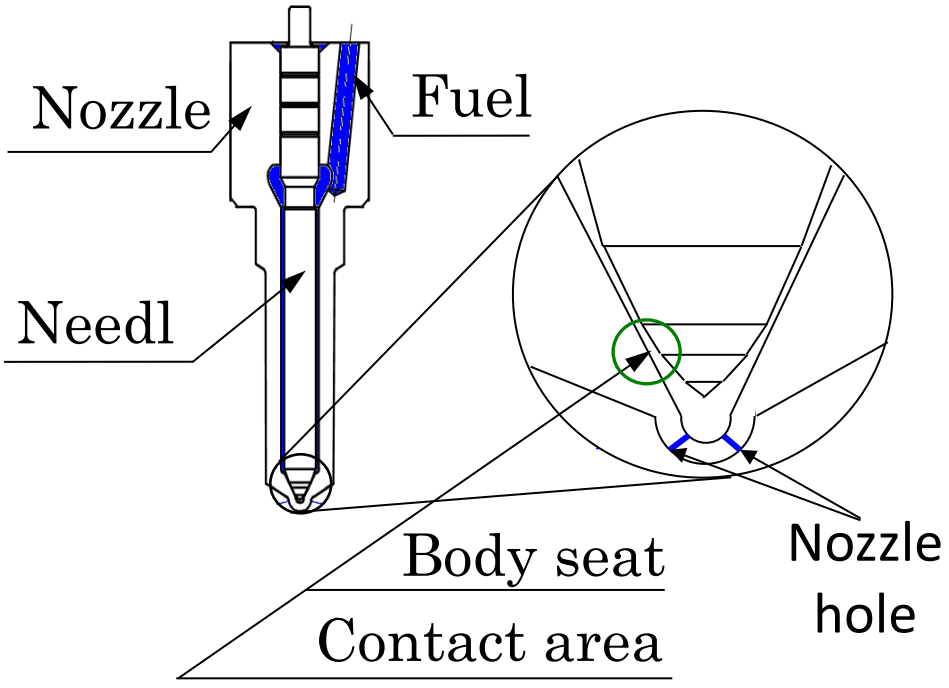

Fig. 2.3 Nozzle body cross-section view and body seat.

2.1.3 Overview and Features of the Testing Machine

Testing machine used in this study are those fabricated based on a common rail fuel injection system used in commercial 6-cylinder diesel engine. A block diagram of the entire apparatus is shown in Fig. 2.4, showing the entire apparatus photograph in Fig. 2.5. Main parts are primarily a common rail, an injector, an injector holder for fixing the injector, an accumulator for the pump and its drive motor, the fuel circulation system, injection control apparatus is configured in such a performance as follows.

Temperature Setting Function of Nozzle

The temperature of the body seat portion of the nozzle is equipped with a heating unit to any set and can be maintained. The heating unit is heating block, electric heater, thermocouple, SSR, is constituted by a temperature controller, it is possible to control the temperature of the body seat of the nozzle from 100℃ to 400℃, which corresponds to the output voltage of the controller.

Recycling and Reuse of Fuel

In this test apparatus, unlike actual engine, the injected fuel collected in the fuel tank is utilized to circulate. This device is used for simplifying the reduction of fuel consumption. In addition, it is necessary to prevent deterioration of fuel in the process of circulating.

Prevention of Fuel Ignition, Oxidation and Degradation

Ignition and oxidation of the injected fuel during to wear test is concerned. It is necessary to control the atmosphere inside injection chamber to prevent fuel deterioration. Argon gas has lower thermal conductivity than other inert gases, it can be suppressed from the environment to be deprived of the heat of the body seat which is heated by a heater.

Injection Interval

In this tester uses the same fuel injection system and a control system intended to be used in actual engines, the injection timing is carried out once injected into the same two rotation actual engine. It has injected 42,000 times per hour in normal test for this.

An overview of the operation of the apparatus will be described below.

(1) The fuel in the fuel tank is fed and pressurized by the fuel pressurizing pump.

(2) High pressure fuel is supplied to each injector through a common rail. The fuel pressure is measured by a pressure sensor attached to the common rail to maintain a predetermined pressure. The amount of fuel supply to pump is controlled.

(3) Carry out the fuel injection by applying a driving pulse voltage to the solenoid valve of the injector. The pressure of the fuel injection in the chamber is maintained at atmospheric pressure. Pulse signal is generated from the dedicated controller based on pump speed, transmitted to the solenoid is amplified to the drive voltage by EDUs (injector drive unit). Non-flammability gas is sent directly to the injector holder.

(4) Injected fuel is fed back to the fuel tank with argon non-flammability gas after cooled by the oil cooler.

(5) The excess gas in the fuel tank is opened to the atmosphere through the mist filter.

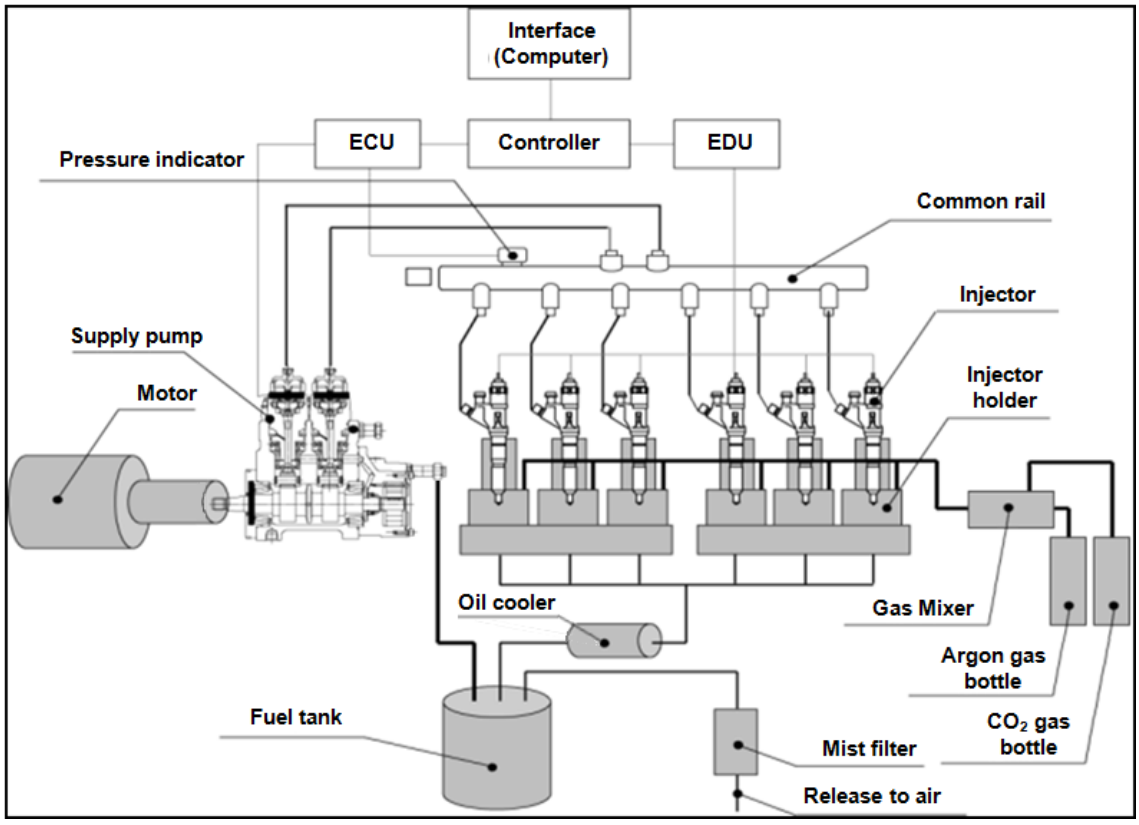

Fig. 2.4 Testing machine configuration diagram.

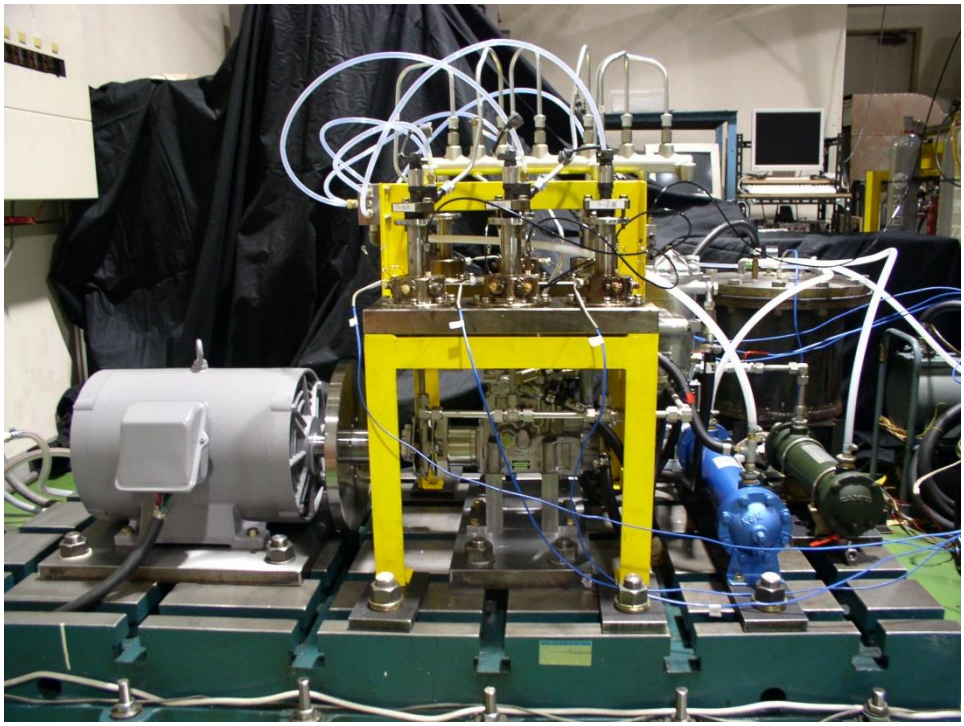

Fig. 2.5 Testing machine.

2.2 The Configuration of the Testing Machine

2.2.1 Drive System

Fuel pump, although the actual engine driven by the crankshaft, in this testing machine is driven by using a three-phase induction motor. The rotation speed can be arbitrarily set using an inverter. Motor and the inverter of three-phase induction motor, MLA8184A and FVR-G7S, are made by Fuji Electric Crop. The specifications of the motor is shown in Table 2.1. Moreover, the flywheel is equipped in order to suppress the vibration of the rotation speed caused by load fluctuations of the pump. Critical speed of the flywheel is at least 2200 rpm, sufficiently larger than the conventional rotational speed used in this tester at 1400 rpm.

Table 2.1 Motor specification.

Power output	18.5 kW
Voltage	200 V
Maximum revolution speed	1460 rpm
Maximum torque	300 Nm at 1300 rpm

2.2.2 Injection System

2.2.2.1 Injector Holder

Fig. 2.6-2.7 show an injector holder external and sectional view. The injector holder is designed to fix the injector for the purpose of pre-injected fuel recovering, it has the following characteristics.

(1) Recovery of pre-injection fuel

Since injected fuel has a large momentum, diameter of the order injection chamber is designed to sufficiently attenuate flow rate of the fuel at the time which the fuel droplets reach the wall surface, the wall is determined as not to be damaged by the injected fuel. In addition, the injector holder is HRC60 and processed by quenching and annealing to improve the durability.

(2) Sealing

In order to purge the injection chamber by the non-flammable gas, it is sealed with an O-ring to prevent purged gas leaks throughout the component contact surface. In addition, the upper and lower contact surfaces of heater holder are sealed by carbon gasket with circle shape which has the high temperature resistance property.

(3) Purge gas inlet

Since the part of heater unit is hot, non-flammable gas is purged to eliminate oxygen through the stainless compression fitting. The position of non-flammable gas inlet is set to be close to the thermocouple.

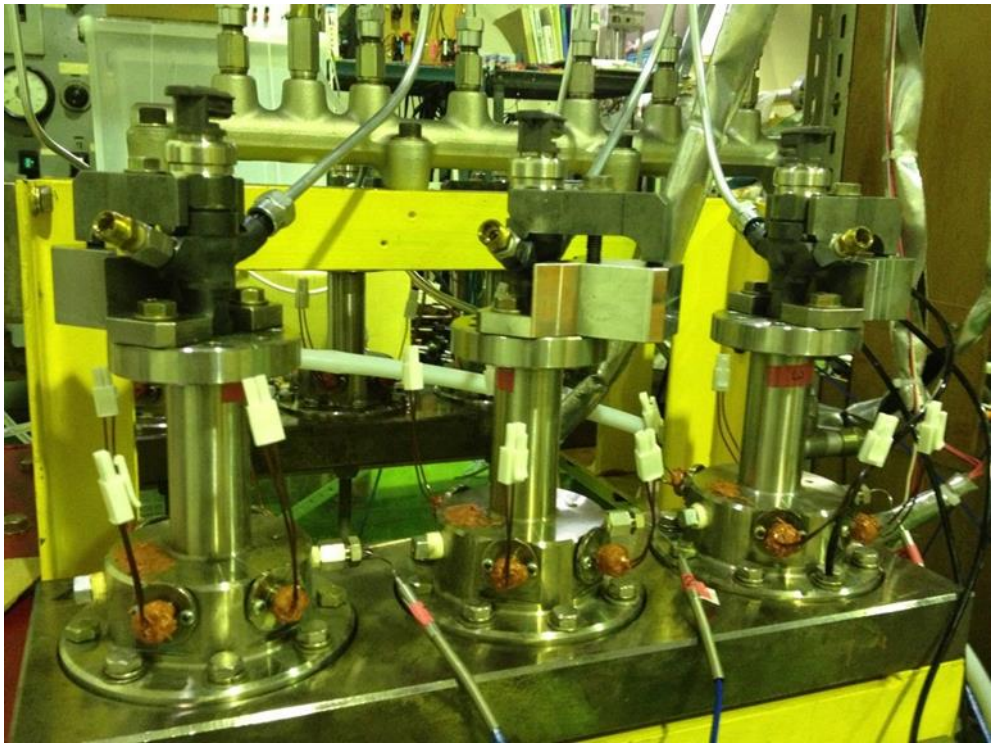

Fig. 2.6 Injector holder.

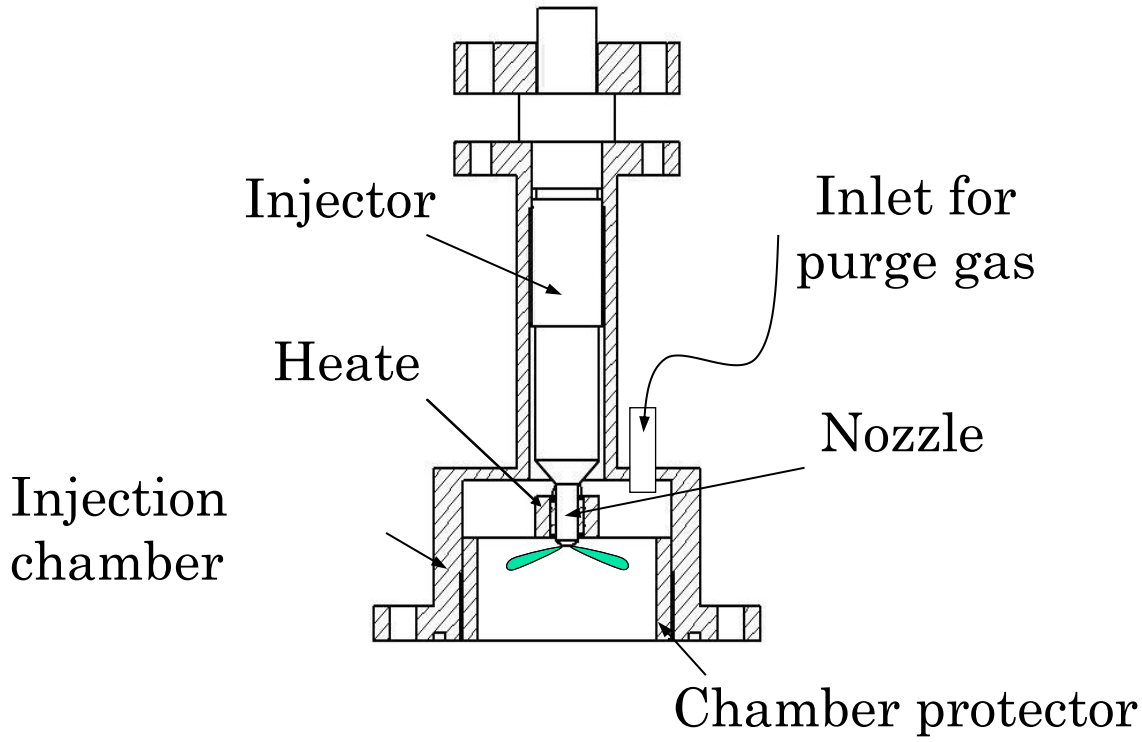

Fig. 2.7 Injector holder cross-sectional view.

2.2.2.2 Injection Pump

Injection pump can feed the fuel with high pressure up to 180 MPa corresponding Denso Corporation diesel engines. Supply pump is employed for boosting the feed fuel and sucking fuel from a fuel tank. Pressurized fuel from the fuel tank will be delivered through the fuel filter, and supplies the high-pressure fuel to the common rail.

2.2.2.3 Common-rail Fuel Injection System

Denso Corp. common rail system is used in this testing machine equipped with the electronic devices such as pressure sensor. The common rail allows the maximum 6 injectors to run in the same time. The maximum injection pressure of the system is limited at 180 MPa. Injector used in this test is G3S model, a third generation of solenoid injectors. The specification of the fuel injection apparatuses is shown in Table 2.2.

Table 2.2 Common rail specification.

Injection pressure	~180 MPa
Injection nozzle diameter	φ 7.2
Orifice diameter	φ 0.11 × 8
Injection pulse duration	0.2~2.0 ms

2.2.3 Control System

The injection of the injector is controlled by using control software provided by Denso Corp., comprising a controller and interface, ECU (engine control unit), EDUs (injector drive unit). It is the same as the fuel injection system mounted on an actual vehicle, the ratio of pump and motor is 1:2.

On the control software, it is possible to instruct the setting the fuel pressure and the injector energizing time of the common rail system. The actual behavior of the injector needle and injector solenoid drive voltage can be observed.

2.2.4 Fuel Circulation System

Fuel circulation system is manufactured as follow features to prevent deterioration of the fuel and control the fuel temperature.

(1) Control of fuel tank temperature

The fuel temperature is raised by being compressed to a high pressure; the influence of the seat temperature due to the change of the fuel temperature is assumed. Thus, water-cooled fuel cooler is provided in the fuel circulation path. OWR-5004G, temperature sensing tube is mounted within the fuel tank through a stainless-steel protective tube, it also controls the circulation fuel temperature by placing the valve in the cooling water system to control the flow rate. This makes it possible to arbitrarily set the fuel tank temperature in the range of 30℃ ~ 60℃.

(2) A method of cleaning an equipment and degradation prevention of the fuel

As means for preventing deterioration of the fuel, no corrosive materials are adopted as the materials of the apparatuses in the fuel flow pipe. The stainless-steel tube is used in the hot section (actual diesel engine component provided by manufacturers) low temperature parts are acrylic tubes or rubber tubes from the viewpoint of maintainability. Fuel tank is made of iron, washing is required before mounting.

To preventing mixing of the heterogeneous fuel, the apparatuses are washed and replaced as following methods.

(1) Drain out the fuel from the high-pressure pipe, oil cooler, fuel filter and fuel tank. Remaining fuel in the pump is possible to be discharged by rotating the motor by hand.

(2) Replace the fuel filter

(3) Performs flushing operation for 1 hour using a same fuel containing the same kind of fuel or additives that will be used next.

(4) Supply the new fuel before conduct a test.

2.2.5 Heating System

2.2.5.1 Electric Heater

The heating of the nozzle is using WATLOW manufactured by small, high-output electric heater. The specifications of the heater are shown in Table 2.3. Electric heaters are cylindrical shape and made of metal magnesium oxide insulator of a specific grain and purity. The wire is made of nickel-chromium resistance.

Table 2.3 Heater specifications.

Model number	E1E61
Diameter	6.25 ± 0.05 mm
Length	31.8 mm
Watt density	60 W/cm^2
Regular voltage	240 V
Power at regular voltage	225 W
Max temperature	890℃

2.2.5.2 Heater Block

For mounting the electric heaters to the nozzle, a heating block is required. Eight of the electric heaters have been designed to be mounted, it is possible to output a total of power at 1800W. The image of heater block is shown in Fig. 2.8. The heating block has the following features.

(1) Heat transfer between the nozzle and the block

Nozzle diameter is formed of a tapered shape with the base and tip as 7.15 mm and 7.05 mm, respectively. The heater block is designed to be adaptable to fit the nozzle shape. Further put a notch in the block, thereby improving the thermal efficiency heat transfer are brought into close contact with the nozzle and the block by bolting. In order to reduce the heat loss of the nozzle and the heater, the thickness between the nozzle and heater is set to 0.2 mm approximately at the thinnest portion.

(2) Thermocouple insertion hole for the nozzle surface temperature measurement

The heater block with eight electric heaters has raised the temperature of the body seat of the nozzle. However, although the ambient temperature inside the holder can be measured by a thermocouple, it is difficult to grasp the body seat temperature of the nozzle. Therefore, a hole of diameter ϕ 1.6 mm is made to insert the thermocouple, it has become

possible to measure the thermal state of the nozzle surface closer to the body seat temperature.

(3) Temperature controller and SSR

Adjusting the voltage using the voltage regulator to the prior, it had raised the temperature of the heater, respectively. However, large variations in the capacity of the heater itself, there is a variation in the thermal conductivity of the heater and the nozzle. It is difficult to provide a constant temperature at the body seat. Therefore, using a temperature controller and a solid-state relay, as shown in Fig. 2.9, to control a certain target value on a nozzle surface temperature, it is possible to keep the body seat temperature constant. Temperature controller and SSR are Omron E5CC and G3PE.

The wiring diagram of a heating apparatus using a conventional heater block is shown in Fig. 2.10. On the other hand, a wiring diagram of an improved heating apparatus using a heater block which is improved is shown in Fig. 2.11. Both systems use a voltage regulator. In the conventional device, heater temperature is controlled by a voltage regulator. Whereas the improved system allows heater temperature to be controlled by SSR and digital heater controller. Thus, the improved system can operate precisely and invariably. Usually, the applied voltage is set to about 140 ~ 160 V.

The above improvements of heater block and SSR, the temperature survey test and various deformation tests using an improved heating device, such as a temperature controller is described later.

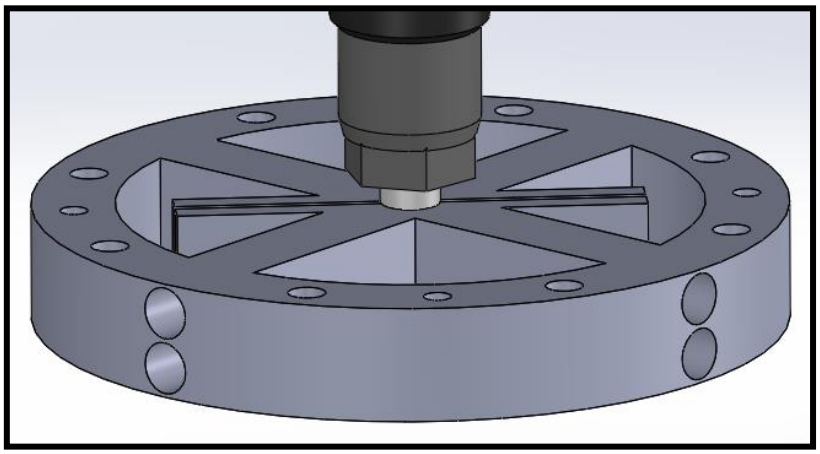

Fig. 2.8 Heater block.

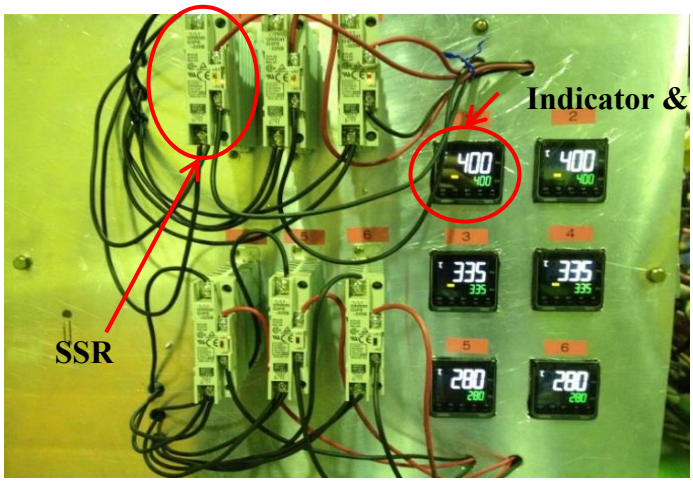

Fig. 2.9 Temperature controller and SSR.

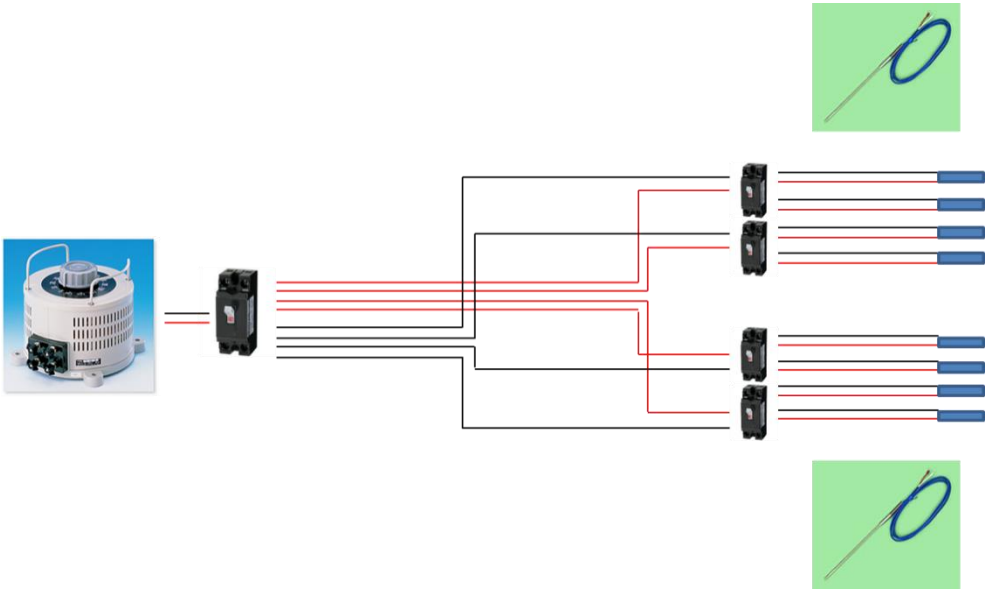

Fig. 2.10 Wiring diagram of a conventional heating devices.

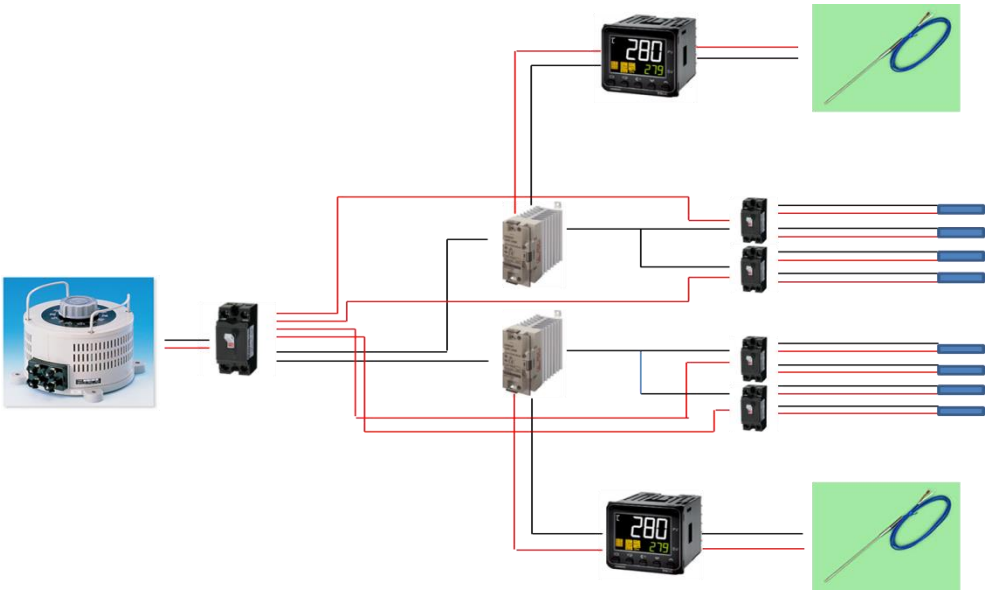

Fig. 2.11 Wiring diagram of the improved heating devices.

2.2.6 Gas Mixing Chamber

In this study, unlike the actual engine which the gas compositions are variation according to the combustion, it is required to control the atmosphere inside the injection chamber to be the same composition of gas. A gas mixing chamber was fabricated and employed to supply the gas to injection chamber in order to imitate the combustion gas. Fig. 2.12 shows a schematic of gas mixing chamber in a cross-sectional view.

In the gas mixing chamber, other gases for most flow-rich gas as a main stream (primarily as main gases Ar, N_2, etc.) has prompted the mixture by causing penetration in opposite directions. Each gas flowing into the gas mixer, the gas after the mixing is prevented from flowing back through the check valves.

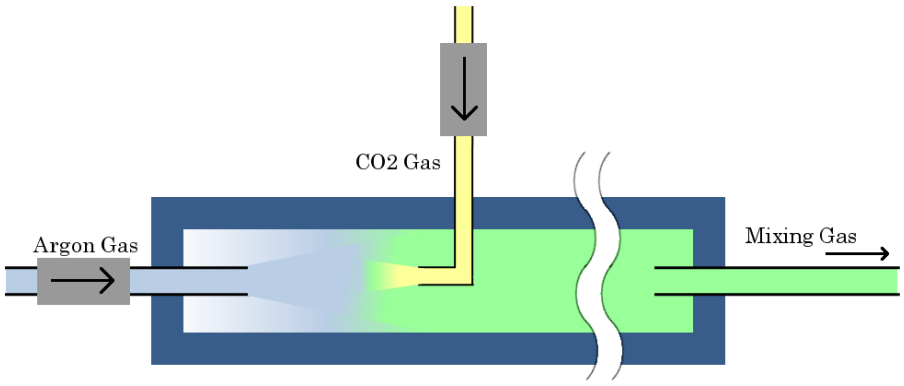

Fig. 2.12 Gas mixing schematic cross-sectional view.

2.2.6.1 Convective Heat Transfer Calculation

-Compare between Argon and CO_2 system

Table 2.6 Gas properties.

Properties	Argon	CO_2
Density @0.15 MPa (kg/m^3)	2.45	2.665
Dynamic viscosity, 20 °C (Ns/m^2)	2.23 x 10^{-5}	1.47 x 10^{-5}
The fluid viscosity at the bulk mean temperature, 20 °C (Ns/m^2)	2.23 x 10^{-5}	1.47 x 10^{-5}
The viscosity at the tube wall surface temperature, 400 °C (Ns/m^2)	4.22 x 10^{-5}	3.08 x 10^{-5}
Conductive heat transfer coefficient (J/mKs)	0.016	0.015

Reynolds number (Re) equation:

$$Re = \frac{\rho u d_h}{\mu}$$

Re = Reynolds Number (non-dimensional)

ρ = Density @0.15 MPa (kg/m^3)

u = Velocity based on the actual cross section area of the duct or pipe (m/s)

μ = Dynamic viscosity (Ns/m^2)

d_h = Hydraulic diameter (m)

Nusselt number (Nu) equation:

*Forced convection, internal flow, laminar flow

$$Nu_D = 1.86 \cdot (Re \cdot Pr)^{\frac{1}{3}} \left(\frac{D}{L}\right)^{\frac{1}{3}} \left(\frac{\mu_b}{\mu_w}\right)^{0.14}$$

$$Nu = \frac{hD}{k}$$

Where,

D= The internal diameter (0.07 m)

L = Length (0.0255 m)

μ_b= The fluid viscosity at the bulk mean temperature (Ns/m^2)

μ_w= The viscosity at the tube wall surface temperature (Ns/m^2)

Pr = Prandtl number (non-dimensional)

k = Conductive heat transfer coefficient (J/mKs)

$$q = h_c A \Delta T$$

q = Amount of heat transferred (W)

h = Heat transfer coefficient (W/m^{2}K)

ΔT = Difference in temperature between the solid surface and surrounding fluid (380 K)

A = Heat transferred area (0.0056077 m^2)

Table 2.7 Calculation results.

Parameter	Argon	CO_2
Re	33.3	37.586
Pr	0.725	0.83
Nu	6.93	7.392
h (W/m^{2}K)	1.584	
q (W)	3.375 (Controlled)	
u (m/s)	0.00433	0.00296
Flow rate (L/min)	1	0.684

2.3 Observation of Nozzle Temperature

In order to simulate a combustion of the injected fuel in the actual engine, it is necessary to raise the temperature of the body seat of the nozzle to 350 °C as the high load condition. Since testing machine used in this study is for circulating the fuel without combustion, the heaters are installed around the nozzle as shown in Fig. 2.8. It is necessary to simulate the temperature of the body seat in the actual engine. This section describes the temperature survey results by the conventional temperature survey results and improvements device as a measurement technique of the body seat temperature.

2.3.1 Body Seat Temperature Measurement Method

In order to measure the body seat temperature of the nozzle, two types of methods are using as described in the following.

[Temperature Test Using a Thermocouple at an Injector Surface]

Embedded thermocouple inside the nozzle using a special injector, it is possible to measure the approximate temperature of the body seat.

Benefits

The temperature measurement by thermocouple is available for immediate measurement.

Disadvantage

Embedded thermocouple inside the nozzle does not measure the real temperature of the body seat. Further, since the fixed using adhesive to the nozzle, cannot be accurately measured exceeds the heat resistant temperature of the adhesive (approximately 300 °C).

[Temperature Test by the Hardness Measurement of the Nozzle]

Steel is based on the principle that the hardness is reduced by tempering, heating with fixed time, a method of estimating the tempering temperature by measuring the amount of hardness decrement of the measurement site of the nozzle. More specifically equipped with a mass nozzle to the apparatus estimates a receiving-heat-temperature by measuring the body seat hardness of each site after operation for several hours.

Benefits

It is possible to get accurate temperature measurement. Further, it is possible to measure for various locations within the nozzle. For example, the temperature near the

nozzle surface of the nozzle and outer wall of the body seat portion is also conceivable different leads to each independent measurement.

Disadvantage

It requires a special tool for hardness measurement, takes time to obtain more results.

In this study, it is necessary to accurately grasp the temperature of the body seat of the nozzle, the temperature was investigated using temperature assay method according to the hardness measurement of the nozzle.

2.3.2 Conventional Temperature Survey Technique

Adjusting the voltage applied to the heater in order to controlled the body seat temperature of the nozzle. The body seat hardness of the injector temperature survey test was measured to estimate the seat temperature on the applied voltage during the test, they were subjected to various tests based on this data.

2.3.3 Temperature Survey Results of the Improved Device

The conventional temperature survey simply to regulate the voltage of the heater, it is difficult to accurately control the body seat temperature of the nozzle. In order to provide a high load of temperature (350°C) to the body seat, it is a need for an improved of the heating device. Therefore, to improve the heater block and thermocouple as shown in Fig. 2.8-2.9, it is possible to immediately measure a nozzle surface temperature close to the temperature of the body seat. Further, it is possible to precisely control the nozzle surface temperature by using a temperature control apparatus and also possible to provide a constant high load temperatures the body seat.

Although, there is a possibility to measure the surface temperature of a nozzle by using an improved apparatus, in order to estimate the temperature of the body seat, it is necessary to examine the relationship between surface temperature and the body seat portion temperature of the nozzle in advance. So, using the improved apparatuses and the temperature was investigated as follows.

2.3.3.1 Test Conditions

The heating apparatuses were modified to achieve the body seat temperature at 350° C during a high load. Test conditions are shown in Table 2.8. In this test, the SSR was examined only relationship of the nozzle surface temperature and the body seat temperature without using a temperature regulator. First, the test under the following test conditions were investigated the relationship between the applied voltage and the surface temperature of the nozzle.

Table 2.8 Temperature measurement test conditions of improved heating devices.

Fuel	Acid 400 μm
Fuel tank temperature	30 ℃
Nozzle surface temperature	220 ℃, 310 ℃, and 420 ℃
Injection pressure	180 MPa
Injection pulse duration	480 μs
Pump speed	1,401 rpm
Test duration	5 h

2.3.3.2 Test Results

It shows a relationship between the nozzle surface temperature and the body seat temperature by a temperature survey test in Fig. 2.13. Measurement of the body seat temperature was investigated under heat temperature in achieving the hardness of the nozzles after the temperature survey test.

Body seat temperature is the temperature results obtained by measuring the hardness of the nozzle body seat at the end of the test. Temperature measurement points of the body seat portion is shown in Fig. 2.14, the temperature of the body seat is expressed as mean values of S1, S2, S3. From this result, the temperature of the nozzle surface temperature and the body seat are plotted to determine the relations. The improved apparatus can grasp the nozzle surface temperature close to the body seat temperature which is considered that it is possible to accurately estimate a body seat temperature than ever.

In the future, when setting the temperature of the body seat, the nozzle surface temperature will be set using a temperature controller and SSR. The controlled temperature is shown in Table 2.9.

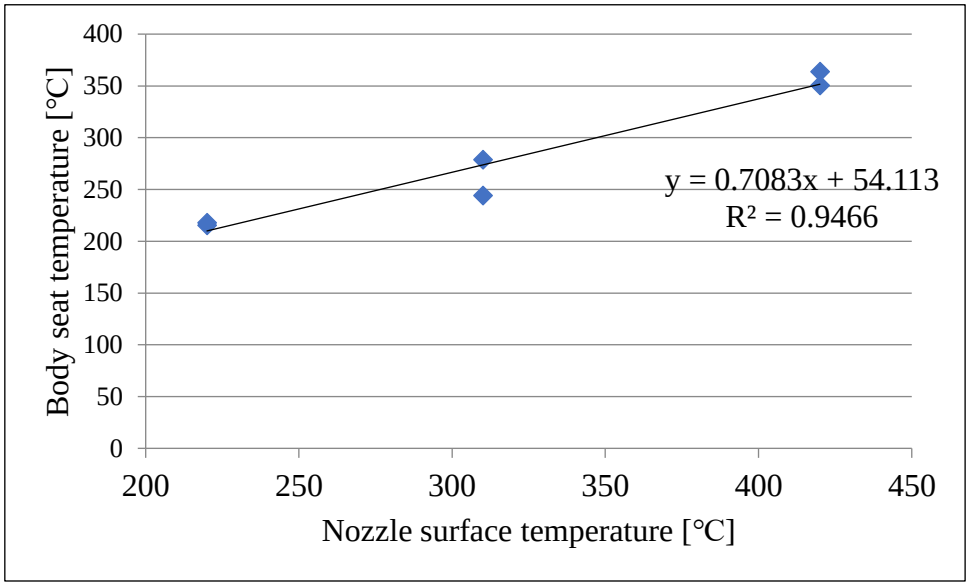

Fig. 2.13 Relations of nozzle surface and body seat temperature.

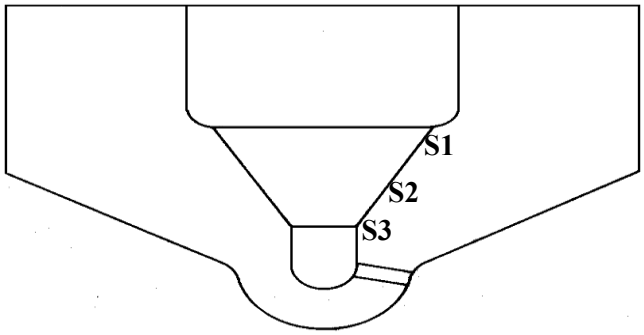

Fig. 2.14 Body seat hardness measurement locations.

Table 2.9 Correspondence table of the body seat and nozzle surface temperature.

Body seat temperature		Nozzle surface temperature
250 °C		279 °C
275 °C	⇔	312 °C
300 °C		346 °C
325 °C		379 °C
350 °C		412 °C

2.4 Surface Observation by Nano Search Microscope

Fig. 2.15 shows the tested nozzle, which was cut by wire electric discharge machining to create a sample for observation. The body seat had a conical surface shape measuring 59°, with the center of the nozzle as the axis. By cutting the body seat part at an angle of 29.5°, it can be measured parallel to the body seat. A nano search microscope (LEXT OLS4500, manufactured by Olympus) was used to measure the surface roughness. The sample was observed using a laser scanning microscope (LSM) and a scanning probe microscope (SPM), which were combined into one instrument. Two-dimensional information can be obtained by selecting a constant line. The accuracy of the measurement is 0.3 μm within the measurement length of this study.

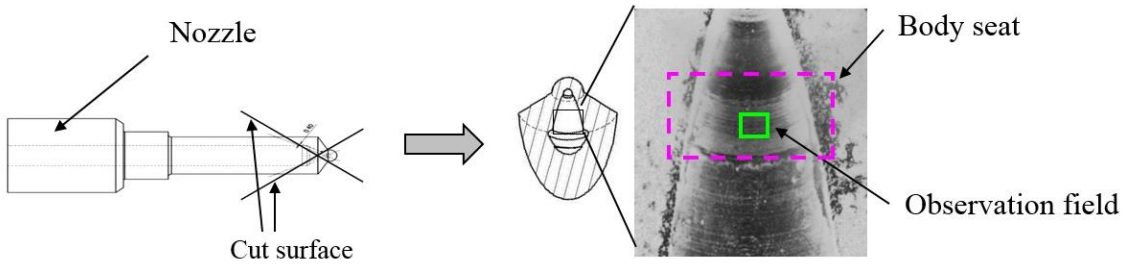

Fig. 2.15 Schematic view of nozzle cutting.

2.5 Definition and Measurement Method of Amount of Deformation

Depth of regression and amount of deformation of body seat were defined by using the results from scanning probe microscope (SPM) and comparing the deformation data before and after the experiment. The shape of the nozzle body seat changed when the body seat collided with the needle shoulder, causing a dent along the needle owing to plastic deformation and wear. The change in the body seat is expressed by the differences in the surface position at the two representative points on the body seat before and after the experiments, denoted as δZ1 and δZ2. Fig. 2.16 shows the outline of surface roughness measuring by SPM method. Fig. 2.17 shows surface shape of body seat before and after the test, and the example data of depth at regression and height of upheaval matching the shape of body seat and the definitions of δZ_1 and δZ_2. The scales in the scanning and depth directions were 200 and 5 μm, respectively. The dotted line in the figure shows the outline of the needle. As shown in this figure, the body seat caved along

the shape of the needle that collided with the body seat. It was speculated that this deformation was associated with plastic deformation, but the contributions of this is yet to be elucidated.

Herein, the depth of regression on the body seat is denoted by δZ_1. The maximum depth of regression is calculated by the distance between the lowest point of the body seat surface and the reference level. However, plastic deformation occurred as the body seat approaches the nozzle tip. The needle surface established contact with the body seat owing to the movement of the needle, and the body seat was plastically deformed. When the needle approached the nozzle tip, the body seat ascended as compared with the scenario before the test. The ascending height was 900 µm away from the location where the most regressed depth was observed; therefore, the deformation or height of the upheaval on the body seat is denoted as δZ_2. As shown in Fig. 2.17, scale in the figure's scanning direction is ~2,000 µm, the depth direction represents 20 µm. Dotted line in the fig. also shows the outline of the needle. The depth at the most regressed point, δZ_1, and the height at the point of 900 µm from the most regressed point, δZ_2, are 3.2 and 2.7 µm, respectively.

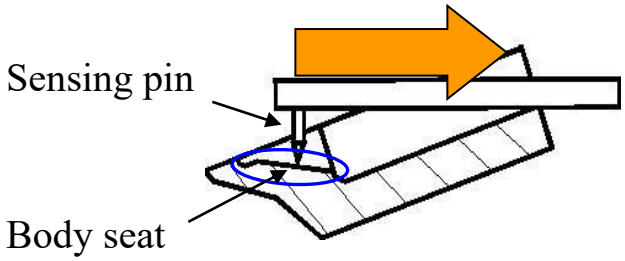

Fig. 2.16 Overview of body Seat measurement by SPM method.

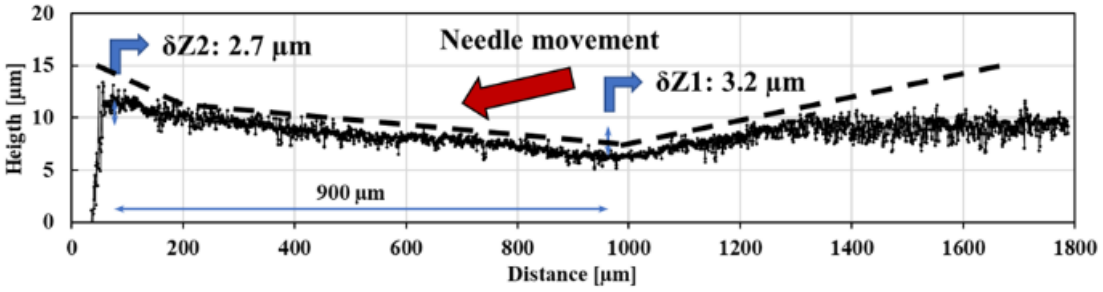

Fig. 2.17 Example of measurement result of the body seat.

2.6 Fuel Injection Measurement

To evaluate the effect of diesel injector deposits, the injector test is carried out using the test machine with non-combustion. At the test time 0, 2, 5, 10 and 20 hours, the amount of fuel injected are measures and reported as the average amount fuel injected loss at injection duration of 480 and 1,000 μs conditions, as shown in Table. 2.10. The fuel injected is sampled for 3 and 2 minutes in injection duration of 480 and 1,000 μs, respectively, with the repeatability of 5 times. The injection pressure is controlled at 180 MPa and the pump revolution is controlled at ,1400 rpm.

Table 2.10 Test conditions for the amount of fuel injected measurement.

Fuel	Additives	HFRR
	Acid	400 μm
Injector model	G3S	
Nozzle	0.11 mm diameter x 8 holes	
Injection pressure	180 MPa	
Injection duration	480 and 1000 μs	
Pump speed	1400 rpm	
Test time	0, 2, 5, 10 and 20 hours	
Test duration	2 and 3 minutes	
Repeatability	5	

2.7 Chemical Composition Analysis

Chemical analysis, which is the most direct method of investigating the composition of samples, is also used in this study in order to study the deposit process. By analyzing compositions of deposits, detailed composition of deposits can be achieved. It is of great importance to identify the source and presence of deposits.

SEM (Scanning Electron Microscope) and EDS (Energy Dispersive X-ray Spectroscopy) techniques were introduced in this study to observe the physical and chemical properties of the deposits, respectively. The tested nozzle is roughly cut in order to prepare for the measurement using electric discharge machining and wire cutting. To access the center of nozzle hole, the cut nozzle is polished by sandpaper and checked by optical microscope. The schematic of observation area of nozzle hole is shown in Fig. 2.18.

The cut nozzle at the center of the nozzle hole was taken as a picture by using SEM to scan the areas of interest. The nozzle hole deposits are observed at three different areas: the inlet, middle, and outlet of the nozzle hole. EDS is good supplementary means to understanding the details of deposit compositions. The interaction of the electron beam and the atoms ids dependent on the element being measured. Elements with a very low are not or hardly detectable. EDS-images are measured during the low magnification investigation with constant boundary conditions. To employ a study using EDS, SEM (Scanning Electron Microscope) is required in order to scan the interest are on the sample with an electron beam. The interaction of surface and electron beam is measured. The measurements are used to build an image of the sample surface. The EDS technique was employed in this study to obtain qualitative information on the element constituents of the deposits. Therefore, the presence of zinc element as a deposit on the injector nozzle surface is observable. The FTIR technique was widely used in many studies to investigate the chemical properties of the deposits [1]. However, it is very difficult to observe in a very narrow area and when the amount of the deposits is very small. Therefore, the ATR-FTIR technique was used to understand the chemical properties of the deposits in this study.

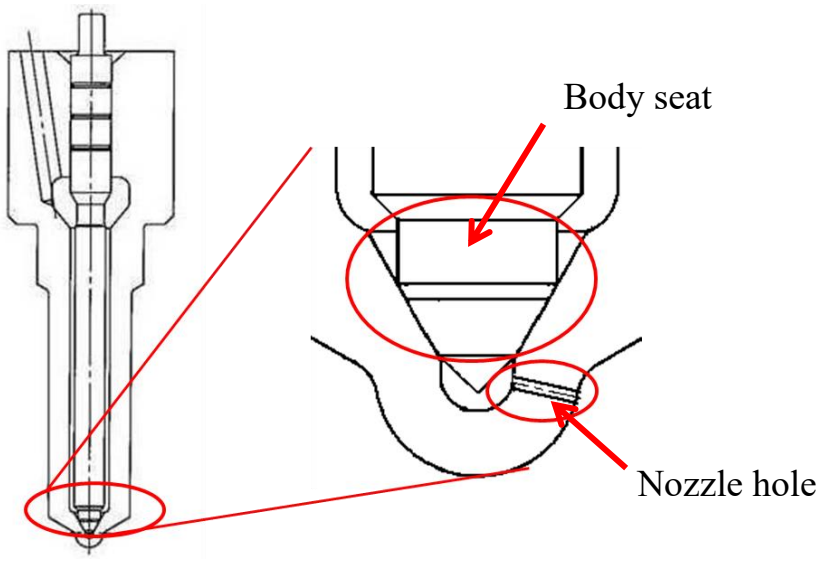

Fig. 2.18 Observation area of nozzle hole.

2.8 Measurement of Injection Rate

This section describes the effects of deposits generated in the injection hole on the injection characteristics, as well as equipment and methods for measuring various fuel injection/spray characteristics. The reduction of the injection hole cross-sectional area due to the accumulation of deposits in the nozzle hole is considered as an indicator of the amount of deposit accumulation because it reduces the injection rate. The principle and method of measuring the fuel injection rate are described. To evaluate the effects of the diesel injector nozzle hole deposit on the fuel injection, the accelerated deposit formation experiment was carried out using the test machine with non-combustion. The fuel injection characteristics were measured by the Bosch technique [2]. This is a method of injecting fuel into a long pipe filled with fuel and deriving the injection rate from the pressure difference due to injection. The results of the measurements were given as the average fuel injection rate and discharge coefficient at the injection of 1,000 μs under different injection pressures ranging from 120 to 180 MPa. The calculation of the injection rate and discharge coefficient were described.

The pressure change caused by the injection is represented by equation (2.1) below.

$$dp = \rho a u \qquad (2.1)$$

dp: Pressure difference of fuel [Pa]

ρ: Density of fuel [kg/m^3]

a: Sound velocity in fuel [m/s]

u: Fuel velocity [m/s]

The derivation of Eq. (2.1) is explained here. When a pressure change of dp occurs in a long pipe due to injection, the state of the change propagates at the speed of sound a. When the inner diameter of the orifice is constant, if the velocity density and pressure in front of the shock wave surface are u, ρ, and p, respectively, then they change to $u+du$, $\rho+d\rho$, and $p+dp$ for the later shock. Applying the law of momentum to an element surrounded by any two adjacent inspection surfaces in a steady flow, the vector sum of the momentum of the fluid entering and exiting the inspection surface is equal to the external force acting on the same inspection surface.

Therefore, the following equation (2.2) can be derived.

$$(a-dU^2)(\rho+d\rho)A-a^2\,\rho A=dpA \qquad (2.2)$$

A: Cross-sectional area of injection hole [m^2]

U: Instantaneous cross-sectional average flow velocity of fuel [m/s]

Considering the shock front, the equation of continuity can be applied, so

$$(a-dU)(\rho+d\rho)A=a\rho A \qquad (2.3)$$

By arranging this and ignoring the second derivative, the following equation (2.4) can be derived.

$$dU/a=d\rho/\rho \qquad (2.4)$$

Simultaneously solving this equation with equation (2.2) yields the following equation (2.5).

$$dp = \rho a \cdot dU \qquad (2.5)$$

Equation (2.1) can be derived from the above.

Here, the fuel injection rate q of the fuel injection device is expressed by the following equation (2.6).

$$dq/dt = AU \qquad (2.6)$$

q: injection rate [m^3/s]

Therefore, by combining equations (2.6) and (2.1), equation (2.7) for the injection rate can be derived from the pressure difference between the atmospheric pressure in the cylinder and the steady state.

$$dq/dt=A/a\rho\,\Delta P \qquad (2.7)$$

ΔP: Injection differential pressure [Pa]

Discharge coefficient can be calculated by Eq. (2.8) [3].

$$C_d = \frac{\dot{m}}{\dot{m}_{theor}} = \frac{\dot{m}}{2A_0\rho_f\Delta P} \qquad (2.8)$$

Where $\dot{m}$ denotes the mean mass flow rate of the fuel calculated from the steady flow, $\dot{m}_{theor}$ refers to the theoretical mass flow rate derived from the Bernoulli's equation, A_0 indicates the cross-sectional area of the orifice at the outlet, ρ_f is the fuel density at the operating temperature, and ΔP for the pressure differential between injection pressure and back pressure.

The fuel injected was sampled at the number of injections at 0, 210,000, and 420,000 times during a heated injection test with a repeatability of 10 times. The rotational speed of the fuel supply pump for the injection rate measurements was controlled at 1,000 rpm for all conditions, as shown in Table 2.11.

Table 2.11 Test conditions for the injection rate measurement.

Fuel	Additives	HFRR
	Acid	400 μm
Injector model	G3S	
Nozzle	0.11 mm diameter x 8 holes	
Injection pressure	180 MPa	
Injection duration	480 and 1000 μs	
Pump speed	1400 rpm	
Test time	0, 2, 5, 10 and 20 hours	
Repeatability	10	

2.8.1 Measuring Equipment

A diagram of the measuring device is shown in Fig. 2.19. The fuel ejected from the fuel injection device attached to the injector holder passes through a long pipe, passes through a throttle valve for attenuating reflected waves, and is discharged from a relief valve for controlling atmospheric pressure during fuel injection and back pressure. The fuel pressure is measured with a pressure gauge just behind the injector holder. Fig. 2.20 shows an example of the pressure waveform and an image of injection rate and injection quantity measurement. The injection quantity obtained in this experiment is from the point where the spray quantity first increases to the point where the spray quantity first drops to 0. On the other hand, the injection rate is the average of the pressure wave data 0.8 to 2 ms after the injection command signal is received, and the fuel flow rate is derived from this.

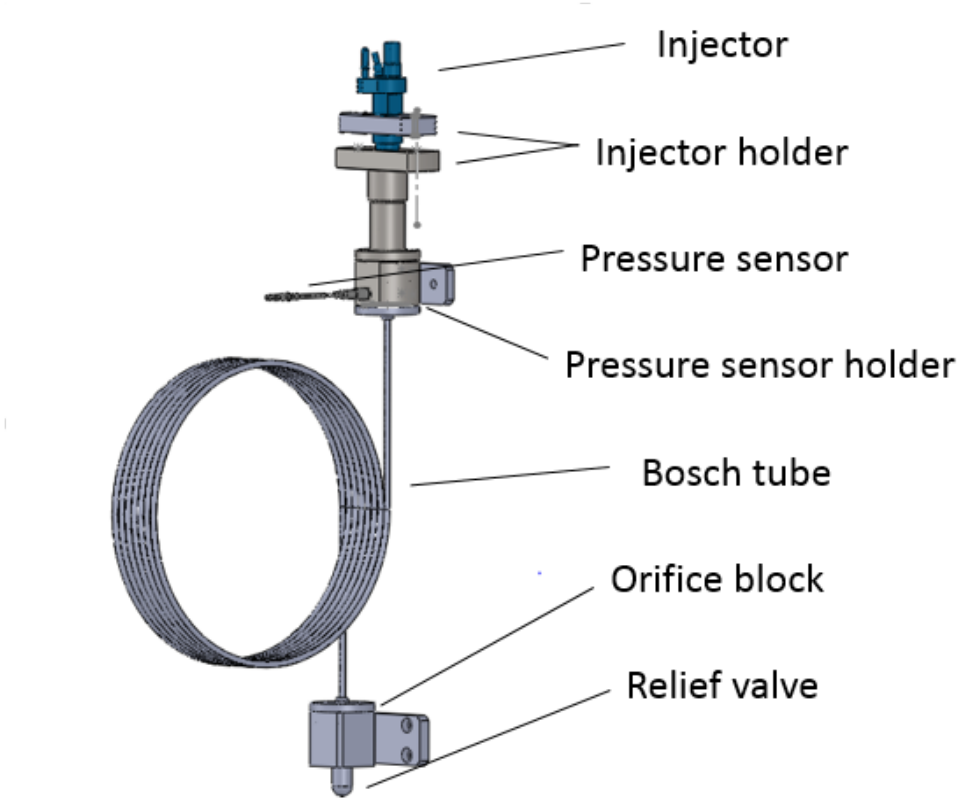

Fig. 2.19 Schematic of injection rate measuring device.

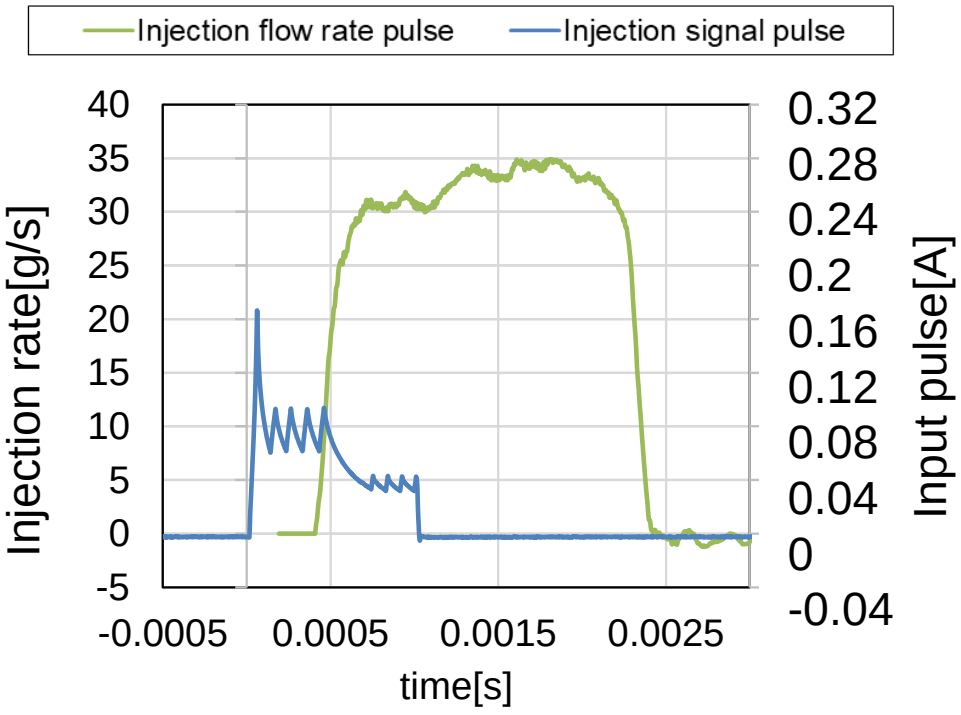

Fig. 2.20 Example of injection flow rate and signal pulse.

2.9 Spray Observation

2.9.1 Photography of Fuel Spray and Measurement of Spray Characteristics by Shadow Photography Technique

As for the deposit generated in the nozzle hole, there are few means to quantitatively evaluate the amount of deposit generated by visualizing the actual fuel injection system because the effect of the nozzle hole is very small. The amount of deposit generated in the nozzle hole affects the spray diffusion angle. In addition, deposits accumulated in the nozzle hole can change the shape of the nozzle hole and change the flow inside the nozzle hole as well. Along with this, there is a possibility that the injection of fuel spray may also be affected.

Therefore, in this study, the fuel spray of each nozzle before and after the test was visualized by the shadowgraph method, high-speed photography was performed, and various spray characteristic values were calculated from the obtained spray images and compared.

2.9.2 Principle of Shadow Photography Technique

The shadowgraph method is used for the optical observation method of the fuel spray. This is a method of photographing and observing light shadows caused by changes in the density of gas or liquid. The principle of the shadow graph method is explained by Fig. 2.21 [4]. Light from a point source S is bent as it passes through an observation gas of non-uniform density, creating an image on a screen P with varying luminosity. For simplicity, we assume that the density change is two-dimensional and does not change in the x direction perpendicular to the paper surface. For a gas whose refractive index n is n=1+Kρ, the angle of refraction of a ray r_A passing through point A is given by Eq. (2.9).

$$\varepsilon_y = \int_0^d \frac{K}{n}\frac{\partial \rho}{\partial y} dz \qquad (2.9)$$

Assuming that the density varies only in the y direction, the total refraction angle of r_A is given by Eq. (2.10).

$$\varepsilon_y = \frac{K}{n}\frac{d\rho}{dy} \qquad (2.10)$$

If the density gradient $d\rho/dy$ is constant in the y-direction, all light will be uniformly bent and the brightness I of the image on the screen will not change. Therefore, it turns out that the change in brightness ΔI is expressed by the change in the density gradient, and there is a relationship of Eq. (2.11).

$$\Delta I \propto \frac{d\varepsilon_y}{dy} \propto \frac{d^2\rho}{dy^2} \qquad (2.11)$$

In the general case where the density varies in both x and y directions, we have Eq. (2.12).

$$\Delta I \propto \frac{d^2\rho}{dx^2} + \frac{d^2\rho}{dy^2} \qquad (2.12)$$

From the above, the contrast on the screen obtained by the shadowgraph method is proportional to the second derivative of the gas density, that is, the change in the density gradient. In practice, light from a point light source is often converted into parallel rays using a lens or a concave mirror.

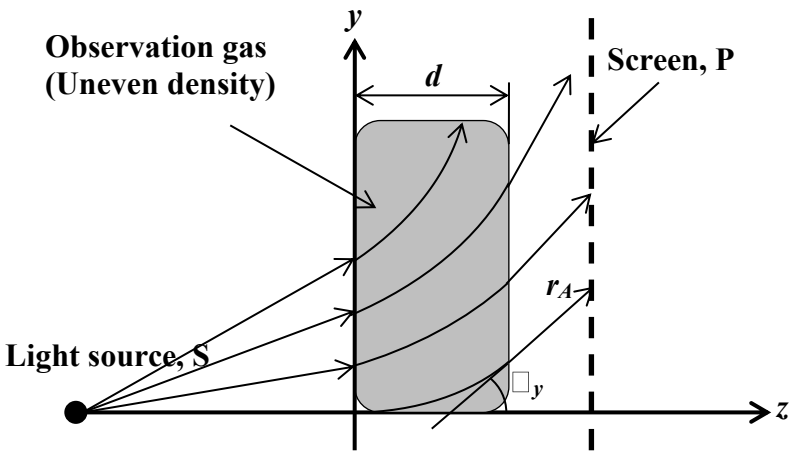

Fig.2.21 Shadow graph method [4].

2.9.3 Spray Observation Optical System

Fig. 2.22 shows the configuration of the optical system for the purpose of high-speed photographing of spray. CVC with a 100 mm in diameter quartz window was used to allow access to spray characteristics. The chamber is filled with nitrogen gas in advance to prevent the spray from igniting. In addition, by setting the pressure inside the CVC to 2.0 MPa and the ambient temperature at 25 ℃, it is possible to photograph the injection under the same atmospheric conditions every time. A photograph of the optically

accessible CVC is shown in Fig. 2.23. The 8-hole, 0.11 mm-diameter nozzle was equipped with a solenoid injector and installed in the chamber to inject the fuel. A high-speed video camera was employed to observe the spray characteristics. The resolution of the image was 464x464 pixels at 10,000 frames per second (fps). Then, a series of images were further analyzed by an image processing process to get the spray penetration, spray cone angle, and spray volume of each nozzle hole, which were then calculated to be the average values of each injector nozzle. The image processing method started with the binarization of the images at a threshold of intensity. In addition, since it is possible that the central axis of the spray fluctuates due to changes in the fuel flow due to deposit in the nozzle, the central axis of each spray was determined and its angle was also investigated. Spray penetration is defined as the distance from the nozzle tip to the tip of the spray image. The spray cone angle is defined as the angle of the spray at 50% of the spray penetration distance from the injector tip [5].

The injection signal was generated by a signal generator which was connected to the EDU directly. The fuel injection duration and pressure were set at 1,000 μs and 180 MPa, respectively. All experiments were conducted at room temperature. A led lamp was used as the light source for the fuel spray. Table 2.12 shows the specifications of the led lamp.

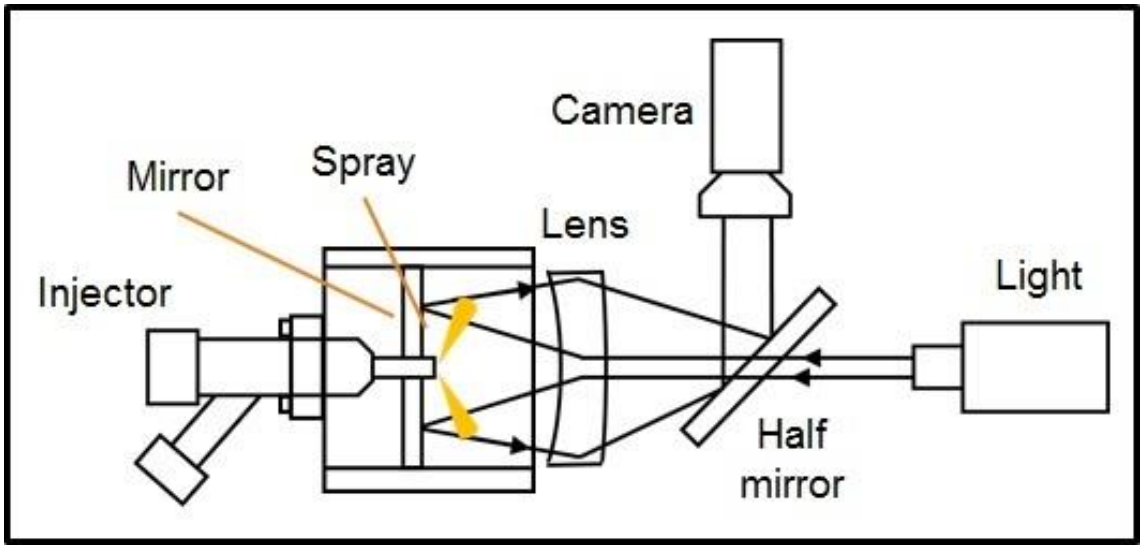

Fig. 2.22 Schematic of spray observation device.

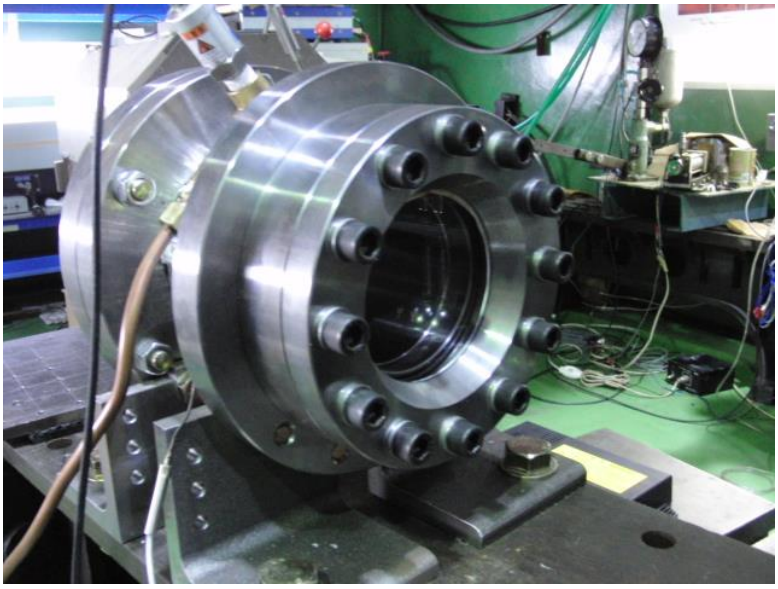

Fig. 2.23 CVC for spray observation.

Table 2.12 Specification of lamp

Light source	LED lamp
Rating of an electric current	100 A
Color temperature	5600 K
Average luminance	17,900 lx

2.9.4 Transmittance-Luminance Ratio Test

The spray in the photograph is identified by binarization using the transmittance as a threshold. Therefore, the relationship between the amount of light that entered the high-speed video camera and the actual transmittance was obtained by pre-testing. First, ND filters with different transmittances are attached to the observation window of the spray observation container, and the images are taken with a high-speed camera. As a result, it is possible to associate the rate of decrease in the amount of light due to transmission through the ND filter with the transmittance specific to each ND filter. The test results are shown in Fig 2.24. In this optical system, the light passes through the ND filter twice, and the vertical axis of this calibration curve is converted to the transmittance when it passes through the ND filter once. The linear equation shown in Fig. 2.24 was used to obtain the transmittance from the high-speed captured image.

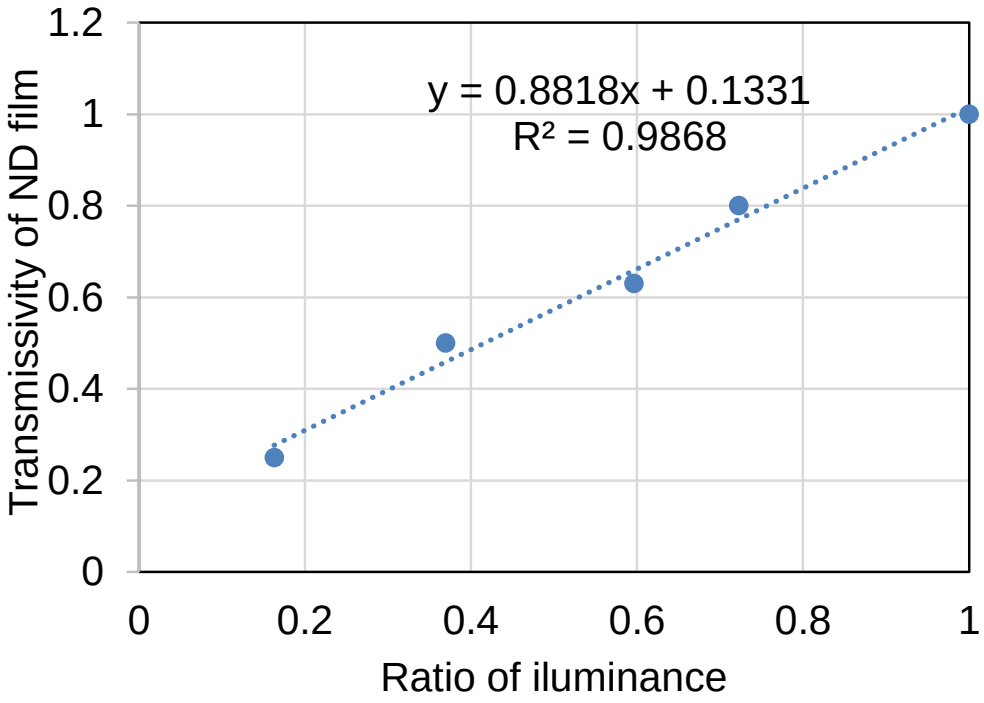

Fig. 2.24 Results of illuminance-transmissivity test.

2.9.5 Analysis of Spray Photographs

From the high-speed photograph of the fuel spray, the spray penetration, spray cone angle, and spray volume were measured. Fig. 2.25 shows an example of a photograph of the spray. First, the transmittance of the spray photograph was binarized to extract the spray. The spray area obtained by binarization is shown in Fig. 2.26. From this binarized image, the pixel position at the center of the nozzle is specified, then the spray penetration is measured from the edge of the nozzle to the tip of the spray, as shown in Fig. 2.27. The spray cone angle is calculated as the angle of the spray at 50% of the spray penetration distance from the injector tip on the clock-wise direction. For the spray volume calculation, the following equation (2.13) reported by Chen et al. [6] is used.

$$V = (\pi/3)^3 s^3 [\tan^3(\theta/2)] \quad \frac{1+2\tan(\theta/2)}{[1+2\tan(\theta/2)]^3} \qquad (2.13)$$

V: Spray volume [mm^3]

S: Spray tip reaching distance [mm]

θ: Spray angle [rad] at half the spray tip reaching distance

In addition, since the photograph of the spray is not taken from the side, it is necessary to consider the inclination of the spray. This correction is applied to the spray volume. In this study, spray image analysis program in MATLAB was created and used, that automatically performs these series of image processing calculations.

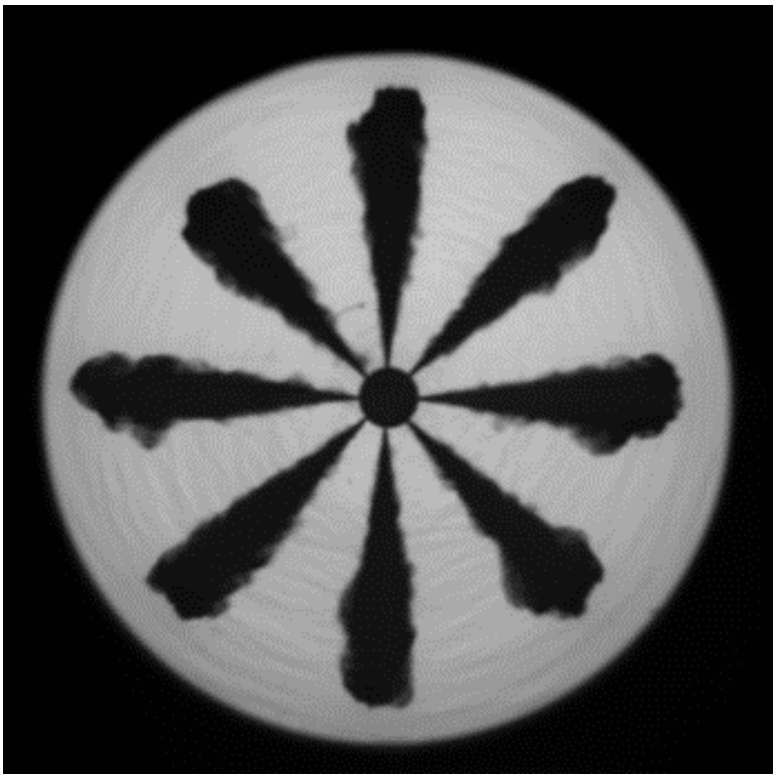

Fig. 2.25 Picture of spray photography captured by high-speed video camera.

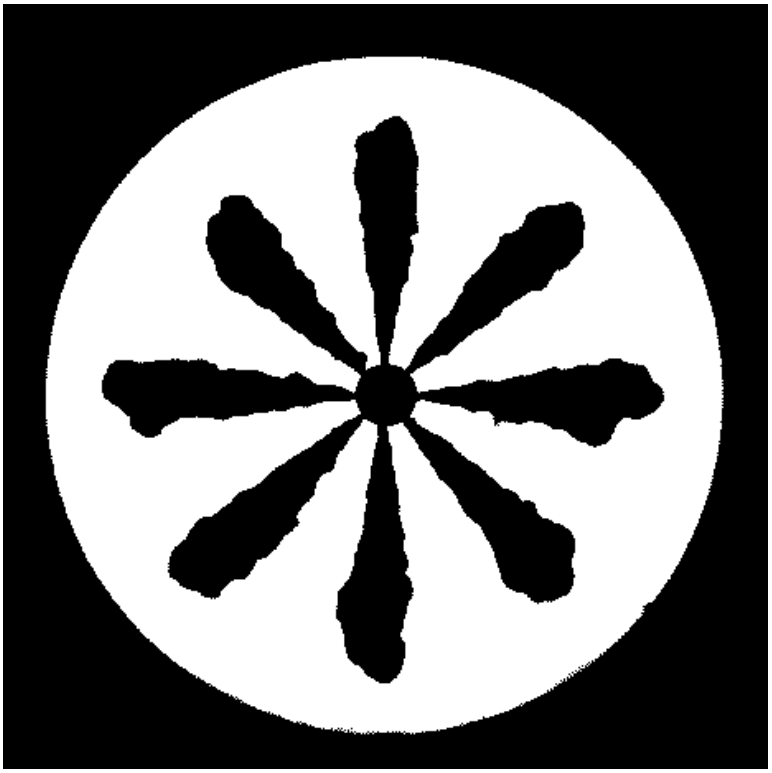

Fig. 2.26 Binarized image of spray.

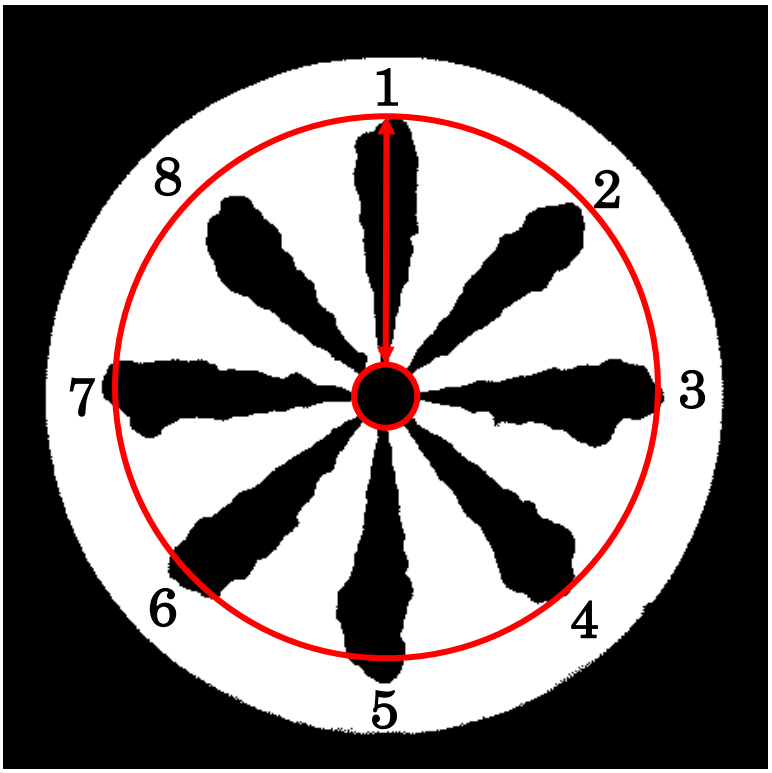

Fig. 2.27 Example of a circle on a spray image.

2.10 SEM Observation of DLC Nozzle Body Seat

The seats of unused nozzles, previously tested DLC nozzles, and non-DLC nozzles were observed by FE-SEM to compare the wear behavior of DLC nozzles and non-DLC nozzles. Fig. 2.28-2.30 depict the respective outcomes. Both tested nozzles had a seat temperature of 240 °C, and the DLC nozzle was tested for 100 hours and the non-DLC nozzle for 50 hours. Other terms are identical to those in Table 2.13.

Table 2.13 Test conditions for the DLC nozzle body seat observation

Fuel	Additives	HFRR
	Acid	400 μm
Injector model	G3S	
Nozzle	0.11 mm diameter x 8 holes	
Injection pressure	180 MPa	
Injection duration	480 μs	
Body seat temperature	240 °C	
Pump speed	1400 rpm	
Test time	50 and 100 hours	

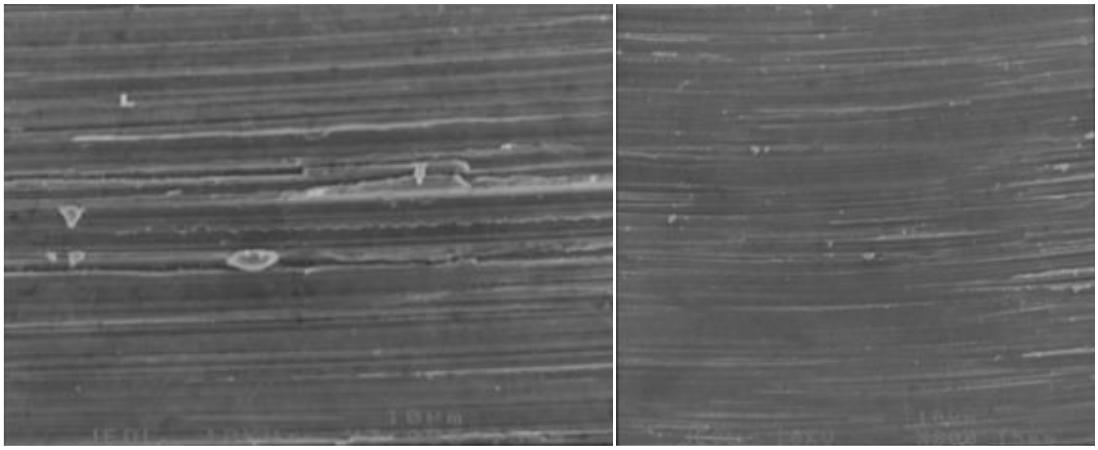

Fig.2.28 SEM images (800x and 3,000x) of non-used nozzle body seat.

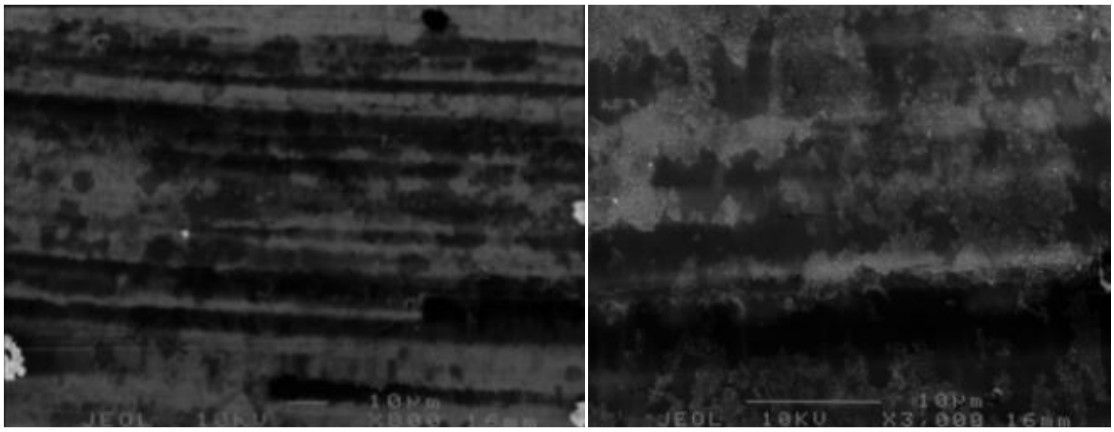

Fig. 2.29 SEM images (800x and 3,000x) of worn surface of body seat in DLC nozzle under 240 ℃ and Acid 400 μm (100 h).

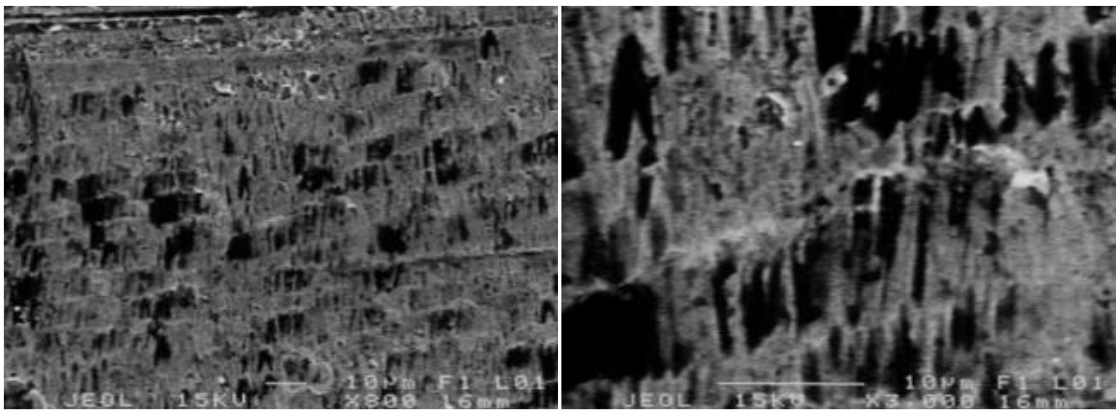

Fig. 2.30 SEM images (800x and 3,000x) of worn surface of body seat in non-DLC nozzle under 240 ℃ and Acid 400 μm (50 h).

The lines on the horizontal in Fig. 2.28 are machining traces made during nozzle fabrication. In Fig. 2.29, which depicts the DLC nozzle, lines that appear to be machining marks were also observed, however, the corrosive wear trace was disappear under the used of DLC nozzle. In Fig. 2.30, the corrosive wear trace and machined flaws were observed. This is presumed to be due to the DLC nozzle's suppression of corrosion wear.

2.11 Deposit Formation Observed by Test Machine

Using the test machine, the effect of zinc-based substances found in engine oil, etc., on the deposits that form inside the nozzle hole was investigated. In this experiment, zinc in engine oil was replicated by adding zinc neodecanoate to the fuel at 100 ppm. The test conditions are shown in Table 2.14.

Table 2.14 Test conditions of deposit formation observed by test machine.

Injection pressure	180 MPa
Injection pulse duration	480 μs
Pump speed	1,401 rpm
Fuel tank temperature	30 ℃
Purge gas	Argon
Test duration	10 hours
Nozzle tip temperature	350 ℃
Additive	Zinc 100 ppm

The evaluation was performed by comparing the injection rate peak values before and after the test. Fig. 2.31 shows the measurement results of the injection rate peak value before the test and 10 hours after the start of the test. Based on this result, it was determined that the injection rate of the nozzle after the 10-hour test decreased by approximately 13.6%, which is lower than the injection rate during the test with zinc-free fuel. It can imply that the simulation of the deposit formation inside the nozzle hole can be done by using test machine. The result from the experiment can confirm the reduction of injection rate which influenced by nozzle hole deposit formation.

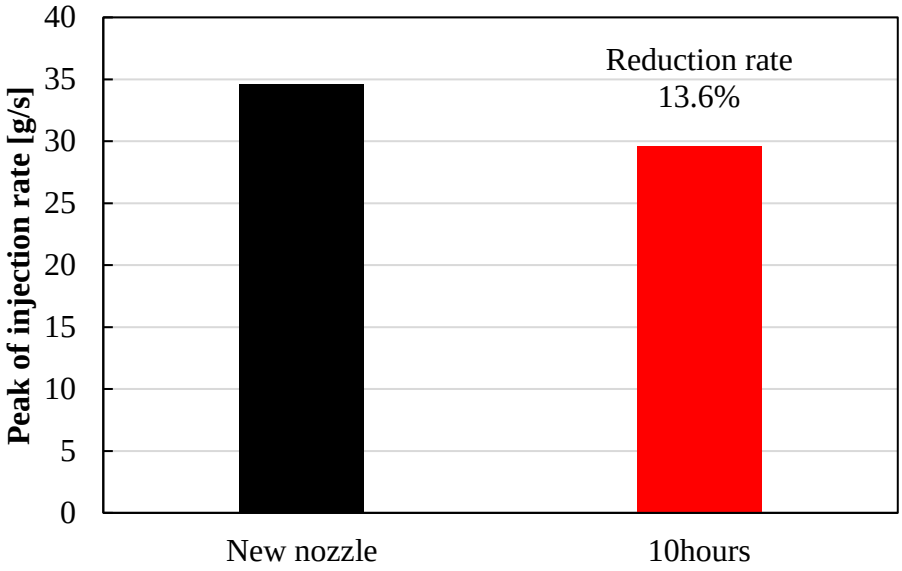

Fig. 2.31 Peak of injection rate (New and tested nozzles).

2.12 Summaries

Chapter 2 describes the specifications and performance of the injection tester used in this experiment. In the following, after summarizing the characteristics of the conventional research, we compare them with the characteristics of this experimental device.

2.12.1 Characteristics of Previous Research

As introduced by many researchers, there is a theory that deposit is formed by the condensation and polymerization of the fuel, and the formation mechanism is being elucidated by Rig tests using an actual engine and a heating plate to identify the formation factors. The test using the actual engine and the Rig test using a heating plate etc. each have advantages and disadvantages. The advantages and disadvantages of each are briefly summarized below.

[The test using the actual engine]

Advantage

As a use of the actual engine, it can faithfully reproduce the deposit that occurs in an actual field of use.

Disadvantage

It is not possible to distinguish whether the components of the deposits accumulated at various locations in the injection hole are products produced by combustion or deposits produced by heating the fuel. Also, it is difficult to control the temperature of the nozzle hole, which greatly affects the amount of deposits.

[Rig test using a heating plate, etc.]

Advantage

As combustion products are not generated, it is easy to clarify the generation mechanism of the generated substances. Furthermore, the parameters such as temperature, injection pressure and duration, and time between injection can be controlled independently, regardless to the load and speed.

Disadvantage

It is difficult to prove that the substances generated in the actual engine can be simulated because the generation conditions are different from those of the actual engine.

As described above, the actual engine and the Rig test each have advantages and disadvantages, and it is necessary to take advantage of each advantage to clarify the deposit formation mechanism.

2.12.2 Features of Experimental Equipment Used in This Study

Since the fuel injection test machine used in this study uses an actual injection system, unlike the conventional Rig test that uses a heating plate, etc., it is possible to simulate the formation of deformation and deposits in the nozzle as close to the actual engine. In addition, since it is possible to control the temperature, which is difficult to test with an actual engine, it is possible to predict the deposit formation mechanism in more detail.

2.13 Conclusions

A testing device was developed based on the injection system of a six-cylinder engine. To investigate the effect of temperature on body seat deformation and deposit formation, the body seat temperature was heated using electric heaters around the nozzle. The fuel temperature in the fuel tank was controlled, whereas the injection pressure and duration were set to 180 MPa and 480 μs, respectively. The revolutions of the pump were varied. Argon gas was purged in the chamber to prevent ignition and degradation of the fuels. The surface roughness measurement, imaging techniques and injection rate measurement used to investigate deformation, and injection characteristics and spray behavior were given. For spray imaging, the shadowgraph imaging technique was used. In classical shadowgraph, a shadowgraph of diesel sprays under non-vaporization shows the shadows of liquid phase. Advantage of using this technique is only using a single high-speed camera, spray characteristics of the liquid phase data such as spray penetration and spray cone angles can be detected. In addition, processing of spray photo was described in order to achieve appropriate processed photograph. In diesel fuel injection rate, the effects of nozzle hole deposit could be studied. The use of the test machine can simulate the deformation of the nozzle body seat as same as in the actual engine. DLC

coating on the nozzle needle can suppress the wear on the nozzle body seat. The test performed using test machine can generate the formation of deposit inside nozzle hole, caused the reduction of maximum flow rate. The main parameters can be controlled independently by the design experimental apparatus. Unlike the actual engine, the test bench allows the study to vary the operating conditions separately. The experiment could run at the most severe conditions in order to accelerate the deformation and reproduce the deposit formation inside the nozzle hole.

Bibliography

[1] D'Ambrosio, S., and Ferrari, A. (April 12, 2012). "Diesel Injector Coking: Optical-Chemical Analysis of Deposits and Influence on Injected Flow-Rate, Fuel Spray and Engine Performance," ASME. J. Eng. Gas Turbines Power. June 2012; 134(6): 062801. https://doi.org/10.1115/1.4005991.

[2] Bosch, W., "The Fuel Rate Indicator: A New Measuring Instrument for Display of the Characteristics of Individual Injection," SAE Technical Paper 660749, 1966, doi:10.4271/660749.

[3] Dernotte, J., Hespel, C., Foucher, F., Houillé, S., and Rousselle, C.M., "Influence of Fuel Properties on the Diesel Injection Process in Non-Vaporizing Conditions," Atomization and Spray 22(6): 461-492, 2012, doi: 10.1615/AtomizSpr.2012004401.

[4] Merzkirch, W. (1987). Flow Visualization. 2nd edn. Academic Press. Massachusetts.

[5] Xu, Q., Xu, M., Hung, D., Wu, S. et al., "Diesel Spray Characterization at Ultra-High Injection Pressure of DENSO 250 MPa Common Rail Fuel Injection System," SAE Technical Paper 2017-01-0821, 2017, https://doi.org/10.4271/2017-01-0821.

[6] Chen Pin Chia，Wang Weicheng，Roberts William L "Spray and atomization of diesel fuel and its alternatives from a single-hole injector using a common rail fuel injection system" ISSN: 0016-2361, Vol: 103, Page: 850-861.

CHAPTER 3
DEFORMATION ON NOZZLE BODY SEAT

3.1 Introduction

In recent years, the use of fossil fuels as a transportation fuel has been a topic of concern. According to reports by the International Energy Agency [1], global energy demand increased continuously over the last decade. The projection of energy demand until year 2030 shows that oil consumption will increase significantly, particularly in the transportation field, at a growth rate of approximately 1.7% annually. Furthermore, in terms of environmental issues, emissions from vehicles or the transportation sector will increase for the same amount of fossil fuel usage. Although excellent combustion technology can provide complete combustion, greenhouse gas and carbon dioxide emissions cannot be reduced when utilizing fossil fuel. Therefore, an energy-saving method that can be used for a significant amount of time must be developed. In Japan, it was reported that 94.9% of the carbon dioxide emitted from energy sources caused global warming. Emission from the transportation sector, such as automobiles and ships, constituted approximately 17.9% of the total emission [2].

Among internal combustion engines (ICEs), diesel engines have been reported to demonstrate the highest thermal efficiency, approximately 40% for commercial engines and up to 45% thermal efficiency for research engines, when compared with other ICEs [3-4]. Therefore, increasing the use of diesel engines can increase the efficiency of liquid fossil fuels. To improve the performance and efficiency of diesel engines, researchers have considered fuel injection systems, high-pressure fuel injection, multi-stage fuel injection, nozzle geometry optimization, and the reformation and reduction of sulfur content in fuel components [5-7]. However, the wear characteristics of the injection system parts are exacerbated by these developments [8-12]. Hence, the wear of the nozzle body seat is accelerated [13-14]. Additionally, the use of high temperatures and fuel additives promotes the production of deposits in diesel fuel injector nozzles [15]. Therefore, regulations pertaining to the restriction of emissions are enhanced appropriately to accommodate the current situation.

It was discovered that the change in injection conditions would not only promote wear, but also affect the deformation of the injector. This is particularly true for the injector nozzle [16-17]. Fuel injection is controlled by opening and closing the needle valve, where the wear and deformation of the nozzle body seat is caused by the collision and the impact of the needle on the body seat of the nozzle, as shown in Fig 1.1. When the nozzle shape is changed, it can affect not only the internal nozzle fuel flow and the fuel spray behaviors, but also the injection characteristics as the change of the internal flow passage, thereby resulting in both combustion and emission characteristics [18-22].

Recently, to reduce the wear of body seats, diamond-like carbon (DLC) nozzles have been widely used to protect body seats that are softer than needles at high temperatures [23]. DLC on a needle can reduce wear on the body seat owing to its smooth surface, low friction coefficient, and low opponent aggression [24-26].

However, deformation still occurs because of the higher hardness of the DLC needle compared with that of the body seat [27]. This results in a change in the internal shape of the injector nozzle, which effects the injection characteristics [28-29].

In this study, the effects of body seat temperature, test duration, and heat treatment of the nozzle on the change in the surface profile of the nozzle body seat, which is due to deformation, was investigated using an injector testing device that was constructed based on a commercial common-rail injection system.

3.2 Effect of Temperature on Body Seat Deformation

This chapter focuses on the impact of temperature on the deformation of the body seat. In the deformation of the injector nozzle which has been carried out so far, there were insufficient data of the amount of deformation due to the limitation of the increment of the body seat temperature. Therefore, the effect of high temperature of the body seat was investigated using a modified heating device. The tested nozzles were measured the depth at the most regressed point and the height of upheaval at the long test duration. By using the improved heating devices which solve the instability problem under the heating situation, it is expected to be able to perform the deformation test machine at the high temperature as same as an actual engine under the high load condition.

3.2.1 Methodology and Results

In order to investigate the effect of high temperature on deformation of the body seat, the test duration was set as 20 hours. The test conditions are shown in Table 3.1. The body seat temperature was set at 300 and 400°C by PID controller system with 150 V of SSR input voltage to supply the power to 8 electric heaters around the nozzle. G3S (3^{rd} Generation of Solenoid) injectors with 0.11 mm diameter of 8 holes were operated at the desired injection pressure and duration as 180 MPa and 480 μs, respectively. The pump speed was set as 1400 rpm to control the injection time with the ratio of 2:1 resulted in 700 times of injection per minute. The fuel temperature was controlled at 60°C and circulated back to the fuel tank after cooling to refrain fuel consumption. Argon gas was purged into the injection chamber with the same heat transfer rate to prevent ignition and degradation of fuels. After finish the test of 300 and 400°C, the injectors were dismantled and the nozzles were cut in order to observe the surface morphology of the body seat, as described in chapter 2. The list of the test nozzle is shown in Table 3.2.

Table 3.1 Test conditions for effect of temperature.

Fuel	Additives	HFRR
	Acid	400 μm
Injector model	G3S	
Nozzle	0.11 mm diameter x 8 holes	
Nozzle seat temperature	300 and 400°C	
Injection pressure	180 MPa	
Injection duration	480 μs	
Pump speed	1400 rpm	
Purge gas	Argon	
Test duration	20 hours	

Table 3.2 List of test injectors.

Injector No.	Body seat temperature
No. 1	300°C
No. 2	400°C

The results of measuring the nozzle body seat surface morphology by Nano Search Microscope after the test are shown in this section. The average values obtained from the measurement are summarized and shown in Table 3.3 and 3.4 as depth at the most regressed point and deformation, respectively. Since the roughness of body seat surface measured by SPM at an initial is not completely flat (roughness value = 0), roughness values of the surface area above body seat are used to be the reference level of the surface of body seat at the initial in order to examine and calculate the depth at the most regressed point and amount of deformation. δZ_1 denotes the depth of regression on the body seat. The depth at the most regressed point is calculated by the distance between the lowest point of the body seat surface and the reference level. As the body seat approached the nozzle tip, however, plastic deformation occurred. Due to the movement of the needle, the needle surface made contact with the body seat, and the body seat was plastically deformed. As the needle approached the nozzle tip, the body seat rose in contrast to the situation preceding the test. $\delta Z2$ denotes the deformation or height of the

upheaval on the body seat because the ascending height was 900 m away from the location where the most regressed depth was observed, towards the nozzle tip direction together with the depth at the most regressed point value. The results of depth at the most regressed point and deformation are shown in Fig. 3.1 and 3.2, respectively.

Table 3.3 Results of depth at the most regressed point measurement.

Injector No.	Depth at the most regressed point [μm]
No. 1	4.41
No. 2	4.43

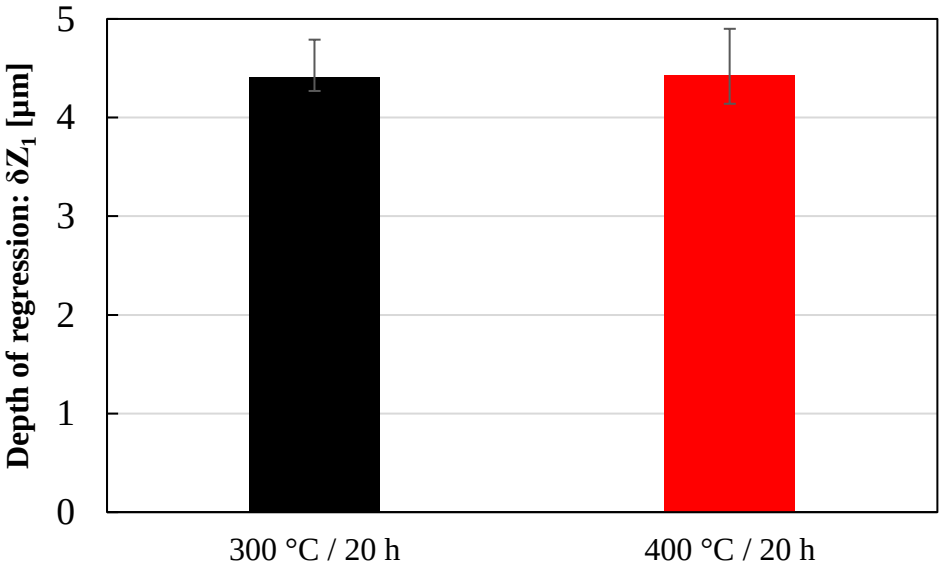

Fig. 3.1 Effect of temperature on depth of regression at nozzle seat.

Table 3.4 Results of deformation measurement.

Injector No.	Deformation [μm]
No. 1	7.02
No. 2	8.24

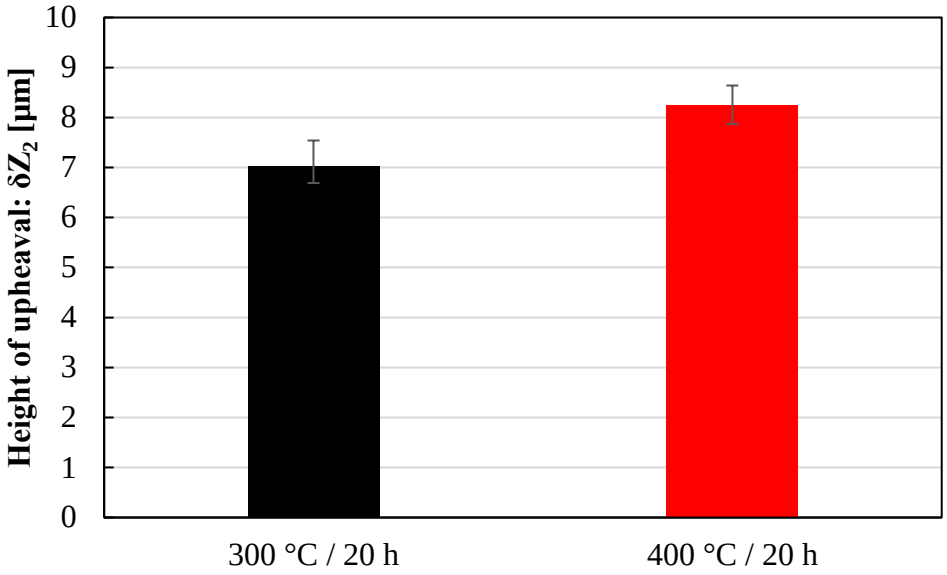

Fig. 3.2 Effect of temperature on deformation at nozzle seat.

Fig. 3.1 shows the results from of depth at the most regressed point from the measurement with the comparison of low temperature and high temperature, 300 and 400°C, respectively. It can be seen that the depth at the most regressed point increases. However, the rate of increment due to the increased temperature is decreases. At 300°C, the depth at the most regressed point increases rapidly to 4.41 µm while it is 4.43 µm at 400°C. This can be considered as the deformation has been settled.

In case of deformation, the results from Fig. 3.2 show that the increment of deformation corresponds to the temperature of body seat. The amount of deformation at 300 and 400°C are 7.02 and 8.24 µm, respectively. This could be explained as the higher temperature strongly effects to the change of body seat hardness more than lower temperature. In addition, the higher temperature allows more dislocation to be released compare with lower temperature.

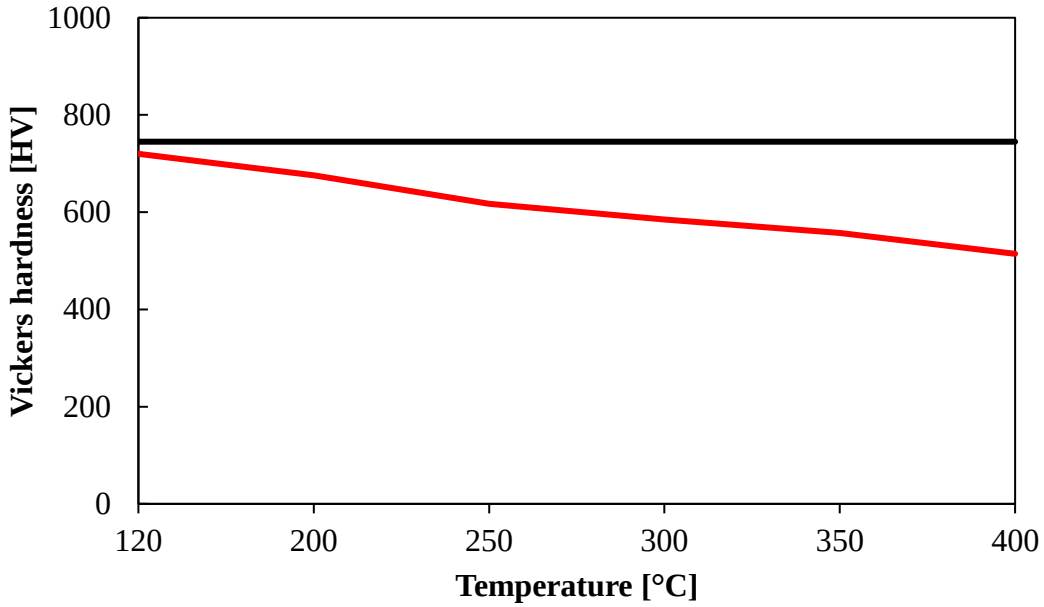

Fig. 3.3 Relationship between hardness and temperature of nozzle body seat and needle.

Fig. 3.3 explains the effect of temperature on the hardness of the nozzle material. The increase in temperature allows more dislocation in the metallographic structure of the material to be released compared with the lower temperature, as clearly indicated by the body seat hardness. By contrast, the hardness of the needle did not change in this temperature range because of the heat treatment process of the needle, i.e., carburization.

3.3 Effect of Test Duration on Body Seat Deformation

The results from section 3.1 show that the higher body seat temperature has a greater effect on the depth at the most regressed point and the deformation of the body seat. Thus, to understand more clearly the deformation mechanism, this section is designed to focus on the impact of test duration on the deformation of the body seat, which has been carried out so far. Therefore, the effect of test duration at high temperatures on the body seat was investigated using a modified heating device. The tested nozzles were measured for depth at the most regressed point and the amount of deformation as the test duration elapsed.

3.3.1 Methodology and Results

In order to investigate the effect of test duration on deformation of the body seat, the set of test duration were set as 10 and 20 hours. The test conditions are shown in Table 3.5. The body seat temperature was set at 400°C by PID controller system with 150 V of SSR input voltage to supply the power to 8 electric heaters around the nozzle. G3S (3^{rd} Generation of Solenoid) injectors with 0.11 mm diameter of 8 holes were operated at the desired injection pressure and duration as 180 MPa and 480 μs, respectively. The pump speed was set as 1400 rpm to control the injection time with the ratio of 2:1 resulted in 700 times of injection per minute. The fuel temperature was controlled at 60°C and circulated back to the fuel tank after cooling to refrain fuel consumption. Argon gas was purged into the injection chamber with the same heat transfer rate to prevent ignition and degradation of fuels. After finish the test at 10 and 20 hours, the injectors were dismantled and the nozzles were cut in order to observe the surface morphology of the body seat, as described in chapter 2. The list of the test nozzle is shown in Table 3.6.

Table 3.5 Test conditions for effect of test duration.

Fuel	Additives	HFRR
	Acid	400 μm
Injector model	G3S	
Nozzle	0.11 mm diameter x 8 holes	
Nozzle seat temperature	400°C	
Injection pressure	180 MPa	
Injection duration	480 μs	
Pump speed	1400 rpm	
Purge gas	Argon	
Test duration	10 and 20 hours	

Table 3.6 List of test injectors.

Injector No.	Test duration
No. 1	10 hours
No. 2	20 hours

The results of measuring the nozzle body seat surface morphology by Nano Search Microscope after the test are shown in this section. The average values obtained from the measurement are summarized and shown in Table 3.7 and 3.8 as depth at the most regressed point and deformation, respectively. Since the roughness of body seat surface measured by SPM at an initial is not completely flat (roughness value = 0), roughness values of the surface area above body seat are used to be the reference level of the surface of body seat at the initial in order to examine and calculate the depth at the most regressed point and amount of deformation. The depth at the most regressed point is calculated by the distance between the lowest point of the body seat surface and the reference level. On the other hand, the amount of deformation is defined as the distance in vertical direction of the point at the distance of 900 μm away from the depth at the most regressed point towards the nozzle tip direction together with the depth at the most regressed point value. The results of depth at the most regressed point and deformation are shown in Fig 3.4 and 3.5, respectively.

Table 3.7 Results of depth at the most regressed point measurement.

Injector No.	Depth at the most regressed point [μm]
No. 1	3.80
No. 2	4.43

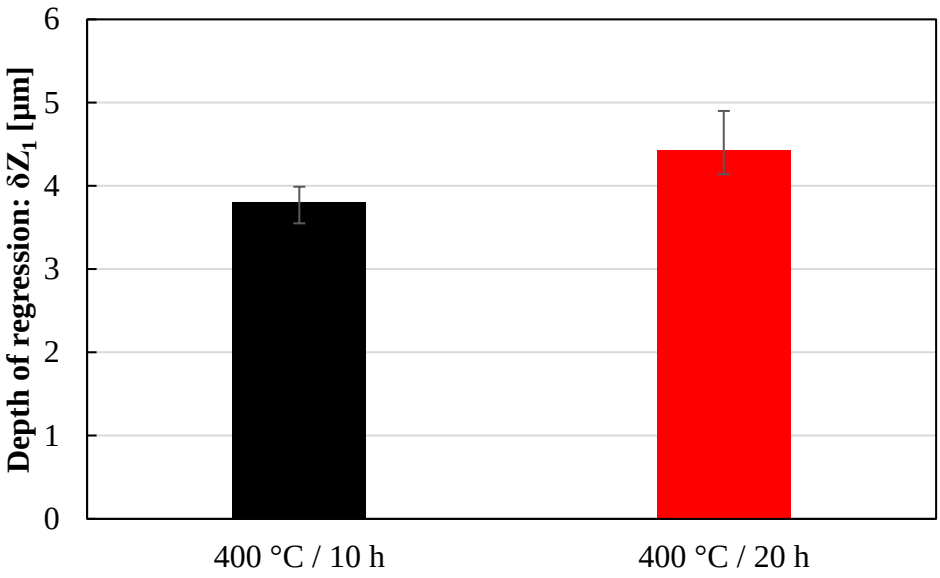

Fig 3.4 Effect of test duration on depth of regression at nozzle seat.

Table 3.8 Results of deformation measurement.

Injector No.	Deformation [μm]
No. 1	8.03
No. 2	8.24

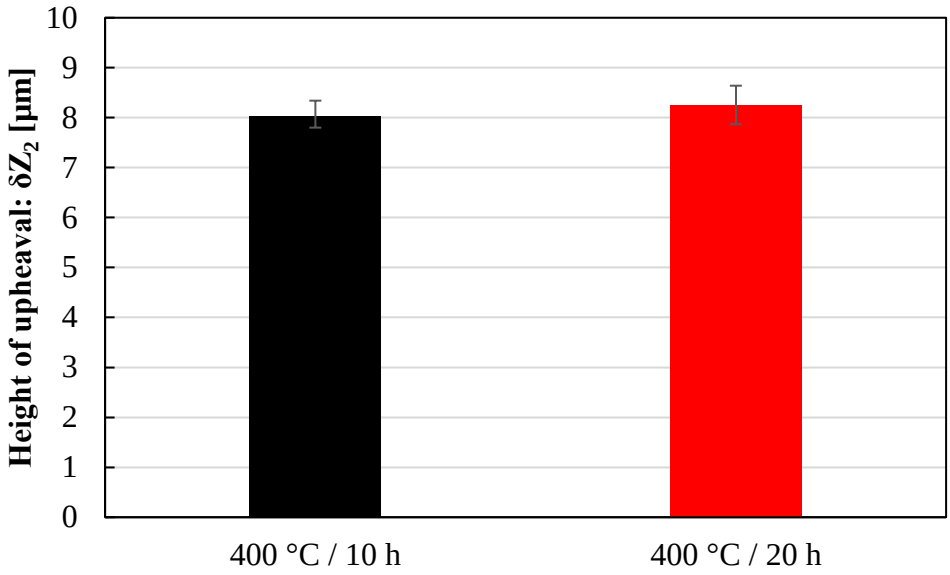

Fig 3.5 Effect of test duration on deformation at nozzle seat.

The results from Fig. 3.4 show the comparison of depth at the most regressed point at 400°C between 10 and 20 h. conditions. The longer test duration results in the larger of depth at the most regressed point. The depth at the most regressed point is 3.80 and 4.43 μm at 10 and 20 h., respectively.

The deformation at 10 h. is 8.03 μm while it is 8.24 μm at 20 h. The increment rate of deformation at the early period from 0 to 10 h. is greater than that of 10 to 20 h., as shown in Fig. 3.5. This could be explained as the adhesion effect and plastic deformation increase with decreasing hardness and shear strength of the body seat due to temperature rise.

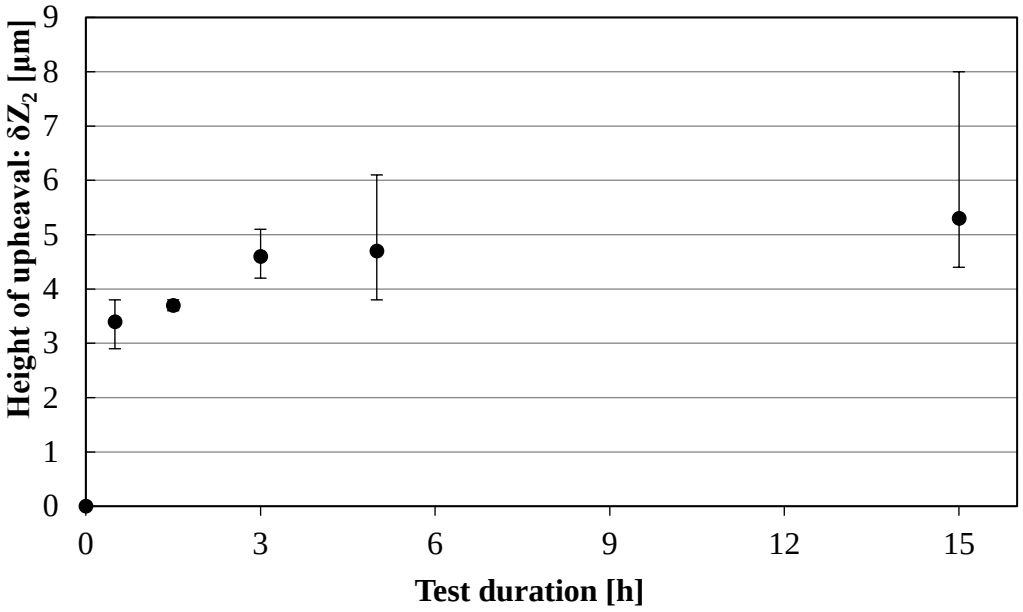

Fig. 3.6 Effect of test duration on deformation of nozzle body seat under 300°C test condition.

To understand the deformation mechanism more clearly, the effect of test time at a constant temperature of the body seat was investigated. The temporal change in the height of the upheaval of the nozzle body seat, which corresponds to the amount of deformation, was measured under 300°C test condition.

Fig. 3.6 shows the effect of the test duration on the height of the upheaval of the nozzle body seat (amount of deformation). The deformations from 0.5, 1.5, 3, and 5 h tests compared with those from the 15 h test were 64.2%, 69.8%, 86.8%, and 88.7%, respectively. The deformation increased rapidly at the early stage of the test, which was assumed to reflect the elimination of dislocations in the metallographic structure. The results suggest that the short-period test should be investigated further to clarify the deformation mechanism on the body seat in the nozzle of a diesel fuel injector.

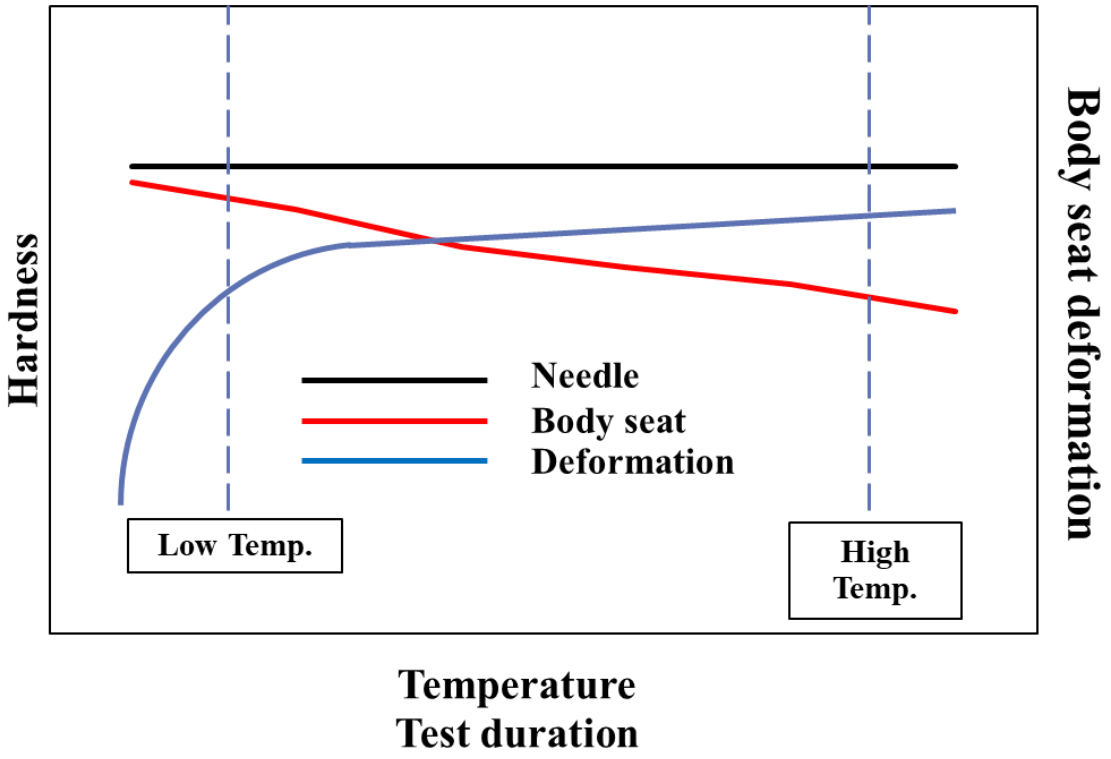

Fig 3.7 Relations of hardness with temperature and deformation with time.

Fig. 3.7 shows the relations of needle hardness constant and higher than that of body seat due to DLC coating process. The mechanism of deformation from the results in chapter 3 could be explained as the higher temperature strongly effects to the change of body seat hardness more than lower temperature. The increment of temperature allows more dislocation to be released compare with lower temperature, it is clearly seen in body seat hardness. On the other hand, the hardness of the needle is constant with the increasing temperature due to the heat treatment process of the needle.

The results in this study can be explained by following mechanism. As the increasing time, deformation is increased with the high rate at the early period. A like creep phenomena, deformation rapidly increases in the first stage due to the external force, stress from opening and closing of the needle, impact between nozzle and needle. Next stage, the deformation of body seat moves slowly and reaches a minimum rate as the dislocation movements and dislocation generation within the crystal structure of the material are almost equal.

3.4 Effect of Temperature Increase Duration on Body Seat Deformation

As mentioned in the previous section, the amount of deformation increased rapidly in the early stage within 5 h after the start of the test. Hence, the rate of temperature increases significantly affected the deformation of the body seat. Several findings have been obtained regarding the large deformation that occurs during microstructural change. and Nishihara et al. [33] reported that deformation decreases with increasing heating rate. It is said that this is because the progression of microstructural changes is suppressed with respect to an increase in the temperature rise rate of the material. However, it is not clear whether deformation is affected when the temperature is maintained for a certain period of time after heating, as is the case with the heat received by the nozzles treated in this study. Therefore, in this investigation, we compared the amount of deformation of nozzles that were tested at a constant temperature for a certain period of time after heating at different heating rates, and investigated how much the heating period affected the overall amount of deformation. investigate.

3.4.1 Methodology and Results

Tables 3.9 and 3.10 show the test conditions and nozzle heating conditions. The seat temperature immediately after the start of the test was 200°C (tempering temperature), the maximum body seat temperature was 300°C, and there were three patterns of temperature rise from 200 °C to 300 °C. Fig. 4.2 to 4.4 show the time course of the surface temperature outside the nozzle during heating. The fuel injection pressure, injection period, and pump rotation speed were constant during the test.

Table 3.9 Test conditions.

Fuel	Additives	HFRR
	Acid	400 μm
Nozzle	0.11 mm diameter × 8holes	
Nozzle seat temperature	300 ℃	
Nozzle surface temperature	346℃	
Input voltage of SSR	110V	
Fuel tank temperature	30℃	
Injection pressure	180 MPa	
Injection pulse duration	480 μm	
Pump speed	1400 rpm	
Purge gas	Argon gas	
Total test duration	5 min+3 h, 1 h+3 h, 2 h+3 h	
Temperature rising duration	Fastest (5min), 1 h and 2 h	
Constant temperature duration	3 h	

Table 3.10 Tested injector and heating pattern.

Injector No.	Elapsed time				
	200 ℃	225 ℃	250 ℃	275 ℃	300 ℃
No. 1					5 min
No. 2					
No. 3	0 min	15 min	30 min	45 min	1 h
No. 4					
No. 5	0 min	30 min	1 h	1.5 h	2 h
No. 6					

Table 3.11 summarizes the amount of surface deformation obtained above. Since the displacement of the surface shape before the test may not be 0, the following results were analyzed by subtracting the displacement in the initial state from the measurement results. Based on the surface shape data above, the amount of deformation was obtained by comparing the displacement from the most recessed part to the part raised at the tip of

the nozzle with the surface shape before the test, and calculating the difference in displacement. Fig. 4.5 shows the amount of deformation after the test for each heating pattern. The bar graph shown here is flat.

Table 3.11 Amount of deformation in heating rate change test.

Injector No.	Temperature rising duration	Deformation [μm]
No. 1	Fastest (5min)	3.3
No. 2		4.7
No. 3	1 h	4.1
No. 4		3.9
No. 5	2 h	4.9
No. 6		4.8

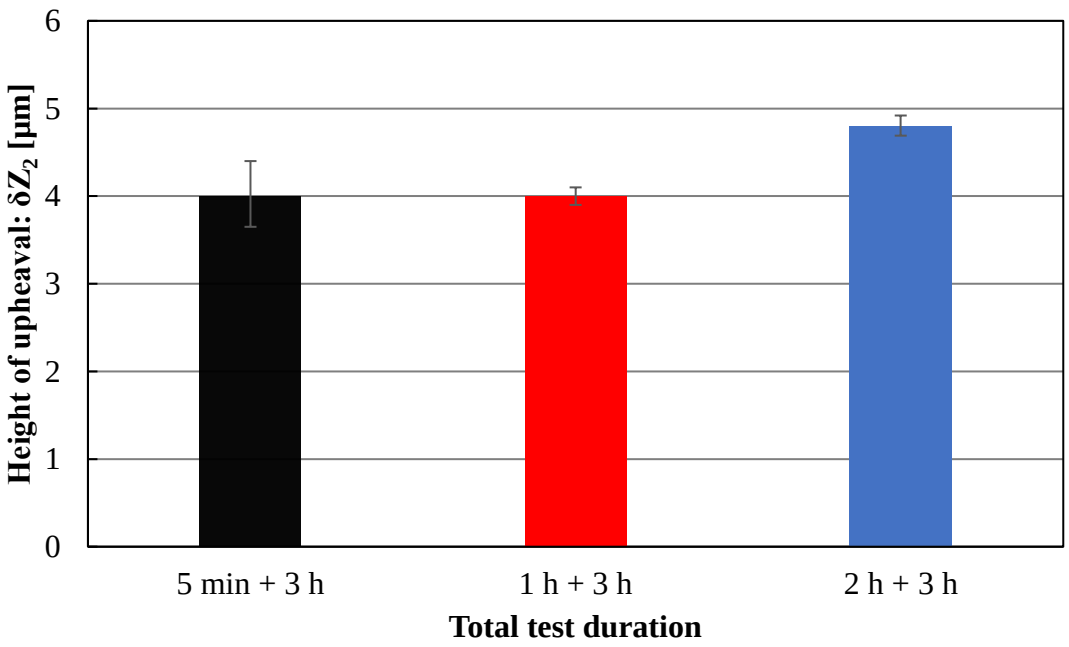

Fig. 3. 8 Effect of temperature increase duration on deformation of nozzle body seat.

As shown in Fig. 3.8, the amount of deformation (δZ_2) did not change significantly when comparing the case involving the fastest temperature increase duration of 5 min and the slowest temperature increase duration of 2 h, and the amount of deformation increased slightly. In addition, compared with the temperature increase duration of 1 h, the same

amount of deformation was obtained. As such, it can be inferred that the dislocation was finally eliminated 3 h into the constant temperature period, which was much longer than the temperature increase period.

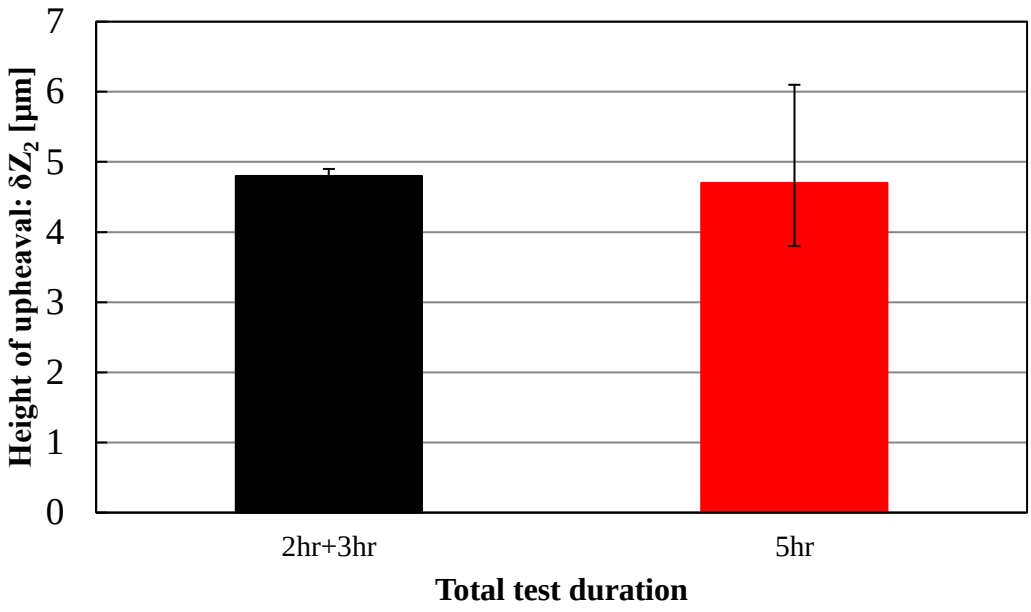

Fig. 3.9 Comparison of deformation between 2-hour heating (2h+3h) and short-term test (5h).

In Fig. 3.9, it can be seen that when the temperature is raised for 2 hours, the deformation amount is almost the same as when the test was performed at 300°C for 5 hours, even though the seat was exposed to 300°C for 3 hours. This is because the time required to reach a stable dislocation density at 300°C is shorter than the constant temperature period of 3 hours set in this study, and the number of dissolved dislocations is the same under each condition, as mentioned above. It is thought that there was no difference in the amount of deformation even if the temperature increased for 2 hours out of 5 hours because the temperature increased to the normal state.

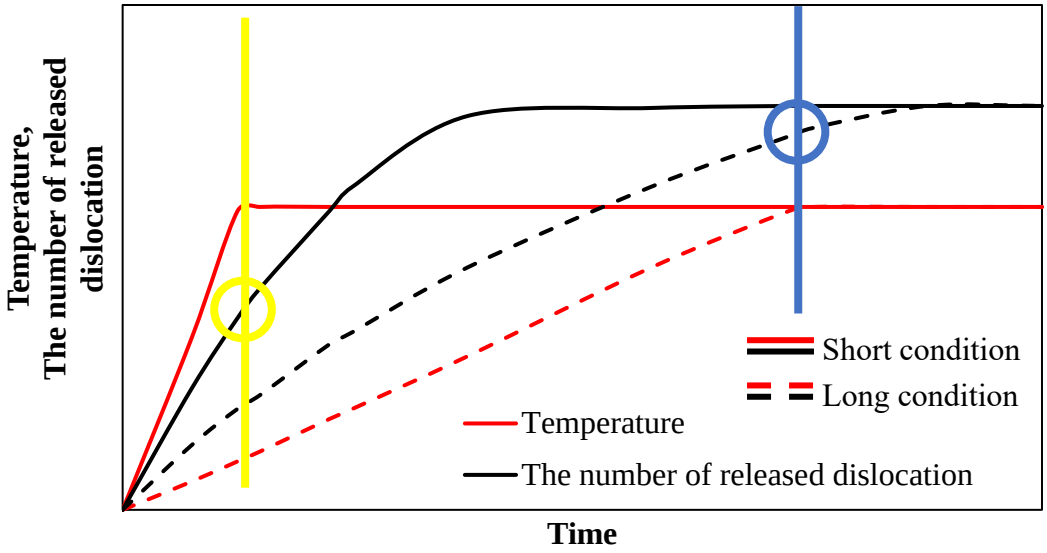

Fig. 3. 10 Relationship between number of released dislocations with temperature and time.

Fig. 3. 10 shows the relationship between the number of released dislocations with temperature and time based on the test results. The solid and dashed lines represent cases involving the short and long temperature increase durations, respectively. For the latter case, the number of released dislocations was limited at the end point of the temperature increase (marked as a blue circle), which was achieved at the desired temperature (marked as a blue vertical line). Compared with the short temperature increase duration, the long duration allows more dislocations to be released. The more released the dislocation, the softer and the easier is the deformation of the body seat. These results of this study are consistent with those of Nishihara [33]. When different heating rates were applied to the materials, it was discovered that the temperature increased to 600 °C for the non-tempered steel, followed by cooling; this can be described as a fast-heating condition. The faster the cycle, the less was the amount of deformation. This is because the progress of the microstructural change during the heating period was suppressed with the increase in the heating rate of the material.

3.5 Effect of Tempering Temperature on Nozzle Surface Hardness

When the structure of a metal changes, its mechanical properties change accordingly. In this study, the effect of structural change due to the tempering temperature on the surface hardness was investigated.

3.5.1 Methodology and Results

The tempering duration for all nozzles in this test was 20 hours at 200 °C, 250 °C, 300 °C, 350 °C, and 400 °C. Because the nozzle material was chromium–molybdenum steel that has been quenched and carburized, the surface layer was treated such that it was harder compared with the center. Therefore, the hardness of the nozzle body seat was measured both at the surface layer and at the center of the nozzle cross-section surface, 2 mm away from the surface. The measurement positions are shown in Fig. 3.11. The hardness of each sample was measured at five or more points in the surface layer and in the center, and the average and standard deviation were calculated. The results of the hardness measurement at surface and center of the nozzle body seats are shown in Table 3.12 and 3.13, respectively.

In the Vickers hardness test, a rigid body (indenter) made of diamond is pushed into the test object, and the hardness is judged by the area of the depression (indentation) that is formed at that time. The indenter is in the shape of a regular quadrangular pyramid with a facing angle of α=136, and the indentation is ideally a regular quadrangle. Fig. 3.12 shows the measured hardness of the sample. The Vickers hardness [HV] is obtained by dividing the test force F [kgf] by the calculated surface area S [mm^2]. In addition, the calculation formula when using the diagonal length d of the indentation is expressed by the following formula.

$$HV = \frac{F\ [kgf]}{S\ [mm^2]} = 1.8544\frac{F\ [kgf]}{d^2\ [mm^2]}$$

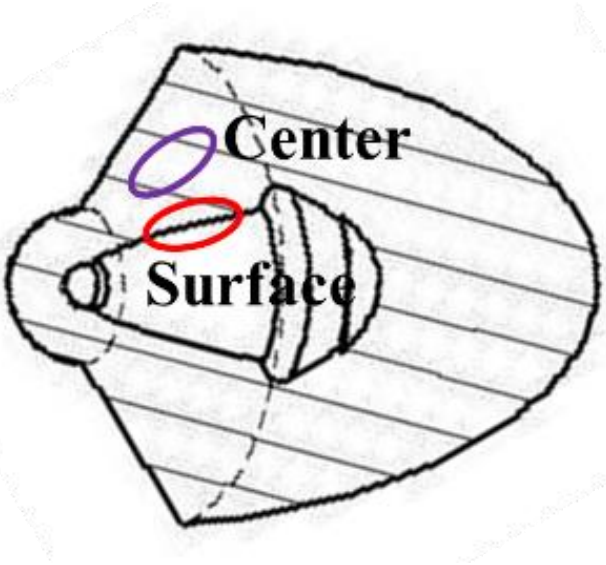

Fig. 3. 11 Hardness measurement positions.

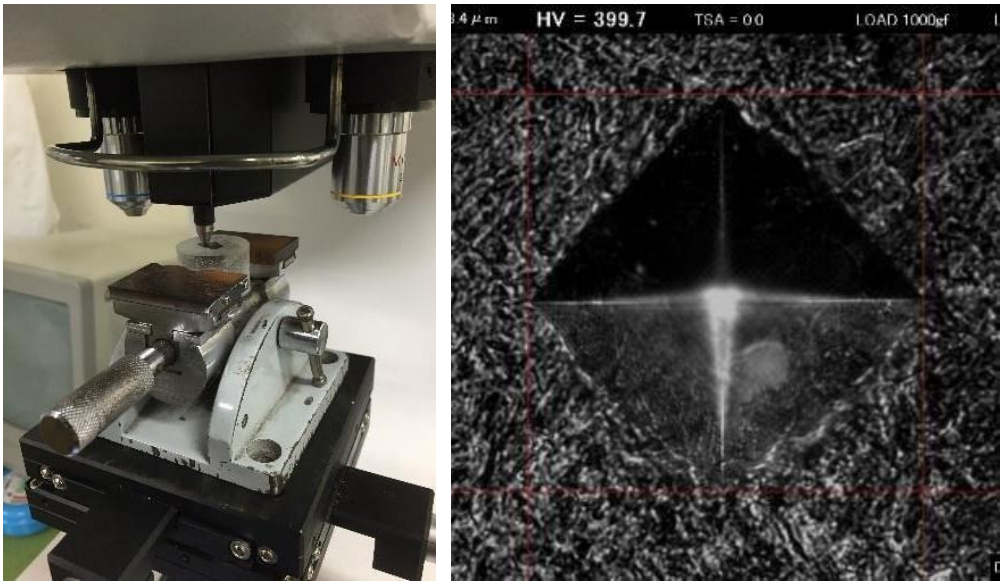

Fig. 3.12 Example of an indentation.

Table 3.12 Hardness measurement near the surface of the body seat.

Measurement position	Near the surface of body seat				
Tempering temperature [°C]	200	250	300	350	400
Hardness [HV]	642.3	533.5	576.9	541.8	502.4
	677.7	627.3	598.6	578.2	512
	694.7	642.4	571.7	556.4	513.2
	693	628.7	598.6	556.4	523.3
	672.7	630	587.5	552.7	520.9
		640.8	574.3		
Average	676.08	617.12	584.6	557.1	514.36
Standard deviation	18.911	37.850	11.047	11.829	7.384

Table 3.13 Hardness measurement at the center of the nozzle.

Measurement position	Inside the nozzle				
Tempering temperature [°C]	200	250	300	350	400
Hardness [HV]	519.8	460.3	400.5	431.7	376.5
	418.6	453.8	412.1	416.1	386.4
	444	479.7	399.7	426.8	383.6
	491.8	457.6	467.9	437.8	405.8
	457.5	446.6	485.7	428.4	396.7
	465.1	458.4	396.7		
Average	466.133	459.4	427.1	428.16	389.8
Standard deviation	32.567	10.102	35.837	7.110	10.300

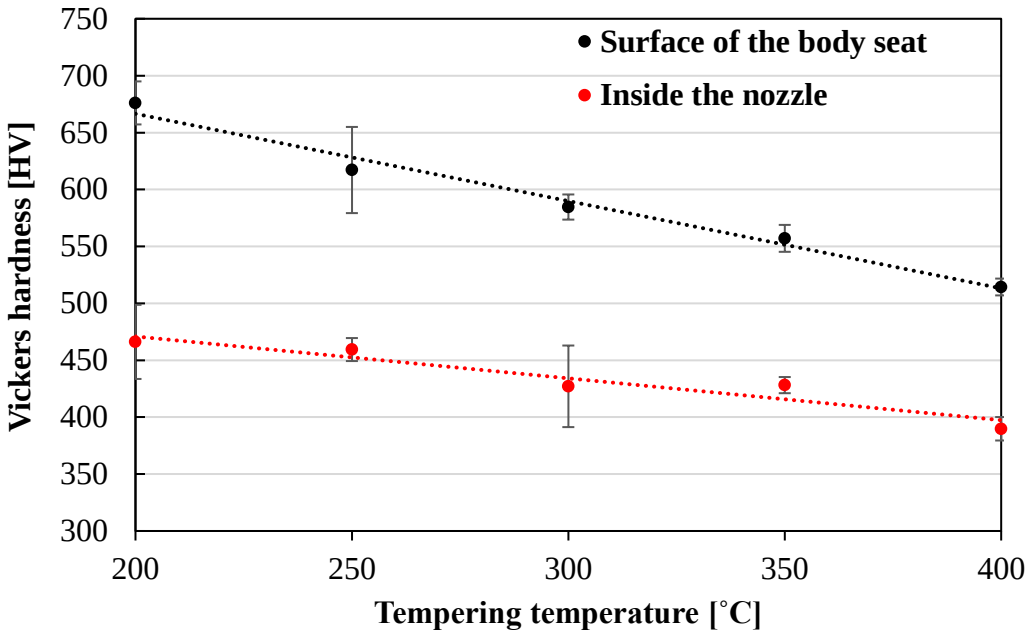

Fig. 3. 13 Effect of tempering temperature on nozzle surface hardness.

The relationship between tempering temperature and hardness is shown in Fig. 3.13. Based on the results, it can be confirmed that the hardness near the surface of the body seat was higher than that at the center of the nozzle. This is because the carburizing treatment was performed before quenching to improve the wear resistance, and the surface layer was hardened by the addition of carbon. Furthermore, it was observed that the hardness decreased in proportion to the tempering temperature. Hence, it was assumed that phenomena such as structural change and elimination of dislocations occurred as the tempering temperature increased. Furthermore, it was assumed that near the surface layer, the rate of decrease in hardness was higher than that in the central part, and structure change was significant.

Generally, the Vickers hardness, yield strength, and fatigue strength exhibit a proportional relationship. Therefore, the yield stress can be converted from the Vickers hardness. Because no direct conversion table exists between hardness and yield strength, a plot of conversion values between hardness and tensile strength based on the SAE hardness was used, as shown in Fig. 3. 14. The yield ratio in chromium steel was assumed to be 85%–90%, and the approximate yield strength was estimated using this ratio and then plotted. Furthermore, the relationship between the Vickers hardness V [HV], tempering temperature T [°C], and yield strength Y [MPa] was obtained as follows:

$$V = -0.7669 \times T + 819.93 \quad (1)$$

$$Y = 3.3614 \times V - 276.47 \quad (2)$$

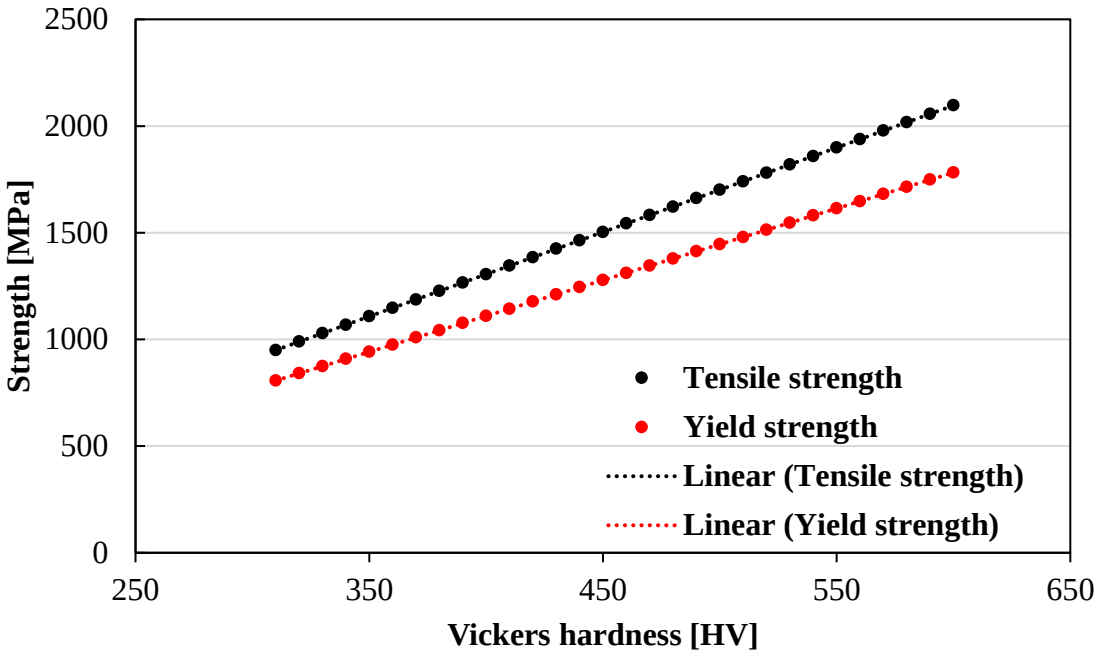

Fig. 3. 14 Relationship between Vickers hardness and strength.

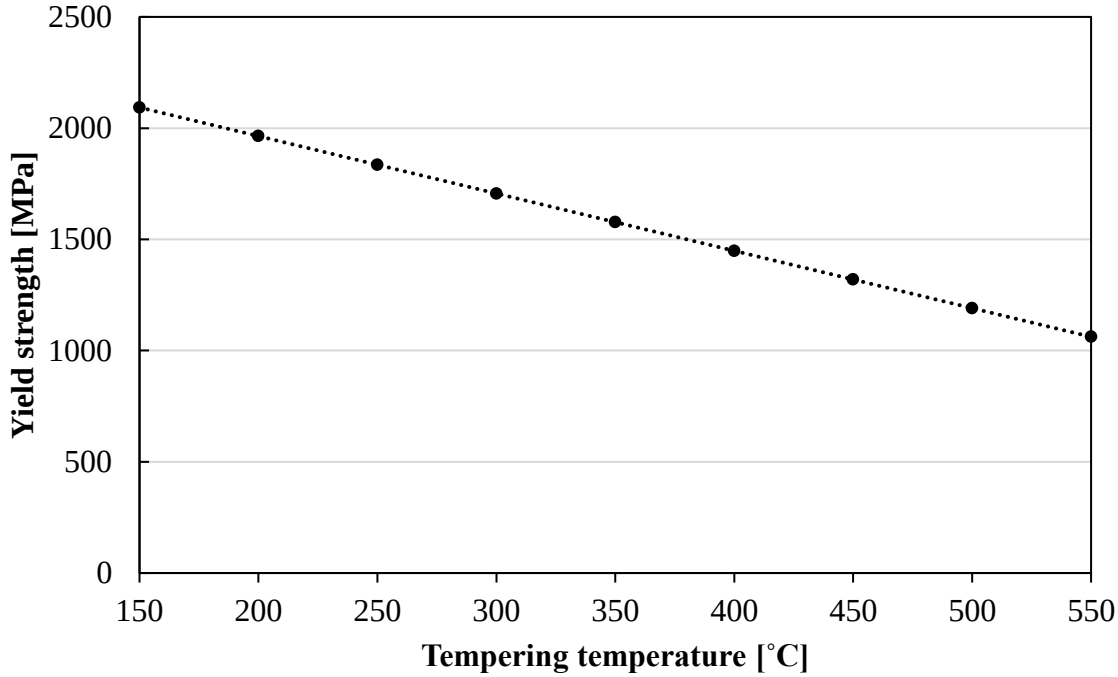

Fig. 3. 15 Relationship between tempering temperature and yield strength.

The relationship between the tempering temperature and calculated yield strength is shown in Fig. 3.15. From the results above, it can be confirmed that the yield strength decreased with the tempering temperature, but the yield strength exceeded 1,500 MPa at tempering temperatures below 400 °C, which was the highest tempering temperature in this experiment. Therefore, it was speculated that the decrease in hardness due to heating was unrelated to the deformation of the body seat, and that a specific phenomenon that caused a decrease in strength occurred during tempering.

3.6 Effect of Injection Pressure on Body Seat Deformation

This section explains how heating causes the yield stress in the body seat to decrease. The structure deforms when heated to a temperature greater than the pre-tempering temperature, according to the experimental findings so far. It is possible to assume that this is caused on by a reduction in the body seat's yield stress as a result of some influence during tempering. Therefore, we carried out tests with various loads applied to the body seat in order to study the decrease in yield stress during tempering. By analyzing the three-dimensional shape of the seat surface with a nano-search microscope measuring instrument, the amount of deformation of the body seat following the test was determined.

3.6.1 Methodology and Results

A wire-cut electric discharge machine was used to cut the nozzle so that the nozzle seat surface could be observed. The body seat was cut at an angle of 29.5° to the nozzle so that measurements can be taken parallel to the body seat. The body seat is shaped like a 59° conical surface that is centered on the center of the nozzle.

The next section will go into more detail regarding how the injector needle is moved by fuel pressure. As a result, fuel pressure has the ability to alter the force applied from the needle to the body seat. In this section, we present the findings from tests we conducted to investigate the yield stress using fuel pressure as a parameter. test circumstances A force is applied to the body seat when the injector repeatedly injects fuel and the needle repeatedly opens and closes the valve. However, in this experiment, the body seat was simply subjected to a static load while remaining in the non-injection state in order to evaluate the yield stress. Table 3.14 displays the test conditions. At 15 to 150 MPa, the fuel pressure was tested. Considering the nozzle temperature to be at a running engine condition, 300 °C was specified. The nozzle is further tempered during the test at a temperature of 200 °C, which is its tempering temperature. 10 hours was chosen as the test duration since it is believed to produce enough deformation.

Table 3.14 Test conditions for investigating the effects of injection pressure.

Nozzle	0.11 mm diameter × 8 holes
Nozzle seat temperature	300 ℃
Input voltage of SSR	130 V
Fuel tank temperature	30 ℃
Injection pressure (rail pressure)	15 - 180 MPa
Injection pulse duration	No injection
Pump speed	1400 rpm
Purge gas	Argon gas
Test duration	10 hours

Table 3.15 Amount of deformation under various fuel injection pressures.

Nozzle No	Fuel pressure [MPa]	Deformation [μm]
No.1	15	0570
No.2	30	0.591
No.3	60	1.771
No.4	90	2.131
No.5	120	2.476
No.6	150	3.186

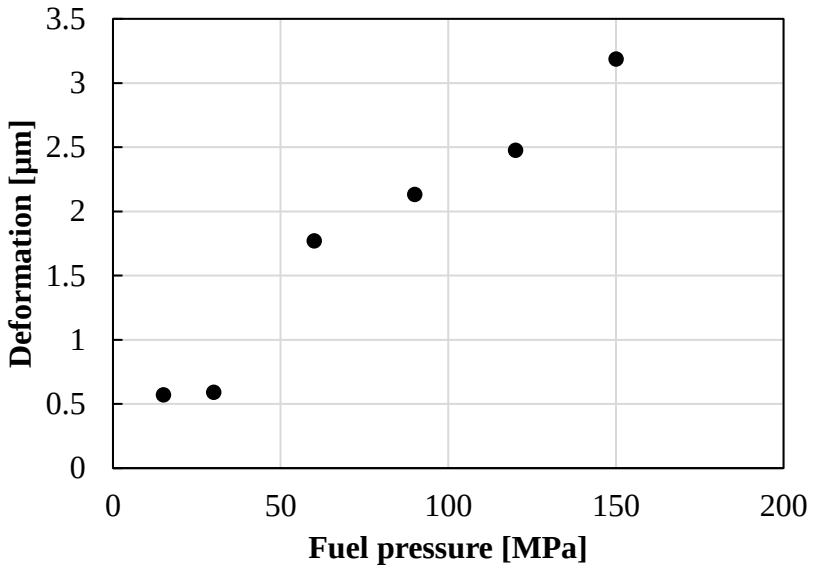

Fig. 3.16 Relationship between fuel pressure and deformation.

The results of evaluating the body seat's shape with a nano-search microscope after the test are shown in Table 3.15. A plot of the relationship with pressure is shown in Fig. 3.16. It is proven that while deformation is negligible between 15 and 30 MPa, it increases in severity as the pressure rises above 60 MPa.

The fuel pressure at which body seat deformation occurs during tempering was also investigated using the pressure parameter test mentioned in the preceding section. The results of the pressure parameter test are used in this section to calculate the amount of yield stress reduction in the body seat.

The structure and workings of the injector must be made clear in order to evaluate the impact of contact pressure on the body seat deformation. The needle in the injector nozzle is moved by the fuel pressure. The load placed on the body seat by the needle rises together with the fuel pressure. In order to describe the force, the fuel pressure exerts on the needle, the injector's construction is first described. A cross-sectional view, an injector schematic diagram, and the workings of the injector are all displayed in Fig. 3.17. A solenoid injector was employed in this study, and the injection was regulated by turning the solenoid on and off. In between injections, the outlet valve closes when the solenoid is turned off due to the force of the spring. The high-pressure fuel from the common rail is at the same pressure both above and below the command piston at this point, and because of the difference in the pressure receiving area, the command piston is being pushed down by more force than the needle valve is being pushed up by, causing the needle to close. The spring located above the needle is also exerting force at this time in the direction of shutting the needle. When the solenoid is turned on for injection, the suction force of the solenoid lifts the outlet valve, releasing the outflow orifice. This causes fuel in the command chamber to exit, lowering the pressure above the command piston. The command piston rises, the needle opens, and the fuel is injected as a result of an increase in the pressure that pulls the needle higher at that point.

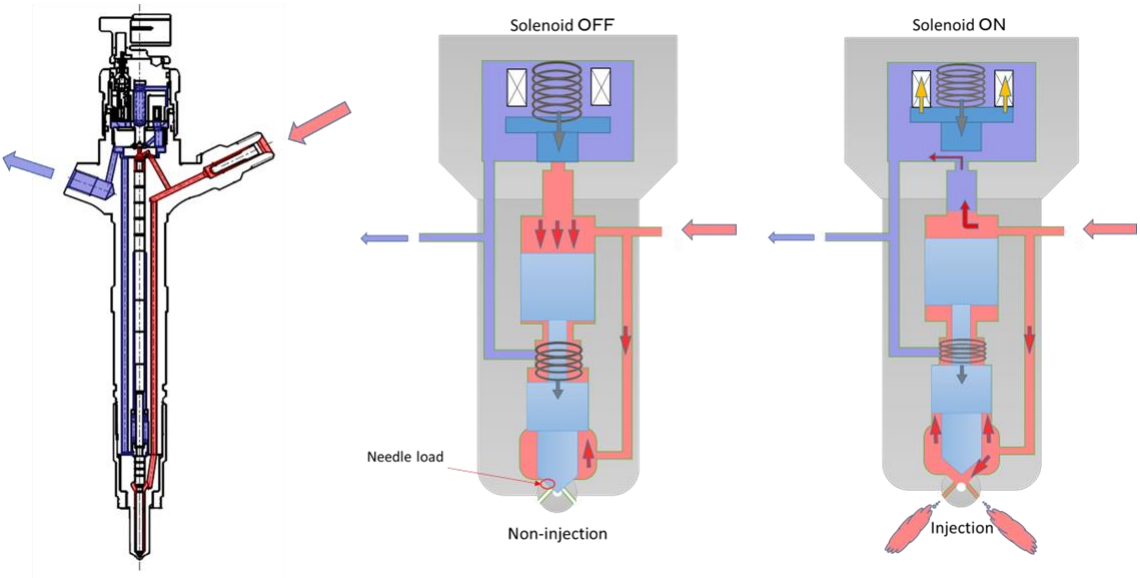

Fig. 3.17 Injector cross-section and operating principle.

According to the operational theory of the injector depicted in Fig. 3.17, the force pushing the command piston down, the force pushing the needle up, and the force of the spring can be used to calculate the load delivered from the needle to the seat during non-injection.

$$S = P\pi R_1^2 - P(\pi R_2^2 - \pi R_3^2) + s$$

Let R_1 [mm] be the radius of the command piston, R_2 [mm] be the radius of the sliding part of the nozzle needle, R_3 [mm] be the radius of the nozzle seat, P [MPa] be the fuel pressure, s [N] be the load of the spring, and S [N] be the seat load.

Here, the surface pressure when the needle and the body seat surface contact each other is discussed. When taking into account the contact points, the Hertzian surface pressure between the flat surface and the cylinder was computed. The body seat surface has a conical shape, and the needle has a curved surface.

The normal force N [N] applied to the body seat is denoted as $N = S/\sin(29.5°)$ since the body seat has a 59° conical form. Additionally, since the needle seat portion's radius is R_2, the contact length is $2R_2$. The body seat is formed of chromium-molybdenum steel, and the needle substance has a diamond-like carbon surface. The needle has a 500 GPa Young's modulus and a 0.2 Poisson's ratio. Young's modulus and Poisson's ratio for the body seat are 205 GPa and 0.3, respectively. The fuel pressure and the contact surface

pressure to the body seat are displayed in Table 3.16 after calculating using the information given above, inputting the precise nozzle dimensions, and comparing the results.

Table 3.16 Relationship between fuel pressure and surface pressure.

Fuel pressure [MPa]	Hertz contact pressure maximum value [MPa]	Contact surface width [mm]
15	365	0.118
30	473	0.153
60	635	0.205
90	764	0.247
120	874	0.283
150	971	0.314
180	1060	0.343

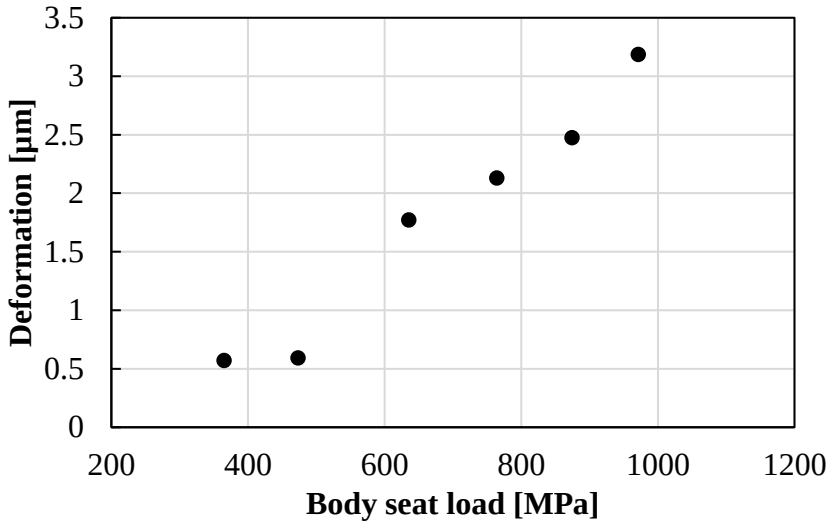

Fig. 3.18 Relationship between body seat load and deformation.

It was found from the results of the pressure parameter test described in the preceding section that nozzles tested at 60 MPa or higher produced deformation along the needle's shape during tempering to 300°C. The conversion of the seat load from the fuel pressure and the degree of deformation are shown in Fig. 3.18. The body seat has likely reached the yield point at about 600 MPa, according to this result.

3.7 Effect of Tempering on Body Seat Deformation

Owing to the different temperatures in the previous test, it was believed that the cause of body seat deformation was the number of dislocations released as the temperature increased [30-32]. When the body seat is subjected to heat above the tempering temperature, the number of dislocations that can be resolved increases, and it is thought that the load from the needle causes deformation. On the other hand, as mentioned above, the number of dislocations that dissolve increases when the injector is heated above the tempering temperature. It is thought that the number of dislocations to be resolved in the center is reduced, and the deformation of the seat can be suppressed. Therefore, in this section, we conducted a deformation test using a nozzle that had been tempered in advance, and investigated the effect of tempering on body seat deformation.

3.7.1 Methodology and Results

Tables 3.17 and 3.18 show the deformation test conditions. The fuel injection pressure is 180MPa and the pump speed is 1400rpm. In this study, we prepared a nozzle that had been tempered to 275°C before the test, and tested it together with a normal nozzle that was non-tempered at a seat temperature of 275°C. As for test time, a normal nozzle was tested for 15 hours. In addition, the tempered nozzle, which is expected to suppress the amount of deformation, has been tested for 20 hours. As for the injectors used, one normal nozzle and five tempered nozzles were used.

Table 3.17 Test conditions for investigating the effects of tempering.

Fuel	Additives	HFRR
	Acid	400 μm
Nozzle	0.11 mm diameter × 8 holes	
Reheating temperature	Non, 275 ℃	
Nozzle seat temperature	275 ℃	
Fuel tank temperature	30 ℃	
Injection pressure	180 MPa	
Injection pulse duration	480 μm	
Pump speed	1400 rpm	
Purge gas	Argon	
test duration	15 h or 20 h	

Table 3.18 Tested injectors with and without tempering.

Injector No.	Reheating treatment
No. 1	Non
No. 2	275 ℃
No. 3	
No. 4	
No. 5	
No. 6	

Table 3.19 summarizes the amount of surface deformation obtained above. Since the displacement of the surface shape before the test may not be 0, the following results were analyzed by subtracting the displacement in the initial state from the measurement results. Based on the surface shape data above, the amount of deformation was obtained by comparing the displacement from the most recessed part to the part raised at the tip of the nozzle with the surface shape before the test, and calculating the difference in displacement. Fig. 3.19 shows the relationship between the amount of deformation and the presence or absence of tempering. The points plotted here represent the mean and the error bars indicate the deviation of the data.

Table 3. 19 Deformation amount of each injector.

Injector No	Reheating treatment	Deformation
No. 1	Non	3.3 μm
No. 2	275 ℃	1.4 μm
No. 3		0.6 μm
No. 4		0.8 μm
No. 5		2.0 μm
No. 6		1.7 μm

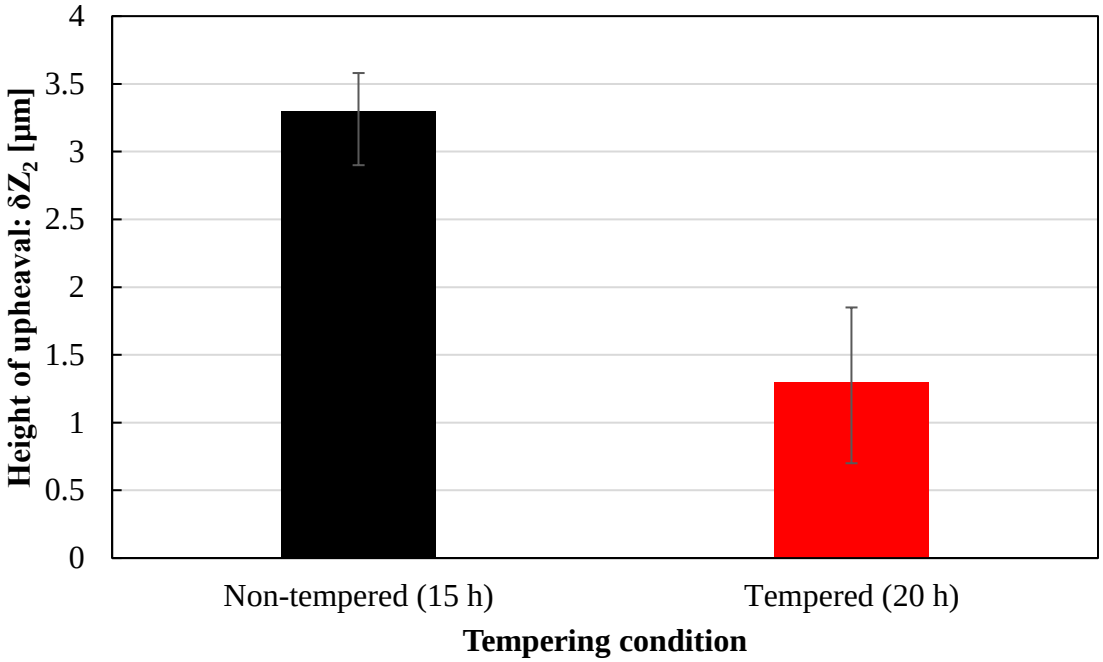

Fig. 3. 19 Effect of tempering on deformation of nozzle body seat.

It was speculated that the tempering released the dislocation density of the nozzle to a stable state at 275 °C, the tempering released the dislocation density of the nozzle to a stable state at 275 °C, which was the temperature in the actual test. During tempering, the material of the nozzle body seat was softened by the release of dislocations. However, δZ_2 was decreased by tempering. This result suggests that the dislocation release of the material affected the strength of the nozzle body seat under the high-temperature corresponding engine operation conditions. Additionally, the structure of the nozzle without tempering might change during the test at high temperatures. In the case

involving the non-tempered nozzle, dislocation was released at high temperatures and high forces owing to the needle contact during the experiment. The release in dislocation of the material under a high load force resulted in deformation. By contrast, in the case involving the tempered nozzle, the dislocation release of the material did not occur during the experiment at temperatures lower than the tempering temperature because the dislocation had already been released and the dislocation density was low. Therefore, the deformation of the nozzle body seat was suppressed by tempering at a temperature higher than the engine operation temperature.

3.7.2 Optical Microscope Observation

To prepare a nozzle that exhibits the required surface and size, a wire cut electric discharge machine was employed to cut the nozzle at the position shown in Fig. 3.20, subsequently, the nozzle was filled with epoxy resin. Polishing was performed using emery polishing papers, followed by mirror polishing using a polishing machine. Tempered nozzles at temperatures 200 °C – 400 °C were etched with nital and picral. The nozzles were observed under an optical microscope. The observation results of the nozzles etched with nital are provided next.

Based on observation results of the nozzle surface etched using nital, as shown in Fig. 3.21 and 3.22, it was confirmed that the material structure of the body seat changed as the tempering temperature increased. The body seat was martensite after quenching and subzero treatment, and the observation results confirmed that needle-like martensite appeared in the tempered nozzles at 200 °C and 250 °C. Furthermore, based on observation results of the tempered nozzles above 300 °C, it was confirmed that the martensite structure contracted as the tempering temperature increased, and the martensite structure could not be confirmed in the 350 °C and 400 °C tempered nozzles. Although the detailed structure could not be determined from the observation results, it was speculated that the structure changed to troostite, which is a mixed structure comprising ferrite and cementite.

In the case of etching with picral, the martensite structure was not revealed; therefore, no characteristic structure was observed in the 200 °C tempered nozzle. It was confirmed that as the tempering temperature increased to 300 °C and 400 °C, a structure that appeared almost white and one that appeared almost black were observed,

respectively. This is because picral revealed the grain boundaries between ferrite and carbide, and it was speculated that an image-like structure appeared as the tempering temperature and carbide precipitation increased. The carbides precipitated by tempering were extremely fine and could not be confirmed by observation using an optical microscope. However, it was speculated that the white structure in the image extruded carbides and transformed into ferrite. The other black areas were assumed to be structures known as troostite.

The optical microscope observation results of the structure etched with nital and picral are as follows:

-A martensite structure was confirmed in the nozzle tempered below 250 °C.

-The martensite structure contracted at the tempering stage at 300 °C and transformed into a structure that comprised ferrite and cementite.

-As the tempering temperature increased above 300 °C, the structure became more prominent in appearance and the structure changed.

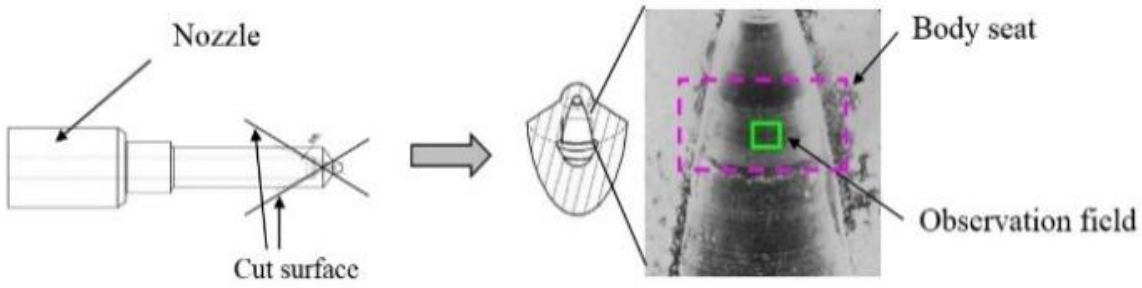

Fig. 3.20 Schematic view of nozzle cutting.

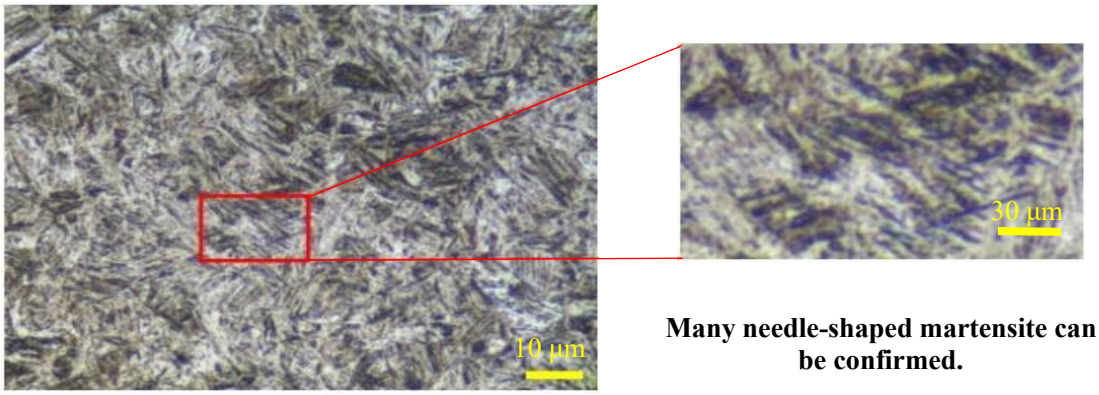

Fig. 3. 21 200 °C tempered nozzle with nital etching (1,000x).

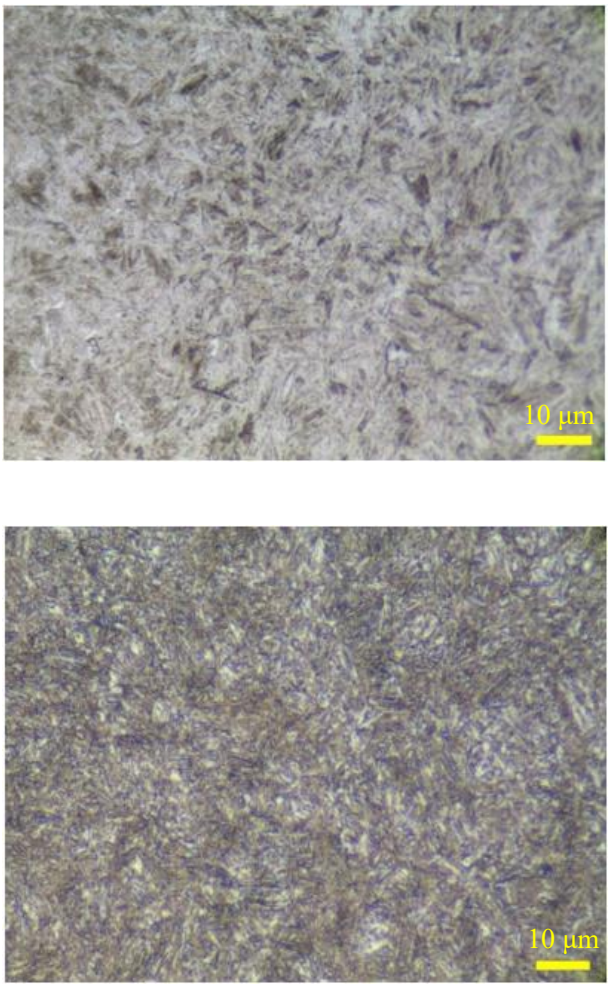

Fig. 3. 22 300 °C (upper) and 400 °C (lower) tempered nozzles with nital etching (1,000x).

3.7.3 FE-SEM Observation

The results of FE-SEM performed in this study are shown in Fig. 3.23. In the case of nital etching, the relief effect was prominent, and the structural change due to tempering was difficult to observe. Therefore, only the observation results of the sample etched with picral are shown.

In the case of the 200 °C tempered nozzles, the main structure was martensite and hence a secondary electron image was obtained. The appearance of standing structures could not be confirmed. However, it was confirmed that many white and long textures appeared in the 300 °C tempered nozzle, assumed to be caused by cementite precipitated by reconstitution. In the 400 °C tempered nozzles, the same structure as the cementite structure observed at 300 °C was confirmed. It was observed that the precipitation of

cementite progressed further from the 300 °C tempered nozzle, accompanied by the further development of the grains.

The following can be inferred from the results of microstructure observation via FE-SEM.

-When tempered at 200 °C, almost no cementite precipitated, and the martensite structure remained.

-The cementite structure precipitated at 300 °C of tempering, and the precipitation progressed further as the temperature increased.

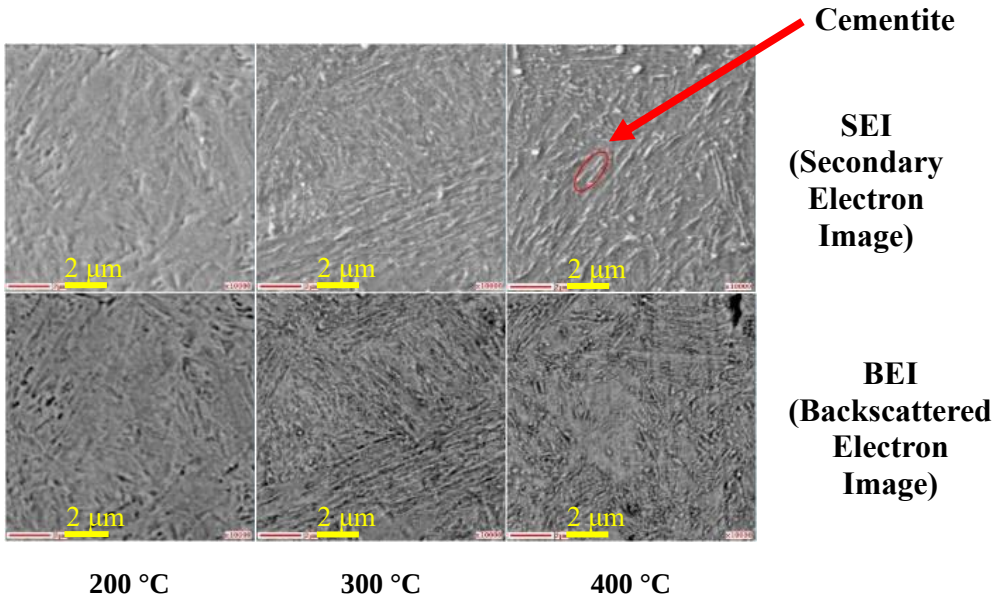

Fig. 3. 23 200 °C, 300 °C, and 400 °C tempered nozzles with picral etching (10,000x).

3.8 Effect of Tempering Duration on Body Seat Deformation

It is assumed that the deformation of the body seat is promoted by the microstructural change that occurs when it is heated above the pre-tempering temperature. Therefore, the deformation is expected to be suppressed by tempering in advance at a temperature above the use temperature to suppress microstructural changes during use. In this section, we analyze the effect of the pre-tempering amount on the deformation and the tempering duration required to suppress the deformation by performing a fixed-time test using multiple nozzles for different tempering durations and by measuring the deformation amount.

3.8.1 Methodology and Results

Five parameters were set from 15 to 240 min as the parameters for the tempering duration. The tempering temperature was set to 300 °C for all cases, which was the actual test temperature. The test duration was 10 h. The fuel injection pressure, injection period, pump speed, and test temperature were maintained constant during the test, and the test conditions are listed in Table 3.20 and 3.21.

Table 3.20 Tempering conditions.

Nozzle No.	Tempering temperature	Tempering duration
No.1	Conventional product (200 ℃, 120 min)	
No.2	300 °C	15 min
No.3	300 °C	30 min
No.4	300 °C	60 min
No.5	300 °C	120 min
No.6	300 °C	240 min

Table 3.21 Test conditions.

Injector model	G3S
Nozzle	0.11 mm diameter × 8 holes
Nozzle seat temperature	300 °C
Nozzle surface temperature	360 °C
Input voltage of SSR	130 V
Fuel tank temperature	30 °C
Injection pressure	180 MPa
Injection pulse duration	480 μm
Pump speed	1400 rpm
Purge gas	Argon
Test duration	10 hours

Table 3.22 shows the amount of deformation of the nozzle seat part obtained from this method, in addition, deformation with respect to tempering duration. A plot of the results is shown in Fig. 3.24.

Table 3.22 Amount of deformation under different tempering duration.

Nozzle No.	Tempering duration [min]	Deformation [μm]
No.1	0	4.392
No.2	15	4.526
No.3	30	3.275
No.4	60	1.071
No.5	120	1.147
No.6	240	1.481

From the results of the measurements at the surface of the nozzle body seat, it was confirmed that in the nozzles with tempering durations of 15 and 30 min, the center was dented along the needle and swelling occurred in the tip direction. By contrast, for the nozzles tempered for 60 min or more, no swelling occurred in the nozzle tip direction. A plot of the amount of deformation against tempering duration is shown in Fig. 3. 24. The

deformation of the 30 and 60 min tempered nozzles was 13.03% and 75.16% lower that of the 20-min tempered nozzle, respectively. Further tempering did not result in any significant deformation suppression.

Based on the results of the tempering temperature and hardness experiments, it was confirmed that the deformation amount of the nozzle body seat was suppressed in cases where the tempering duration exceeded 60 min. This is likely because the tempering was completed in approximately 60 min, and further tempering did not occur when the tempering duration was extended. When the tempering duration was less than 60 min, the structural change was incomplete during tempering; therefore, further structural change occurred via heating during the test, and deformation was promoted. When the tempering duration exceeded 60 min, the deformation amount slightly increased as the tempering duration increased. Although the error margin was not exceeded in this case, it might be affected by the decrease in hardness due to long-term tempering.

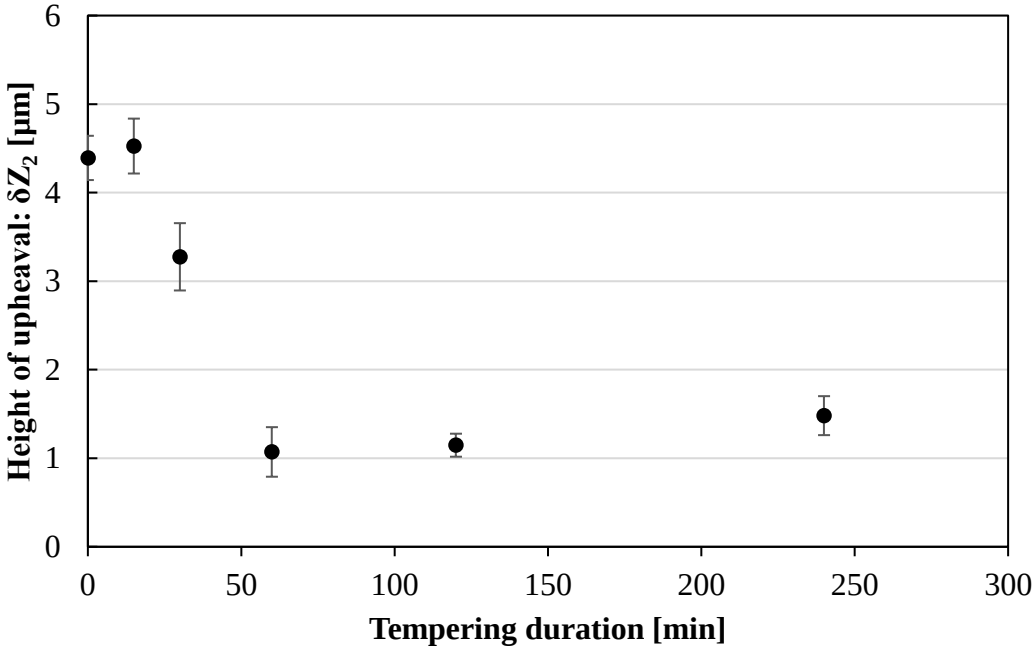

Fig. 3. 24 Effect of tempering duration on deformation of nozzle body seat.

3.9 Effect of Tempering Temperature on Body Seat Deformation

The structural change due to tempering progressed further as the temperature increased. In this study, different tempering temperatures were considered. The tests were conducted using nozzles tempered at different temperatures to investigate the relationship between the tempering temperature and deformation amount.

3.9.1 Methodology and Results

Tempering conditions are shown in Table 3.23, and test conditions are shown in Table 3.24. As a parameter of tempering temperature, tempering was performed at 200 °C, 250 °C, 300 °C, and 350 °C. The tempering duration was 30 min for all nozzles. This is because tempering at 350 °C for a long time exceeds the heat resistance temperature of the nozzle and does not work well. Tempering was also performed for 240 minutes at a temperature of 250 °C. The fuel injection pressure, injection period, pump speed, and test temperature were all constant during the test.

Table 3.23 Tempering conditions

Nozzle No.	Tempering temperature	Tempering duration
No.1	250 °C	30 min
No.2	300 °C	30 min
No.3	350 °C	30 min
No.4	250 °C	240 min

Table 3.24 Test conditions.

Injector model	G3S
Nozzle	0.11 mm diameter × 8 holes
Nozzle seat temperature	300°C
Nozzle surface temperature	360°C
Input voltage of SSR	130V
Fuel tank temperature	30°C
Injection pressure	180 MPa
Injection pulse duration	480 μm
Pump speed	1400 rpm
Purge gas	Argon
Test duration	10 hours

These are the results of the surface morphology measured by the nano-search microscope. It can be confirmed that deformation occurs along the shape of the needle in the products tempered at 250°C and 300°C for 30 minutes. On the other hand, at 350°C, deformation is suppressed regardless of the tempering time of 30 minutes. In addition, although the deformation was suppressed by tempering for 240 minutes at 250°C, it can be confirmed that some deformation occurred. The summarization of the body seat deformation amounts obtained from Table 3.25. is shown in Fig. 3.25.

Table 3.25 Amount of deformation in tempering temperature parameter test.

Nozzle No.	Tempering temperature [℃]	Tempering Duration [min]	Deformation [μm]
No.1	250	30	3.039
No.2	300	30	3.270
No.3	350	30	0.723
No.4	250	240	2.209

The surface shape measurement showed that deformation occurred along the needle at the nozzle body seat surface. The effect of the tempering temperature on the deformation (δZ_2) is shown in Fig. 3.25. In the case involving a tempering temperature of 350 °C, the tempering duration was only 30 min. This is because when tempering at 350 °C for a significant amount of time, the temperature exceeded the heat-resistant temperature of the nozzle. Therefore, the complete tempering process could not be completed at a tempering duration of 30 min. Tempering was performed for both 30 and 240 min at 250 °C and 300 °C.

The deformation amount of the nozzle body seat decreased as the tempering temperature increased. In particular, at 350 °C, the deformation was suppressed by 83.54% compared with the tempered nozzle at 200 °C for 120 min, even though the tempering duration was shorter (30 min). However, when tempered at 300 °C with a tempering duration of 30 min, the deformation suppressed was less than that at a lower temperature of 250 °C. This is attributable to the short tempering duration. In the case involving a tempering duration of 240 min, the deformation amount decreased when the tempering temperature increased from 250 °C to 300 °C. The tempering duration of 30 min was insufficient to release the dislocation of the material. However, at the tempering temperature of 350 °C, it was confirmed that the amount of deformation reduced significantly even after 30 min. Hence, it can be concluded that pre-tempering at a temperature higher than the operating temperature can effectively suppress deformation. Furthermore, it can be concluded that even if the temperature is below the operating temperature, a nozzle that has been tempered for a sufficient duration imposes a certain degree of deformation suppressing effect, and that a higher temperature results in a more prominent effect.

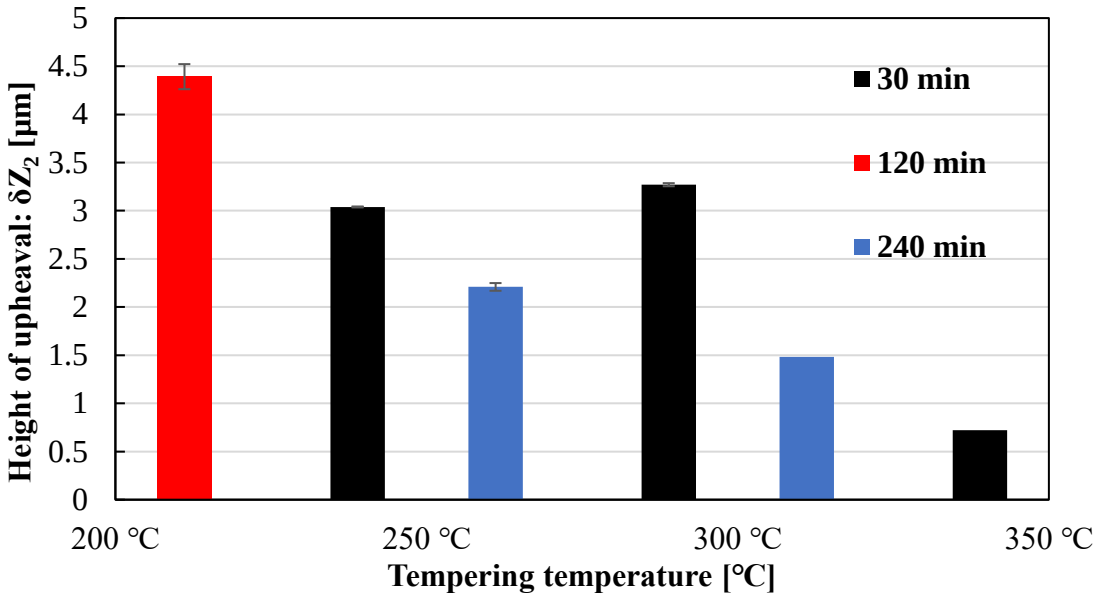

Fig. 3. 25 Effect of tempering temperature on deformation of nozzle body seat.

3.10 Deformation Mechanism

3.10.1 Estimating Mechanism of Body Seat Deformation

To explain the mechanism of the body seat deformation, the state of the nozzle material must be focused on, particularly the dislocation behavior.

As shown in Fig. 3. 26, when the nozzle was exposed to heat above the tempering temperature under no load, the number of dislocations that can be eliminated increased with temperature. Because the elimination of dislocations at this time occurred isotropically, it was assumed that the material did not deform or deformed slightly based on a micro viewpoint.

In addition to being heated, the seat received a load from the needle during injection, and it was assumed that this load resulted in dislocations that can be transformed to anisotropic owing to the effect of the load direction, as shown in Fig. 3. 27.

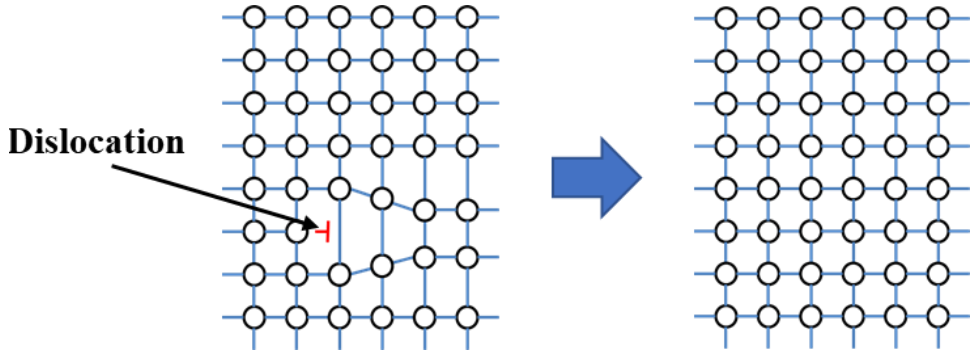

Fig. 3. 26 Dislocation elimination due to increased heat.

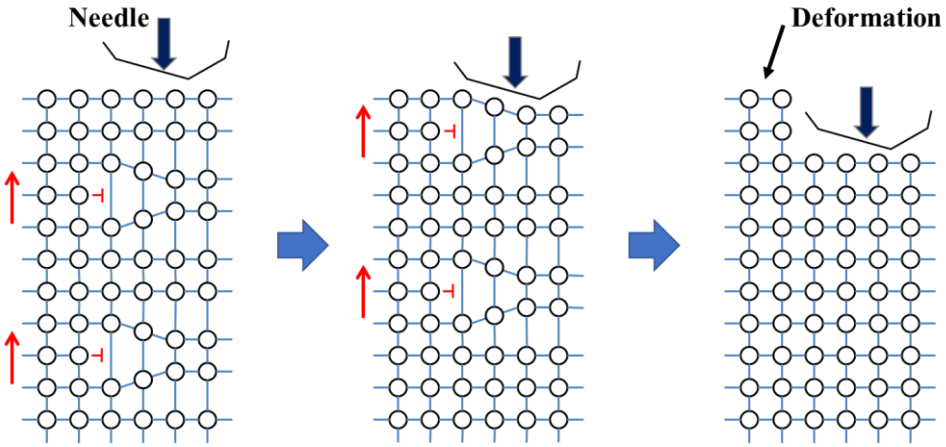

Fig. 3. 27 Process of seat deformation estimation.

In the nozzle that was subjected to tempering, dislocation was isotropically resolved until it became stable at the tempering temperature. When the test was performed at the tempering temperature, only a few dislocations were anisotropically resolved. Therefore, the deformation was suppressed.

It was confirmed that the nozzle seat used in this study was plastically deformed by a stress lower than the yield stress during tempering. Furthermore, it was confirmed that by heating the nozzle, carbide, which is considered to be cementite, precipitated from the martensite structure. Based on the phenomenon explained in the previous section, i.e., the deformation mechanism of the body seat, internal stress was generated in the material owing to the precipitation of cementite by tempering, and a needle load was applied in the state where the dislocation movement was promoted in the high-temperature environment. Hence, it can be concluded that macroscopic deformation was promoted. Fig. 3.28 shows an image of internal stress generation due to the precipitation of cementite (blue region in Fig. 3. 28) and an illustration of the body seat deformation. Deformation was suppressed by tempering in advance because the microstructure did not change during the test, and an internal stress was generated.

The nozzle seat was carburized to improve its wear resistance; consequently, the surface hardness increased. However, when the amount of carbon on the surface was significant, the precipitation of carbides by tempering increased; therefore, the appearance of new phases by tempering and the effect of internal stress became more prominent, and it was assumed that plastic tempering was promoted. However, in this study, the internal stress could not be measured, and hence the abovementioned phenomenon could not be validated. To confirm the acceleration of deformation due to internal stress, in situ observation of stress during heating is necessitated.

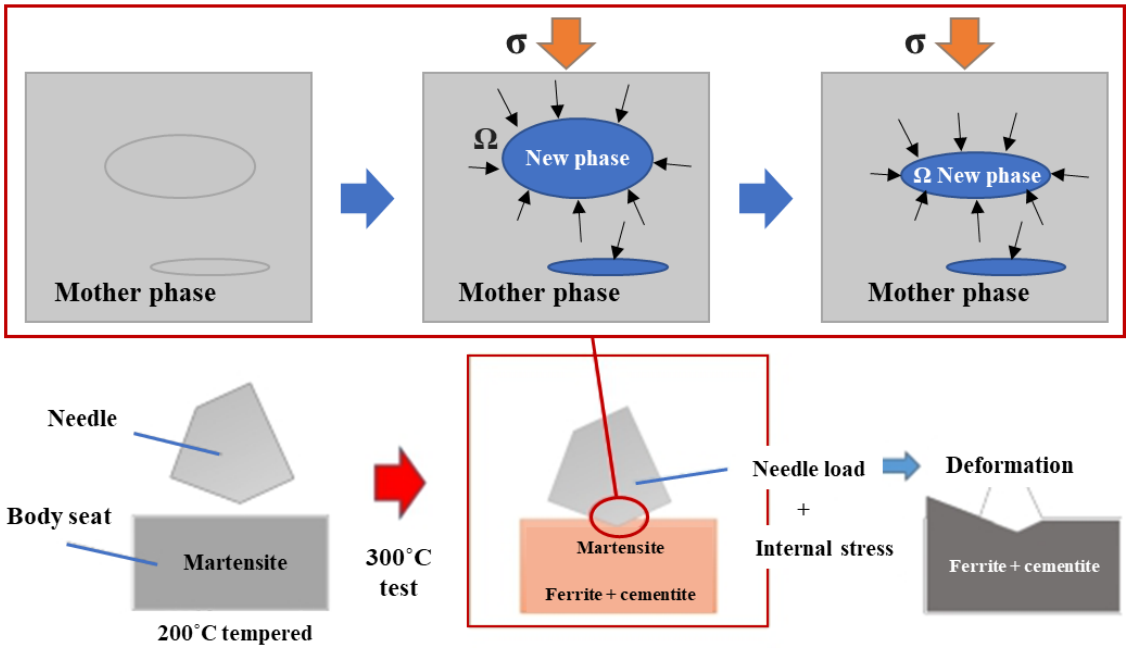

Fig. 3. 28 Estimation process of body seat deformation.

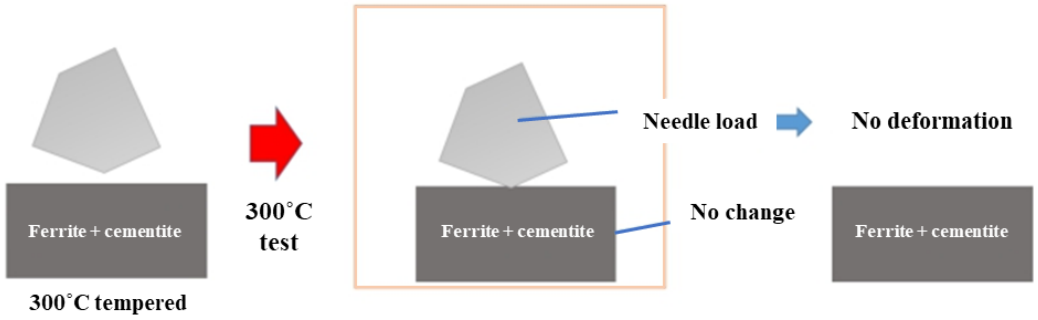

Fig. 3. 29 Estimation process of body seat deformation suppression.

3.10.2 Deformation Suppression Method

Based on the body seat deformation described above, a method for suppressing the deformation can be considered, as described below.

Heat treatments were considered to suppress the plastic deformation that accompanied the microstructural changes in the body seat. Heat treatment was performed to avoid any microstructural change occurs, as shown in Fig. 3. 29. As shown by the results, deformation was suppressed by completing tempering at the operating temperature or at a temperature higher than the operating temperature. In particular, deformation did not occur in heat-resistant steel that had been subjected to high temperature tempering at 530 °C to 630 °C.

When the nozzle was subjected to tempering, the structure of the nozzle changed from martensite to cementite and ferrite. Because of the brittleness of cementite, the cementite layer served as a hard obstacle to dislocation propagation. Therefore, the deformation can be suppressed via tempering, as illustrated in Fig. 3. 30.

From the viewpoint of material composition, when tempering was performed at 250 °C–350 °C, a decrease in toughness known as low-temperature temper brittleness occurred. This is attributed to the precipitation of cementite at the grain boundaries. Because silicon suppressed the precipitation and growth of cementite, the brittle zone was shifted to the high-temperature region.

Therefore, silicon must be added to set the tempering temperature to above 250 °C. When softening due to tempering becomes problematic, an effective solution is to increase the addition number of carbide-forming elements such as chromium, molybdenum, tungsten, and vanadium, which exhibit tempering softening resistance.

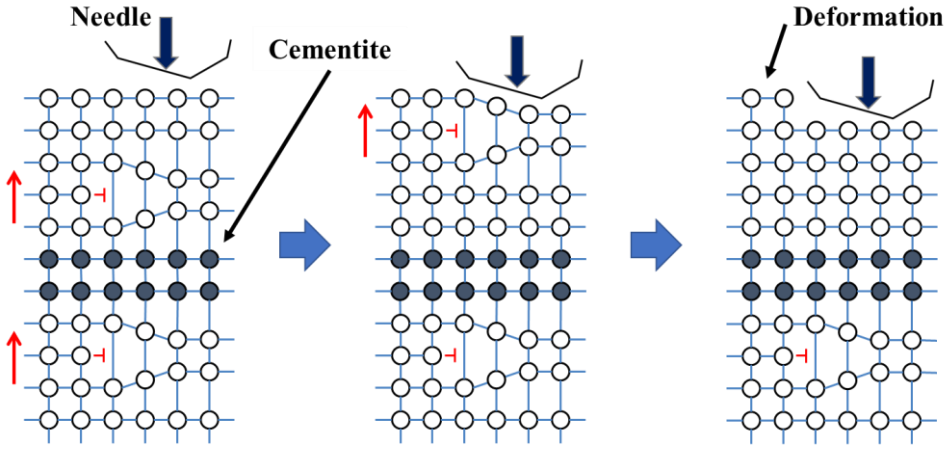

Fig. 3. 30 Estimation process of body seat deformation suppression from micro viewpoint.

3.11 Conclusions

The effects of body seat temperature, test duration, temperature increase duration, tempering temperature, and tempering duration on nozzle body seat deformation were investigated using surface roughness, hardness, and optical measurements. The experiments were run on the wear testing machine which was designed base on the commercially used common-rail system from Denso. The injection pressure was controlled at the maximum which was 180 MPa and the injection duration was control at 480 μs. The electric motor was employed to control the injection time at 1400 rpm with the ratio of 2:1 resulted in 700 times of injection per minute. The nozzle seat temperature was controlled at 300, 350 and 400°C by 8 electric heaters around the nozzle. The fuel temperature was controlled at 60°C by shell and tube heat exchanger and fuel was circulated back to the fuel tank after cooling to refrain fuel consumption. Argon and CO_2 gases were purged into the injection chamber with the same heat transfer rate to prevent ignition and degradation of fuels. The following findings were obtained from the tests of body seat deformation of the diesel fuel injector nozzle.

-As the temperature increased, the depth at the most regressed point and deformation of the body seat increased. The temperature significantly decreased the hardness owing to the release of dislocations. This resulted in the plastic deformation of the body seat.

-The amount of deformation increased with the test duration, and the amount of deformation at 0.5 h was 64.2% of that at 15 h, whereas it reached 88.7% at 5 h.

-The results of the nozzle that underwent reheating indicated that the amount of deformation reduced to less than half of that of the normal nozzle without reheating. The heat treatment eliminated the isotropic dislocations, thereby resulting in a low density of dislocations released during the test.

-After increasing the temperature based on the different heating patterns, a test was performed where the temperature was maintained constant for 3 h. The results indicated no significant differences in the amount of deformation. This is because the time required for the nozzle material to saturate when the nozzle was heated to 300 °C was shorter than the constant temperature period of 3 h set, and the number of dislocations to be resolved was fewer, even when the temperature increase rate was changed. It was assumed that the final dislocation density and the deformation remained unchanged.

-The hardness measurement results of the body seat revealed a decrease in the body seat hardness and yield strength with the tempering temperature. It was confirmed that the yield strength of the body seat was sufficiently high and that ordinary plastic deformation did not occur when tempering was performed at 400 °C or lower.

- From the relationship between the obtained load and deformation results, it was confirmed that the yield strength of the body seat decreased to about 600 MPa when tempering occurred. The nozzle material undergoes structural changes such as cementite precipitation as the tempering temperature rises, and the hardness decreases accordingly. The non-tempered or lower tempering temperature nozzle deformed during the test even though the hardness before the test was higher than that of the high-temperature tempered nozzle. The strength temporarily decreases and deformation occurs when the material is used at a temperature higher than the pre-tempering temperature while the nozzle is being further tempered.

-The material structure observation results of the body seat confirmed that the conventional 200 °C tempered nozzle exhibited a martensitic structure. Furthermore, when tempering was performed at 300 °C or higher, a structure such as cementite, which was assumed to be composed of carbide and precipitates, as well as precipitation progressed as the tempering temperature increased.

-By performing injection tests using nozzles for different tempering durations, the relationships among tempering duration, amount of deformation, tempering temperature, and amount of deformation were determined. It was confirmed that tempering at the same temperature as during the test for 1 h or more was necessary to suppress deformation. In addition, a higher tempering temperature resulted in a more prominent deformation suppressing effect, and at a temperature higher than the test temperature, the effect was achieved even with a short tempering.

-Based on the experimental results, it can be concluded that body seat deformation is a plastic deformation associated with transformation plasticity. The precipitation of cementite from martensite during tempering caused internal stress, and it was speculated that plastic deformation was promoted even under low stresses.

- With the use of a DLC needle, due to the strength and smoothness of the material, wear on the nozzle body seat was eliminated. Only the results of plastic deformation were found. Therefore, the deformations on the nozzle body seat are mainly influenced by

plastic deformation.

-In this experiment, the results can be obtained by using the test rig, which is constructed based on the actual fuel injection equipment. The test conditions can be varied independently of the severe conditions of the actual engine. This allows the short-duration test using the test rig to predict and simulate the same phenomena that occur in the actual engine use without complexity of the parameters.

Bibliography

[1] IEA (2019), https://www.iea.org/reports/world-energy-outlook-2019.

[2] Greenhouse Gas Inventory Office of Japan (GIO). (2016). http://www-gio.nies.go.jp/aboutghg/nir/2016/NIR-JPN-2016-v3.0_rev_web.pdf.

[3] Heywood, J. B. (1988). Internal Combustion Engine Fundamentals. 2nd edn. Mcgraw-Hill. New York, USA.

[4] Takaishi, T., Numata, A., Nakano, R. and Sakaguchi, K. (2008). Approach to High Efficiency Diesel and Gas Engines. Mitsubishi Heav Ind Tech Rev. 45(1), 21–24.

[5] Ficarella, A., Giuffrida, A. and Lanzafame, R. (2005). Common rail injector modified to achieve a modulation of the injection rate. Inj. J. Automotive Technology, **6**, **4**, 305−314.

[6] Park, J., Kim, D. and Park, S. (2020). Effects of nozzle L/D on near-field development and macroscopic spray characteristics of common-rail diesel sprays. Inj. J. Automotive Technology, **21**, **3**, 657-666.

[7] Wang, F., He, Z., Liu, J. and Wang, Q. (2015). Diesel nozzle geometries on spray characteristics with a spray model coupled with nozzle cavitating flow. Inj. J. Automotive Technology, **16**, **4**, 539−549.

[8] Caprotti, R., Fowler, W. J., Lepperhoff, W. J. and Houben, M. (1993). Diesel additive technology effects on injector hole erosion/corrosion injector fouling and particulate traps, SAE Paper No. 932739.

[9] Dhar, A. and Agarwal, A. K. (2014). Effect of Karanja biodiesel blend on engine wear in a diesel engine. Fuel, **134**, 81-89.

[10] Gondal, A. K. and Nautiyal, P. C. (1991). Wear investigations of injector nozzle using radionuclide technique. Wear, **147**, 375-384.

[11] Khanafi, B. N., Loucif, K., Montmitonnet, P. and Felderb, E. (2010). Plastic

deformation of 25CrMo4 steel during wear: Effect of the temperature, the normal force, the sliding velocity and the structural state. Wear, **268**, **1-2**, 23-40.

[12] Caprotti, R., Fowler, W. J., Lepperhoff, W. J. and Houben, M. (1993). Diesel additive technology effects on injector hole erosion/corrosion injector fouling and particulate traps, SAE Paper No. 932739.

[13] Sachdev, K., Sharma, R. K. and Kumar, V. (1967). Study of injector nozzle wear while using different fuels by radiotracer technique. IIP Report. 44/256.

[14] Tuteja, A. D. (1966). Wear rate of injector nozzle while using different fuels. IIP Report. 44/212.

[15] Cernej, A. (1984). Fuel Introduction in Internal Combustion Engine. UNDP Technical Report.

[16] Lazarev, V. E., Lazarev, E. A., Lomakin, G. V. and Wloka, J. (2014). Injection Nozzle Design for Longer Life at Higher Injection Pressures. MTZ industrial, **4,** 64–69.

[17] Listewnik, J. (1970). Maintenance Limits to Marine Diesel Engines Fuel Injectors on Board Ships. WIT Transactions on the Built Environment, **27**.

[18] Jung, D., Wang, W. L., Knafl, A., Jacobs, T. J., Hu, S. J. and Assanis, D. N. (2008). Experimental investigation of abrasive flow machining effects on injector nozzle geometries, engine performance, and emissions in a DI diesel engine. Inj. J. Automotive Technology, **9**, **1**, 9-15.

[19] Pielecha, I., Skowron, M. and Mazanek, A. (2018). Evaluation of the injectors operational wear process based on optical fuel spray analysis. Maintenance and Reliability, **20**, **1**, 83-89.

[20] Pischinger, F., Hilger, U., Finsterwalder, G. and Kupper, H. (1984). Operation and exhaust emissions behavior of the direct-injection alcohol diesel engines, Proceeding. 6th International Symposium on Alcohol Fuels Technology, **1**, 1,319-1,325.

[21] Su, T. F., Chang, C. T., Reitz, R. D., Farrel, P. V., Pierpont, A. D. and Tow, T. C. (1995). Effects of injection pressure and nozzle geometry on spray SMD and D.I. emissions. SAE Paper No. 952360.

[22] Yasutomi, K., Hwang, J., Manin, J., Pickett, L., Arienti, M., Daly, S. and Skeen, S. (2019). Diesel injector elasticity effects on internal nozzle flow. SAE Technical Paper, 2019-01-2279.

[23] Liu, Y., Erdemir, A. and Meletis, E. I. (1996). An investigation of the relationship

between graphitization and frictional behavior of DLC coatings. Surface and Coatings Technology, **86-87**, 564-568.

[24] Costa, R. P. C., Oliveira, D. A. L., Marciano, F. R. and Airoldi, V. J. T. (2012). Tribological behavior of DLC films in space and automotive oil under boundary lubrication. Journal of Aerospace Engineering, Sciences and Applications, **4**, **1**.

[25] Hershberger, J., Ozturk, O., Ajayi, O. O., Woodford, J. B., Erdemir, A., Erck, R. A. and Fenske, G. R. (2004). Evaluation of DLC coatings for spark-ignited, direct-injected fuel systems. Surface and Coatings Technology, **179**, 237-244.

[26] Liu, Y., Erdemir, A. and Meletis, E. I. (1996). A study of the wear mechanism of Diamond-Like Carbon films. Surface and Coatings Technology, **82**, 48-56.

[27] Magee, L. C. (1966). Transformation kinetics, microplasticity and aging of martensite in Fe-31 Ni. Carnegie Institute of Technology. Pennsylvania.

[28] Asi, O. (2006). Failure of a diesel engine injector nozzle by cavitation damage. Engineering Failure Analysis, **13**, 1,126-1,133.

[29] Greenwood, G. W., Johnson. R. H. (1965). The deformation of metals under small stresses during phase transformations. Proceedings of the Royal Society of London. Series A, **283**, 403-422.

[30] Haiko, O., Kaijalainen, A., Pallaspuro, S., Hannula, J., Porter, D., Liimatainen, T. and Komi, J. (2019). The effect of tempering on the microstructure and mechanical properties of a novel 0.4C press-hardening steel. Applied Sciences, **9**, **4231**.

[31] Koneva, N. A., Esipenko, V. F., Kozlov, E. V., Tailashev, A. S., Demyanov, B. V. and Popov, L. E. (1975). Effect of temperature on the dislocation structure of the ordered alloy Ni3(Fe, Cr). Soviet Physics Journal, **18**, 1596–1601.

[32] Lee, W. S. and Huang, Y. C. (2016). Mechanical properties and dislocation substructure of 6061-T6 aluminum alloy impacted at cryogenic temperatures. Materials transactions, **57**, **3**, 344-350.

[33] Nishihara, T. (1978). On the abnormal plastic phenomena of eutectoid steel during tempering. Bulletin of Faculty of Engineering, Kokushikan University. 11, 1978-03.

CHAPTER 4
DEPOSIT FORMATION INSIDE NOZZLE HOLE

4.1 Introduction

Diesel engines have the highest combustion efficiency among other internal combustion engines (ICEs) [1]. Many of the fuel injection systems of diesel engines (also referred to as injectors, Fig.4.1), employ a common rail fuel injection system. As the stricter emission regulations are developed to reduce the emitted pollutants of the engines all the time, the injection system has also been developed in order to increase the combustion efficiency and meet the new emission regulation standard. Therefore, the smaller size of the injector hole and high fuel injection pressure were introduced in order to get better combustion efficiency. The smaller size of the nozzle hole diameter and high fuel injection pressure show the improvement of vaporization, atomization and air-fuel mixing results in a shorter combustion duration [2]. However, it is found that the small size of the injector hole and high fuel temperature at high injection pressure led to the coking of the nozzle hole by the injector nozzle hole deposit. Injector nozzle hole deposit in high pressure common rail fuel injection systems is a relatively new problem in diesel applications. This deposit is generated inside the nozzle hole. Deposits have been generated with the use of diesel engines for a long time. There are many factors that affect the generation of deposits and lead to the differences in locations, compositions, and mechanisms of deposit generation. These result in the change of the internal shape of the injector nozzle, which influences not only the fuel injection but also the fuel spray characteristics as well [3-11].

The dominant factors of deposit formation have been studied and proposed by many researchers. Fig. 4.2 shows the dominant parameters and the effects of the deposit inside the nozzle hole on the injection and spray characteristics. When a deposit forms inside the nozzle hole, it affects both the injection and spray characteristics. As reported, the fuel composition, temperature, and nozzle geometry are the main causes of the deposit formation. Carbon contained in fuel basically relates to pyrolysis, polymerization, and carbonization [12-17]. Metallic components such as Zn, Cu, Ca, and Na in the fuel have an impact on deposit formation inside the nozzle hole, especially Zn as the accelerator for

the deposit formation [18-19]. The temperature was found to be a key to intensifying the deposit formation. Due to the chemical reaction of the carbon molecules in the fuel, the high temperature promotes the formation of deposits [20-23]. The internal geometry of the nozzle also plays an important role in the nozzle hole deposit. Recently, hydro grinding and convergent nozzle holes have been introduced to improve the flow efficiency inside the nozzle by reducing cavitation [24-25]. However, the formation of nozzle hole deposit has increased when the cavitation disappears. Therefore, the deposit is found in the nozzle [26-28]. Although many deposit formation mechanisms were proposed in previous research, it has not been clearly clarified yet.

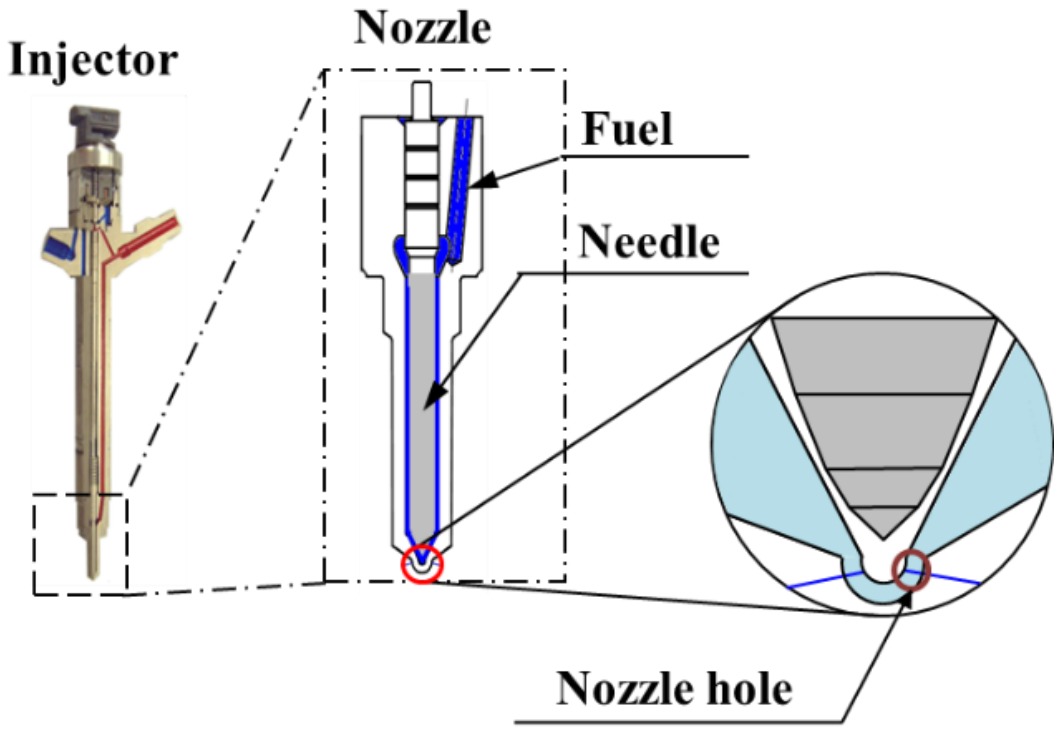

Fig. 4.1 Schematic diagram of diesel injector nozzle.

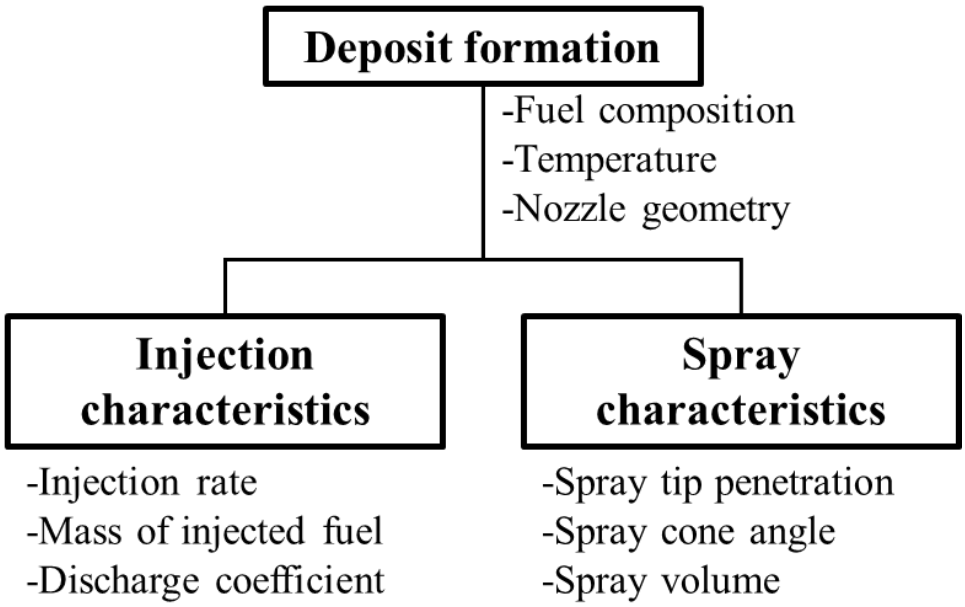

Fig. 4.2 Dominant parameters.

In this study, the effects of fuel additive, ambient gas, and time between injections and number of injections on the deposit inside the nozzle hole and the effects of the deposition on injection and spray characteristics were investigated with an injector testing device, which was constructed based on a commercial common-rail injection system. The results from measurements not only showed the effect of the nozzle hole deposit on the fuel injection but also the spray characteristics.

4.2 Effect of Fuel Additive on Deposit Formation

The study in this chapter focuses on deposits inside the nozzle hole of diesel injector. As described in chapter 1, the deposit which occurs at the fuel injection equipment (FIE), particularly inside the nozzle hole, directly affects to the injection characteristics of the injector leads to the power loss during long term operation in the actual engine. The intended investigation on the fuel additive parameter zinc is desired to blend into the fuel tank to precipitate the formation of deposits.

4.2.1 Methodology and Results

Since the experiment is run on the non-combustion environment, the injected amount of fuel from to injector is employed to be the indicator the appearance of deposits in the injector instead of the power loss from the actual engine. The G3S injector is operated at the conditions as shown in Table 4.1 The pump speed is controlled at 1,400 rpm. The injection pressure and duration are 180 MPa and 480 μs, respectively. Argon gas is purged in to the injection chamber to prevent the degradation and ignition of diesel fuel with zinc 3 ppm. The amount of injected fuel is desired to be measured at 0, 2, 5, 10 and 20 h. to compare the reduction of injected fuel which can leads to the conclusion of deposits formation.

Table 4.1 Test conditions for effect of fuel additive.

Fuel	Additives
	Acid (HFRR 400 μm)
	Zinc 3 ppm
Injector model	G3S
Nozzle	0.11 mm diameter x 8 holes
Nozzle seat temperature	350°C
Injection pressure	180 MPa
Injection duration	480 μs
Pump speed	1400 rpm
Purge gas	Argon
Test time	0, 2, 5, 10, and 20 hours

The average results from injected fuel measurement are shown in Table 4.2. The measurement is separated into two injection duration conditions as 480 and 1,000 µs. The injection duration is concerned due to the different injection duration causes the different injector needle lift which strongly effects to the flow inside the injector.

Table 4.2 Fuel injected amount measurement.

Injector No.	Seat temperature (°C)	Fuel additive	Test duration (h)	Fuel/Injection @480 µs (mg)	Fuel/Injection @1,000 µs (mg)
No. 1	350	Zinc	0	19.7257	66.1358
			2	19.4978	63.8438
			5	19.1637	61.8830
			10	19.0554	59.9178
			20	18.2681	58.0172

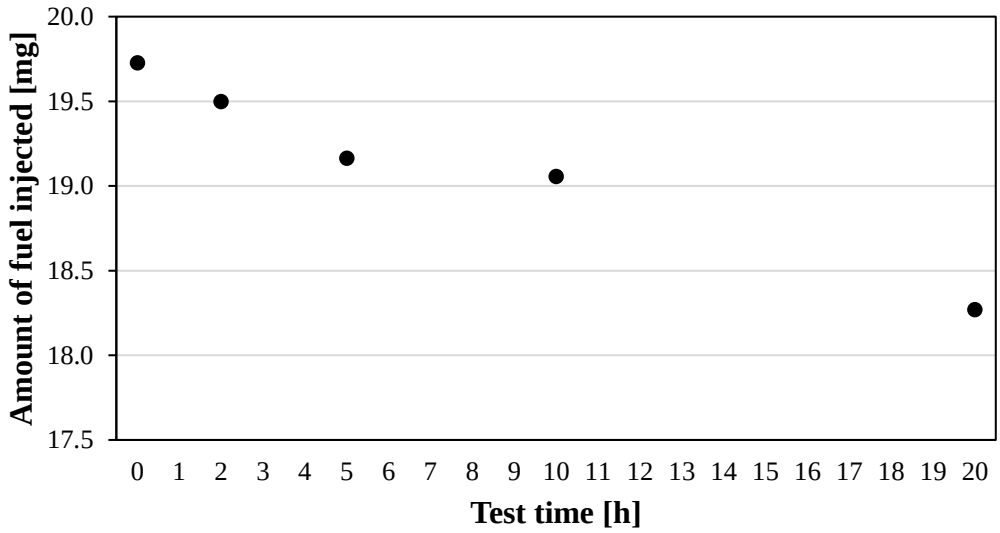

Fig. 4.3 Amount of fuel injected at 480 µs.

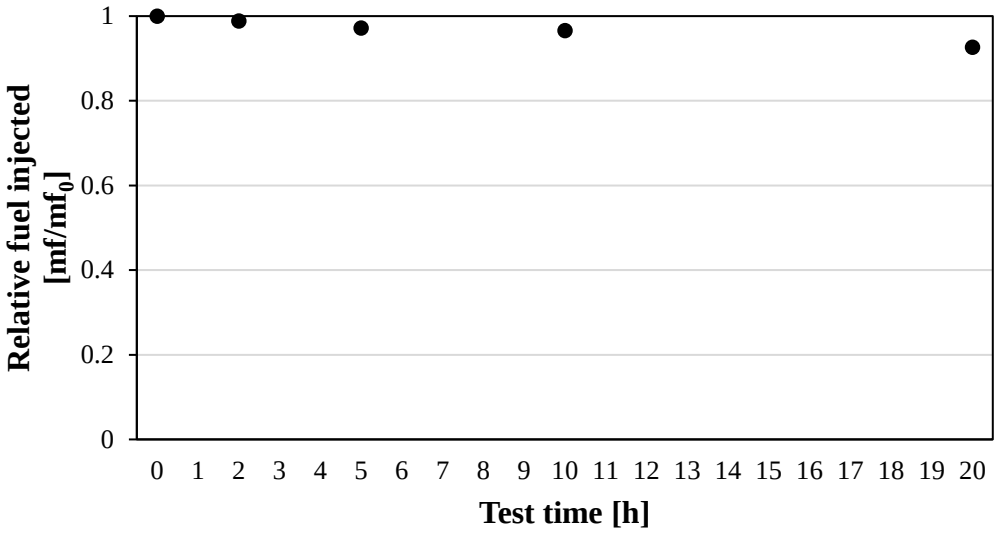

Fig. 4.4 Relative fuel injected amount at 480 μs.

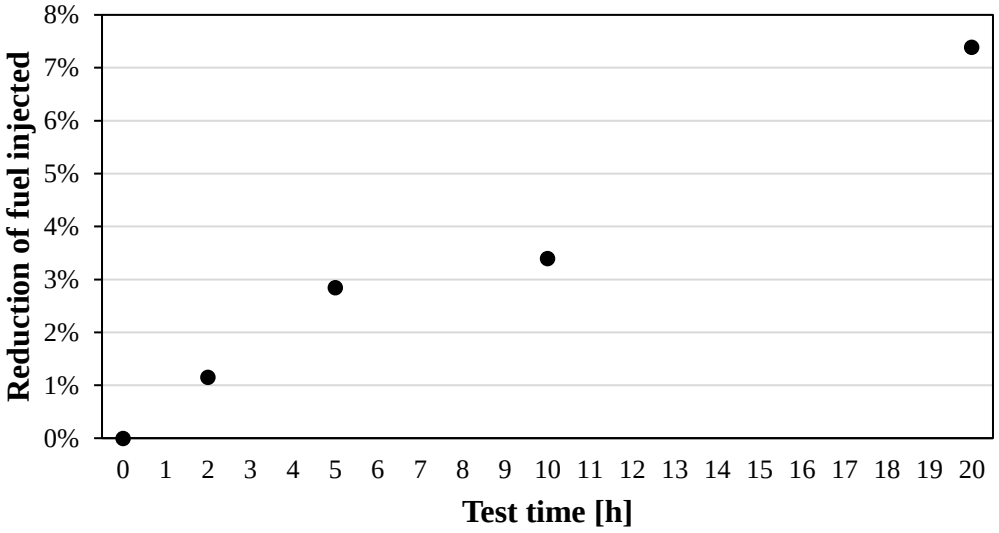

Fig. 4.5 Fuel injected difference at 480 μs.

Fig 4.3-4.5 show the result of fuel injected, relative fuel injected and reduction of fuel injected, respectively. The amount of fuel injected decrease with the increment of test time. At 10 h., amount of fuel injected is 19.06 mg the decrease to 18.27 mg at 20 h. The tendency of fuel injected reduction is almost linear for this experiment. The reductions of fuel injected are 3 and 7.5% at 10 and 20 h., respectively.

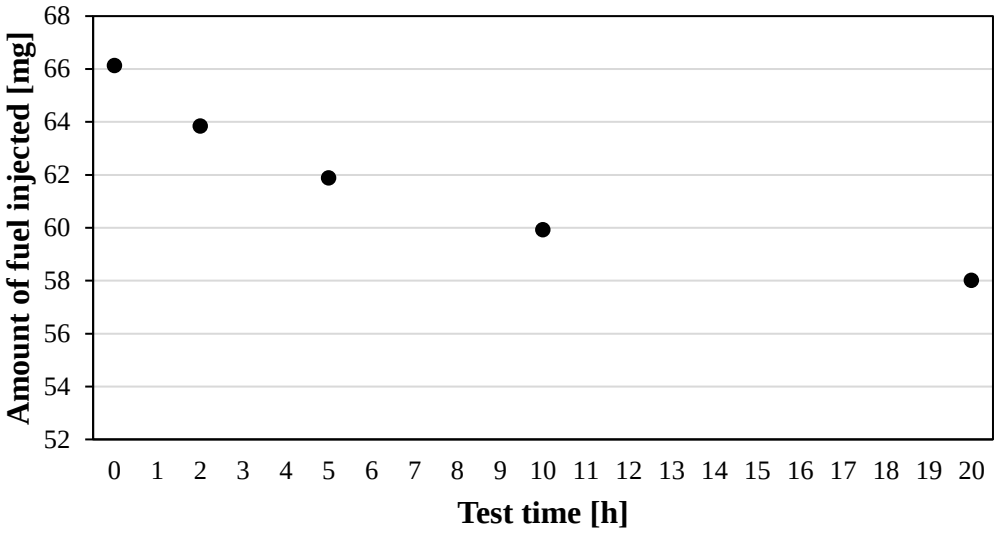

Fig. 4.6 Amount of fuel injected at 1,000 μs.

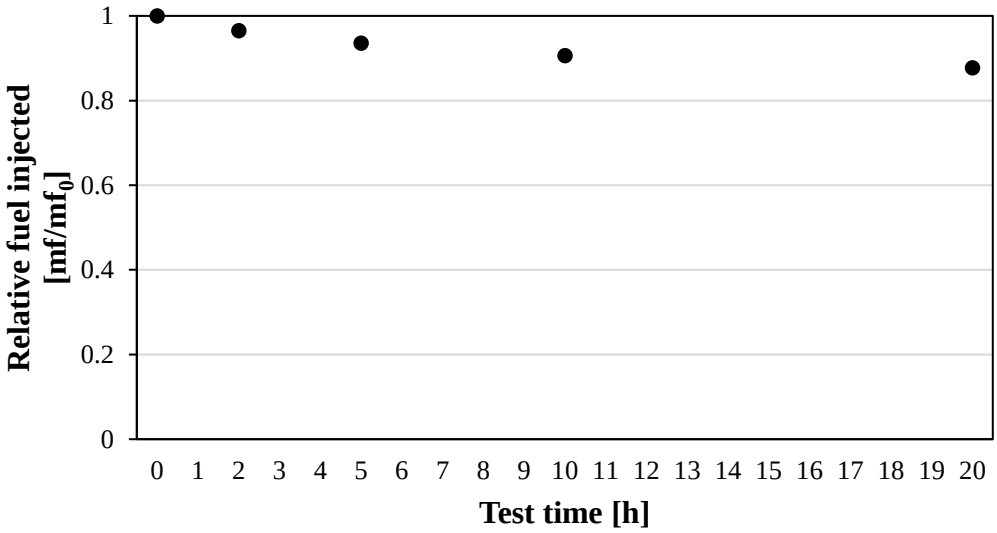

Fig. 4.7 Relative fuel injected amount at 1,000 μs.

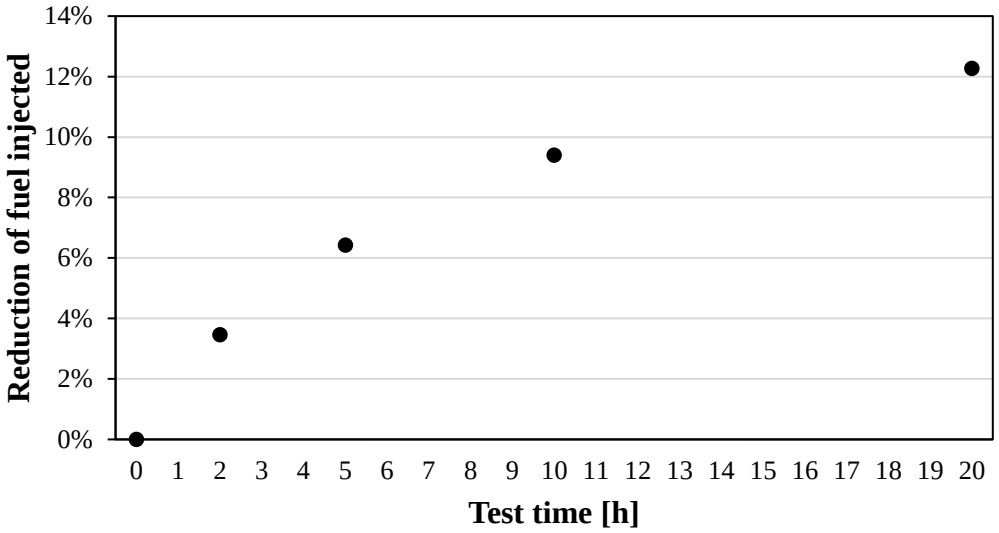

Fig. 4.8 Fuel injected difference at 1,000 μs.

The amount of fuel injected which shown in Fig. 4.6-4.8 decrease with the higher rate in the early period of the test from 0-10 h. compare with 10-20 h. In Fig. 4.6, at the beginning of the test, the fuel injected is 66.14 mg then substantially drops to 59.92 mg at 10 h. At the end of the test, fuel injected slightly decreases to 58.02 which is 12% if the reduction from the initial. These can be roughly concluded that the reduction of fuel injected with time may occurred by the formation of deposits. Thus, the investigation on chemical composition of deposits at nozzle hole is needed. In addition, the difference of fuel injected reduction tendency between 480 and 1,000 μs conditions may affected by the needle lift distance.

4.2.2 Deposit Analysis by Means of the EDS Technique

The cut nozzle at center of nozzle hole was token a picture by using SEM technique to observe the physical properties and positions of deposits. Fig 4.9-4.11 show SEM image of deposits in nozzle hole at different locations. Unlike the deposits from actual engine. The results of SEM images show black color of the nozzle hole surface which could be confirmed as the presence of deposits. In particularly, Fig. 4.11 shows that the nozzle holes are clearly blackened by the covering of deposits. It is considered that the fuel has been deteriorated by the heat from the body seat to form deposits.

Fig. 4.12-4.26 show characteristics EDS-spectra of the deposits at nozzle hole of each test conditions as shown in Table 4.3. The nozzle hole deposits are observed at three different area as inlet, middle and outlet of the nozzle hole, as mentioned in chapter 2.

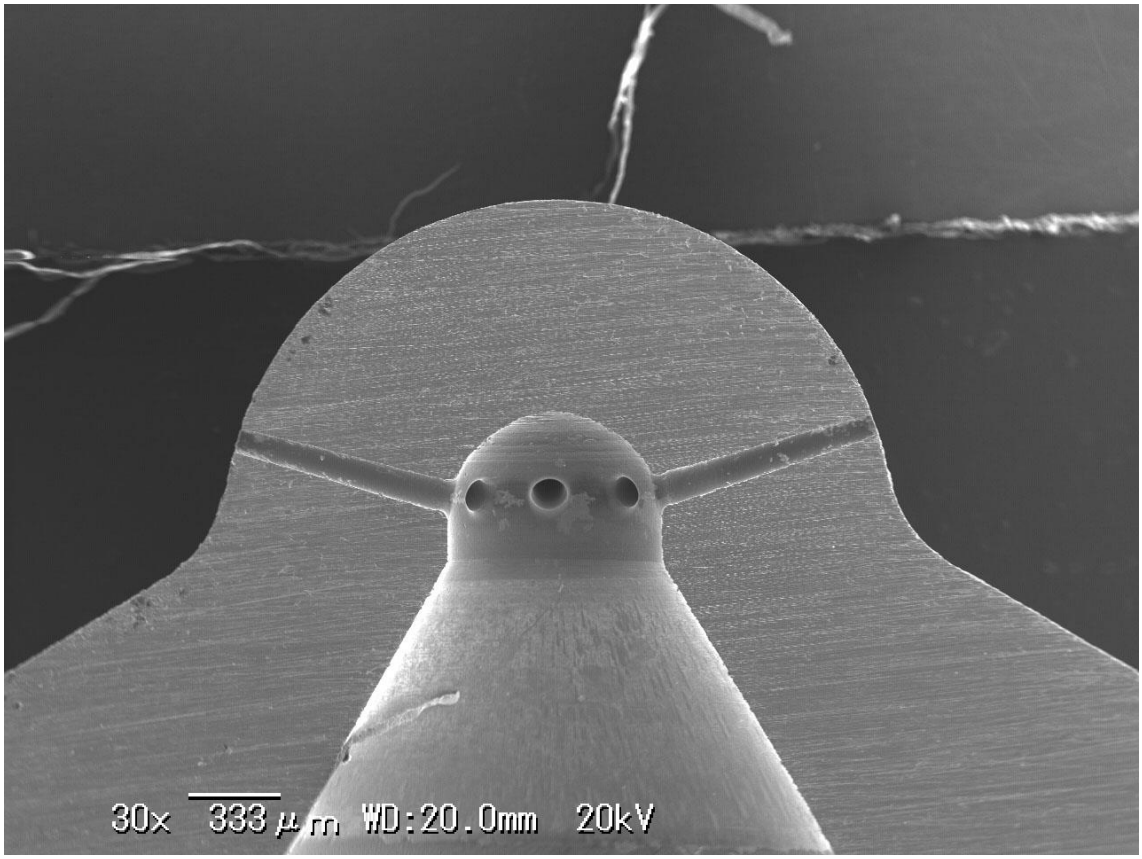

Fig 4.9 SEM image of deposits in nozzle hole.

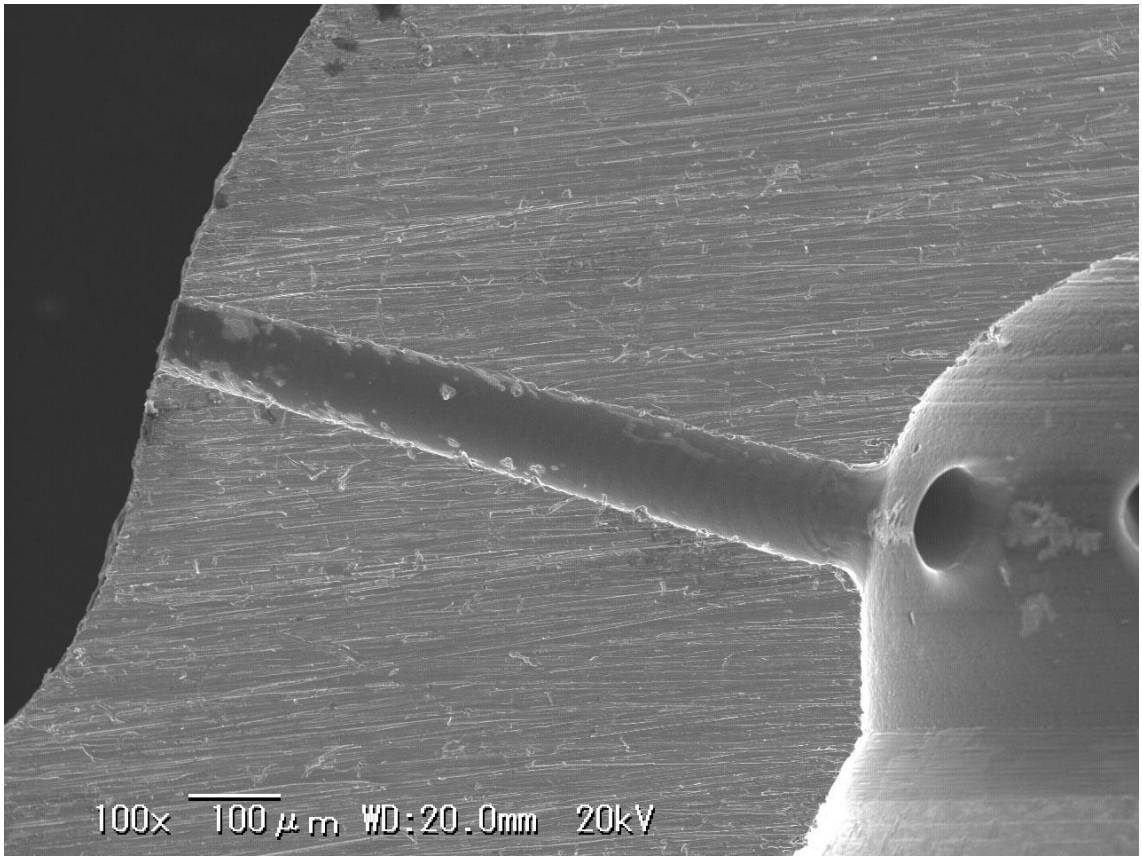

Fig 4.10 SEM image of deposits in nozzle hole.

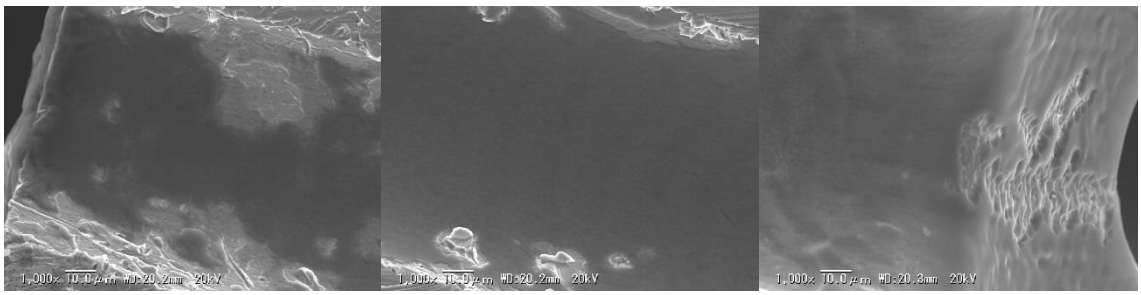

Fig 4.11 SEM images of deposits in nozzle hole at outlet, middle and inlet (Left, middle, and right).

Table 4.3 List of tested injectors.

Injector No.	Seat temperature (°C)	Fuel additive	Test duration (h)
No. 1	350	None	20
No. 2	300	Zinc 3 ppm	10
No. 3			20
No. 4	350		10
No. 5			20

[Nozzle no.1: 01P21216: inlet / middle / outlet]

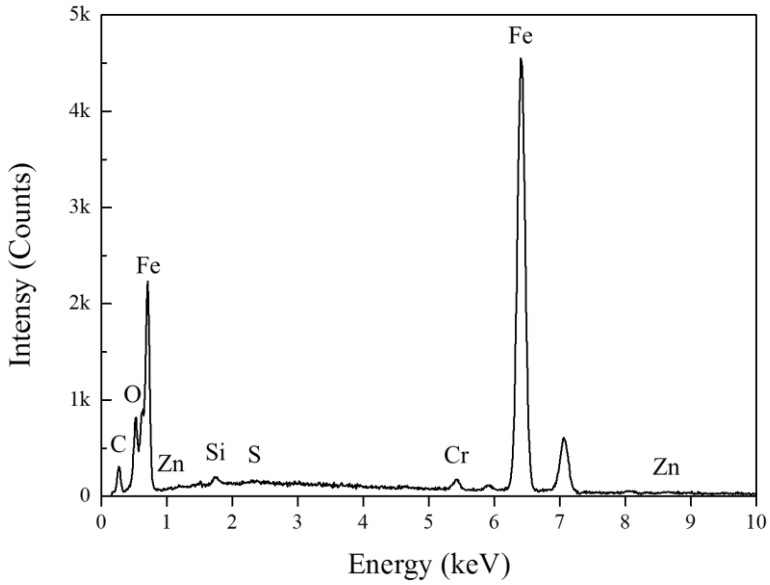

Fig. 4.12 Characteristic EDS-spectra of injector no.1 at the inlet of hole.

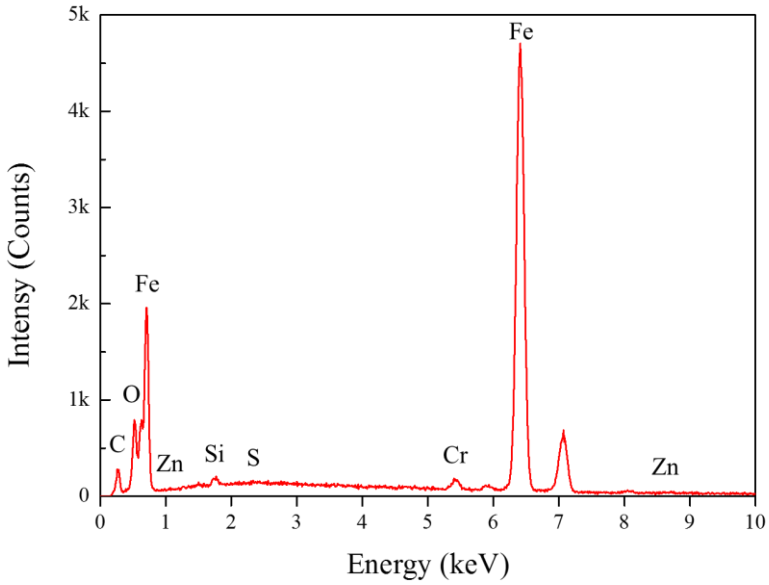

Fig. 4.13 Characteristic EDS-spectra of injector no.1 at the middle of hole.

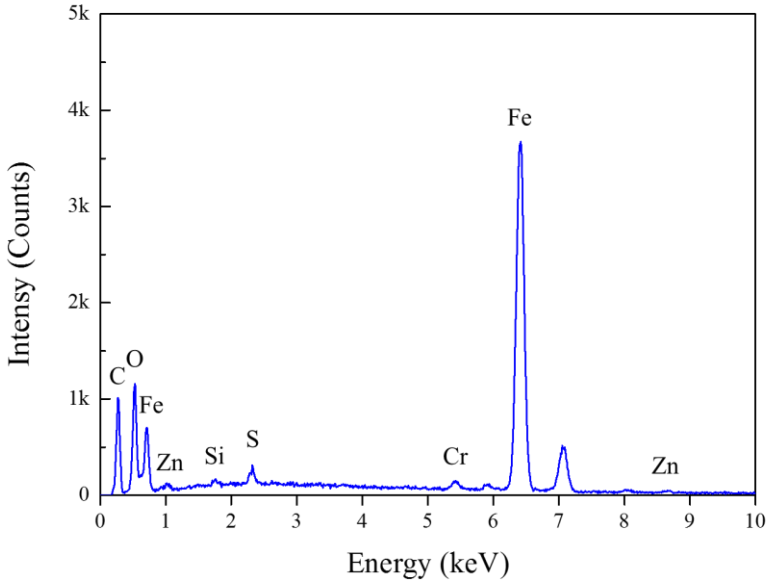

Fig. 4.14 Characteristic EDS-spectra of injector no.1 at the outlet of hole.

[Nozzle no.2: 01P23461: inlet / middle / outlet]

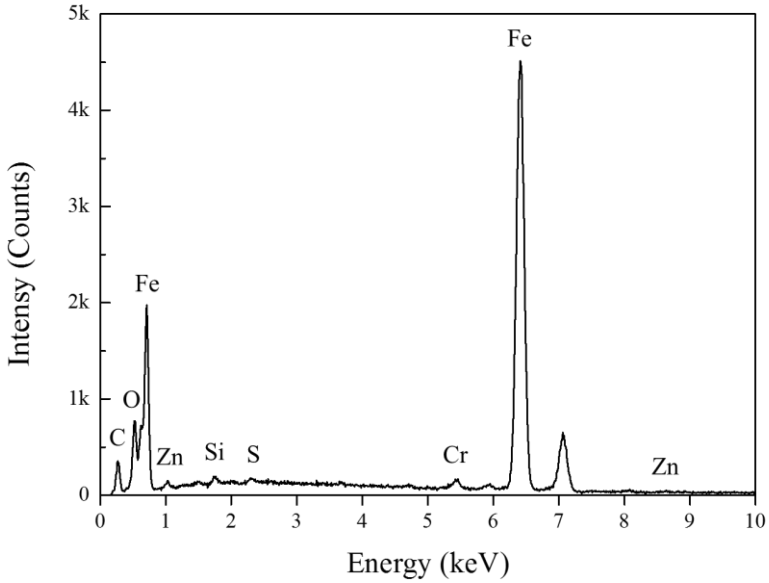

Fig. 4.15 Characteristic EDS-spectra of injector no.2 at the inlet of hole.

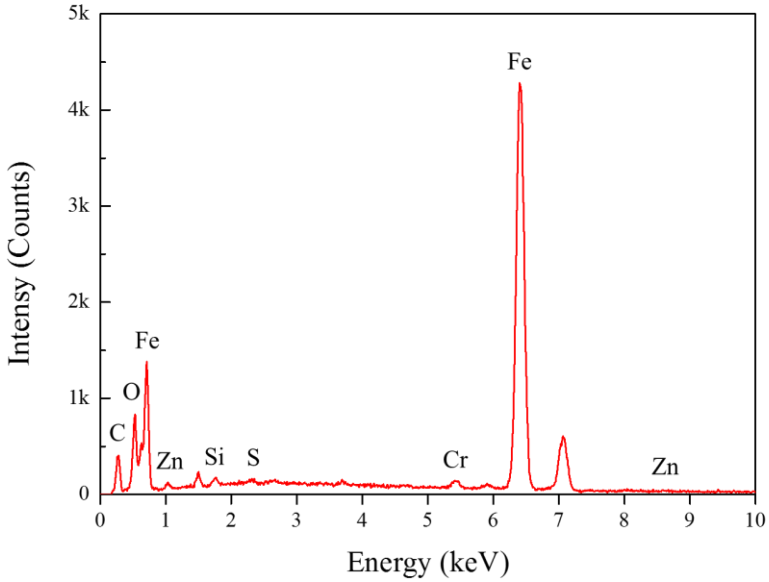

Fig. 4.16 Characteristic EDS-spectra of injector no.2 at the middle of hole.

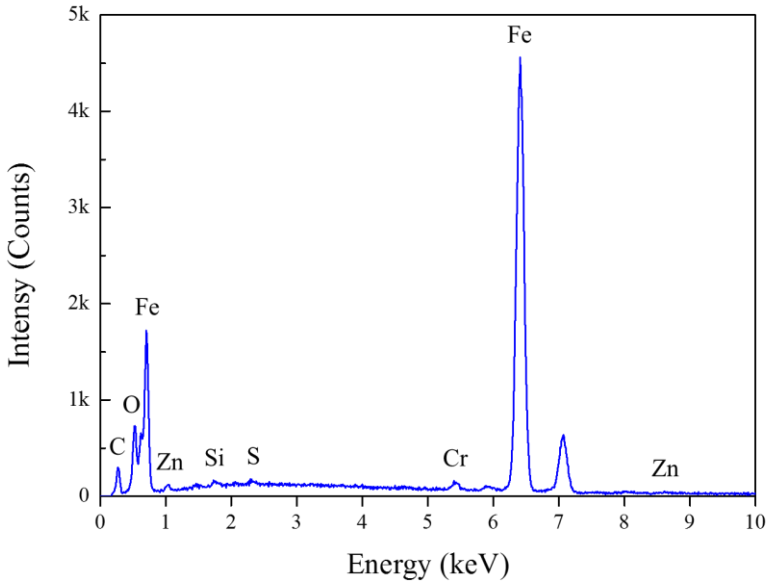

Fig. 4.17 Characteristic EDS-spectra of injector no.2 at the outlet of hole.

[Nozzle no.3: 10N00837: inlet / middle / outlet]

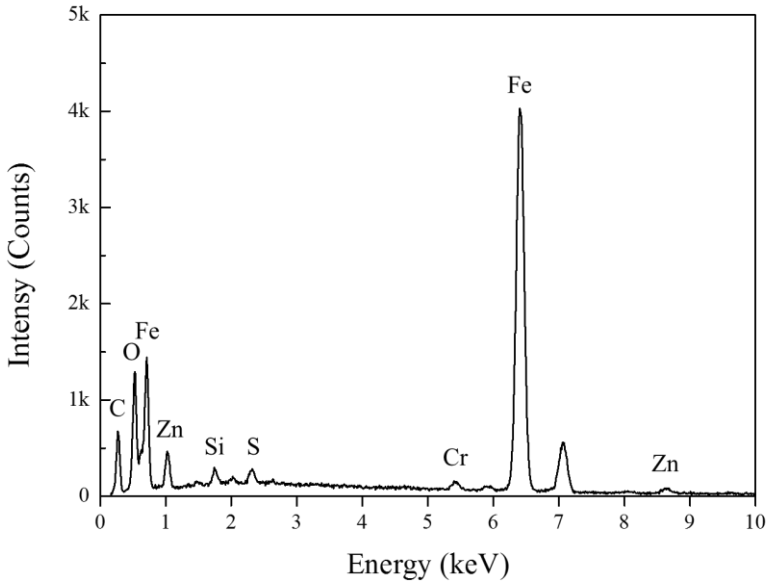

Fig. 4.18 Characteristic EDS-spectra of injector no.3 at the inlet of hole

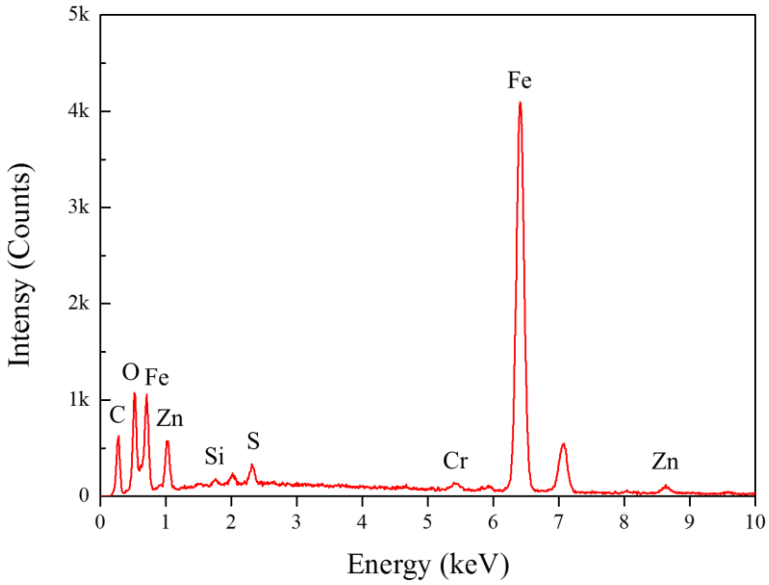

Fig. 4.19 Characteristic EDS-spectra of injector no.3 at the middle of hole.

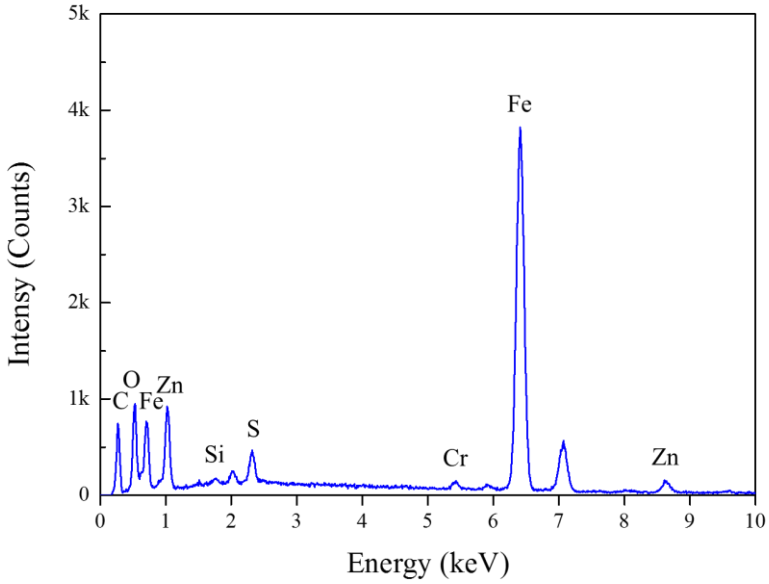

Fig. 4.20 Characteristic EDS-spectra of injector no.3 at the outlet of hole.

[Nozzle no.4: 01P21238: inlet / middle / outlet]

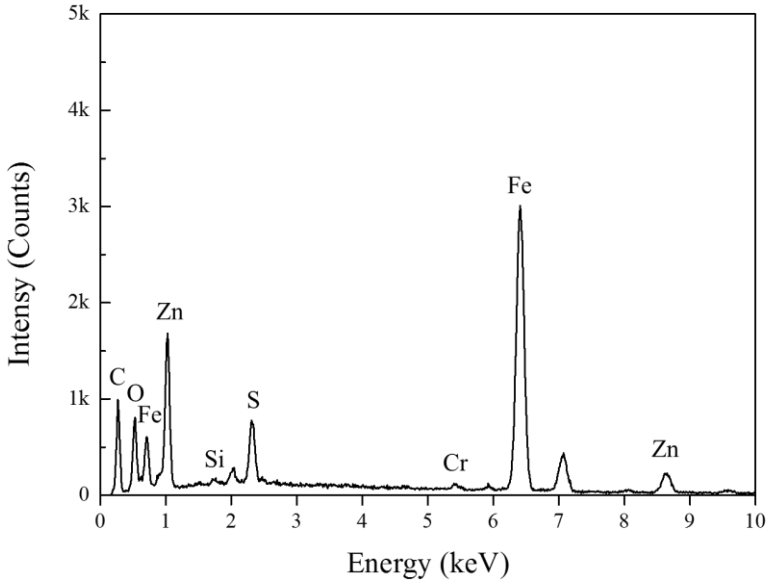

Fig. 4.21 Characteristic EDS-spectra of injector no.4 at the inlet of hole.

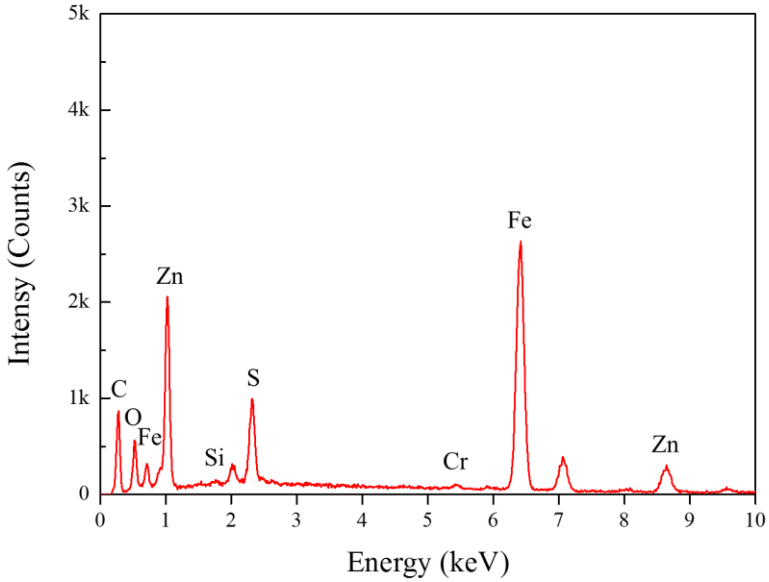

Fig. 4.22 Characteristic EDS-spectra of injector no.4 at the middle of hole.

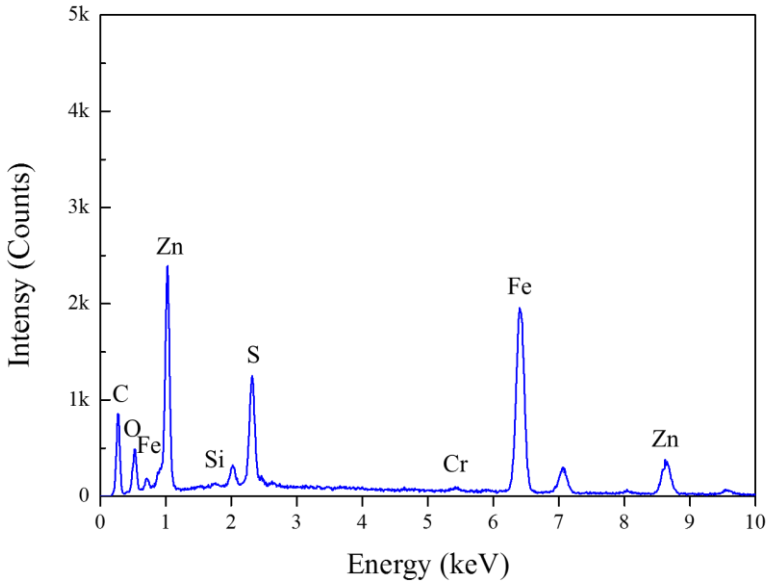

Fig. 4.23 Characteristic EDS-spectra of injector no.4 at the outlet of hole.

[Nozzle no.5: 01P23447: inlet / middle / outlet]

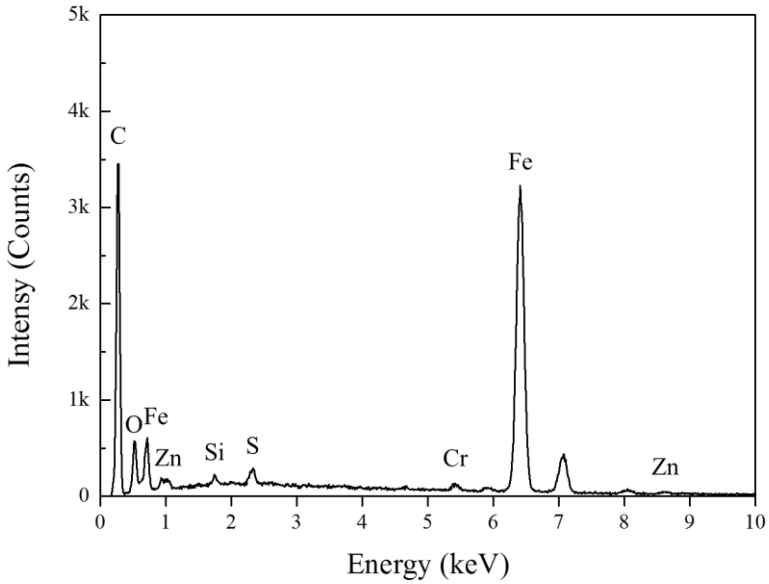

Fig. 4.24 Characteristic EDS-spectra of injector no.5 at the inlet of hole.

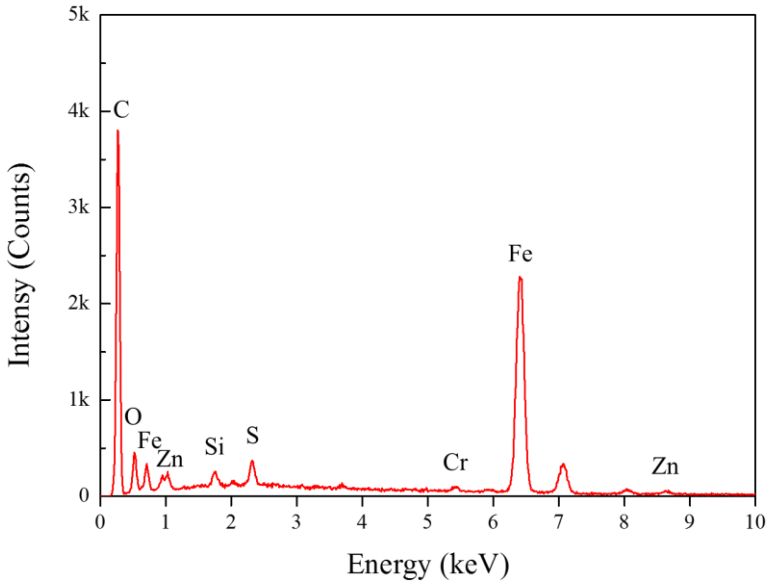

Fig. 4.25 Characteristic EDS-spectra of injector no.5 at the middle of hole.

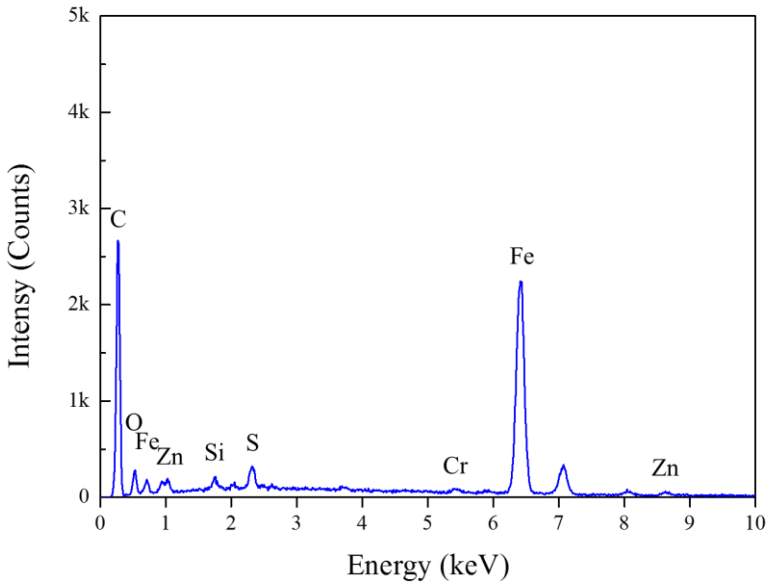

Fig. 4.26 Characteristic EDS-spectra of injector no.5 at the outlet of hole.

The received EDS-spectra display quantitative information about the nozzle hole deposits. The values of y-axis correlate are a function of the element-specific response to the primary electron beam and the concentration of this element in the area under observation.

Deposits formed in the presence of zinc 3 ppm within the fuel. The concentration of zinc in deposits cannot be used to conclude neither the effect of test time nor temperature. The peak of zinc in EDS-spectra can be used to ensure that the used of zinc as the fuel additive causes the fouling of the injector and reduction of the fuel injected.

The results also show that in the different areas of interest the deposits compositions are slightly different. These can be explained as the effects of nozzle geometry that leads to the difference of flow characteristics on each area of the nozzle hole.

4.3 Effect of Ambient Gas on Deposit Formation

CO_2 is one of the main gas emissions emitted from the combustion of internal combustions engines. According to the difference between non-combustion and combustion system, the use of CO_2 at the various concentration is concerned in this experiment to see the chemical compositions of deposits at nozzle hole.

4.3.1 Methodology and Results

Table 4.4 shows the test conditions. The non-combustion test machine is run by electric motor at 1,400 rpm. G3S injector is operated at the maximum injector 180 MP and injection duration 480 μs. Fuel tank and body seat temperature are kept constant at 60 and 350 °C in every experiment. Flow rates of argon and CO_2 are controlled at 1:0, 0.5:0.35 and 0:0.7 L/min for non-CO_2, 50% of argon and CO_2, and non-argon conditions, respectively. The experiments are operated for 20 h. with the interval at 2, 5 10 h. in order to measure fuel injected together with the operation.

Table 4.4 Test conditions for effect of ambient gas.

Fuel	Additives	HFRR
	Acid	400 μm
Injector model	G3S	
Nozzle	0.11 mm diameter x 8 holes	
Nozzle seat temperature	350°C	
Injection pressure	180 MPa	
Injection duration	480 μs	
Pump speed	1,400 rpm	
Purge gas	1 L/min of Argon	
	0.5 L/min of Argon + 0.35 L/min of CO_2	
	0.7 L/min of Argon	
Test time	20 hours	
Interval	At 2, 3, 5 and 10 hours	

Table 4.5 concludes the amount of fuel injected from each condition related to test durations. Injector no.01P23447 represents the effect of argon as ambient gas to be the base condition. Mixing of 50% argon and 50% CO_2 is employed at injector no.10N00725. In addition, the completely use of pure CO_2 is injector no.01P13462, as shown in Table 4.5. The results in Table 4.5 are subsequently plotted to show the fuel injected trend of each test conditions.

Table 4.5 Fuel injected amount.

Injector No.	Seat temperature (°C)	Ambient gas	Test duration (h)	Fuel/Injection @480 µs (mg)	Fuel/Injection @1,000 µs (mg)
No. 1	350	Argon	0	19.7257	66.1358
			2	19.4978	63.8438
			5	19.1637	61.8830
			10	19.0554	59.9178
			20	18.2681	58.0172
No. 2		*Argon + CO_2	0	19.4321	66.9654
			2	18.9016	65.7833
			5	18.6297	64.1619
			10	18.3982	62.3947
			20	17.7325	60.3225
No. 3		CO_2	0	19.6939	67.1593
			2	18.3461	63.5258
			5	17.8595	61.1995
			10	17.7389	59.8315
			20	17.6847	57.4945

*Ar 50% + CO_2 50%

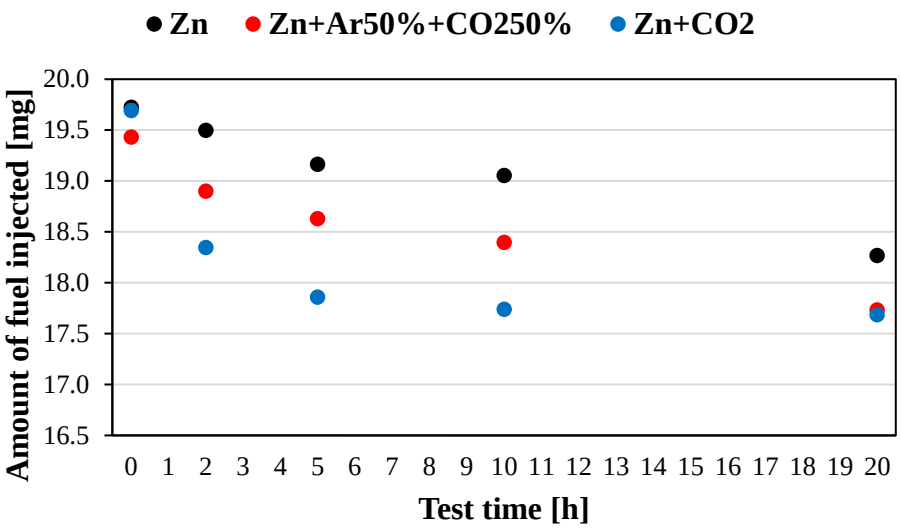

Fig. 4.27 Amount of fuel injected at 480 µs.

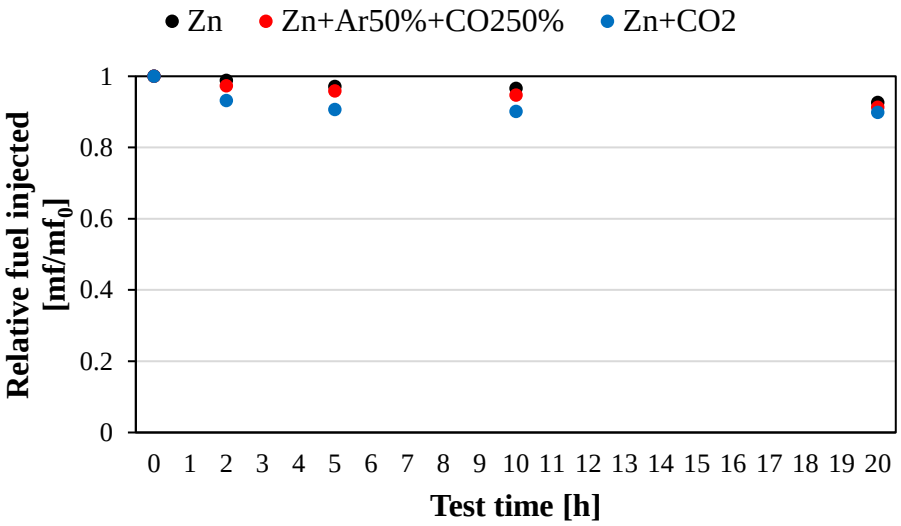

Fig. 4.28 Relative fuel injected amount at 480 µs.

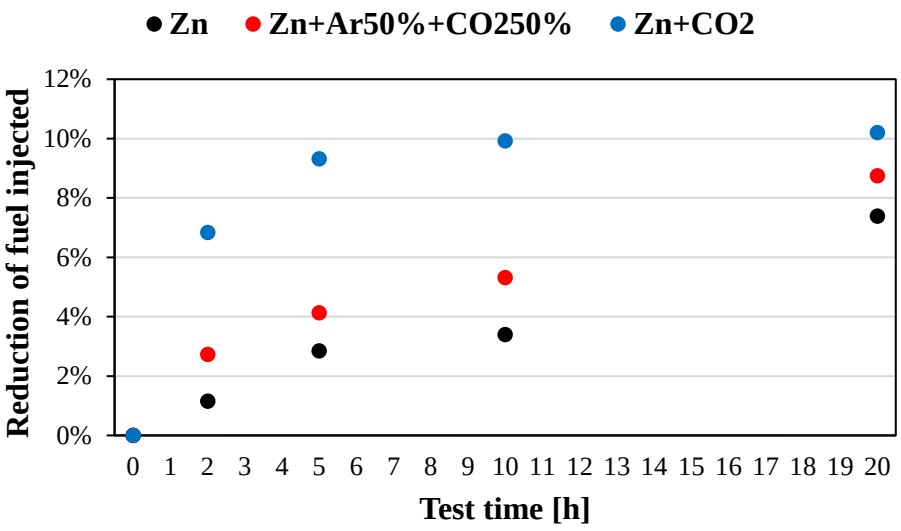

Fig. 4.29 Fuel injected difference at 480 µs.

Fig 4.27-4.29 show the relations of fuel injected with time in different information as amount of fuel injected, relative fuel injected and reduction of fuel injected. At 480 µs, the amount of fuel injected under the use of CO_2 are less that argon in all cases. It is found that fuel injected decreases continuously from 0 to 20 h. with the faster reduction rate in the early period. At 20 h., the maximum reduction of fuel injected is found in pure CO_2 condition at 10% while 9% and 7% in 50% and 0% of CO_2 conditions, respectively.

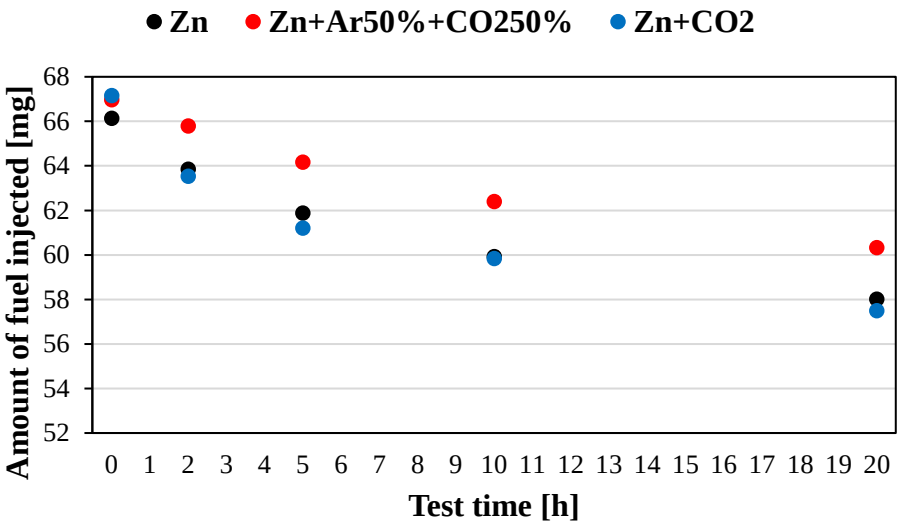

Fig. 4.30 Amount of fuel injected at 1,000 µs.

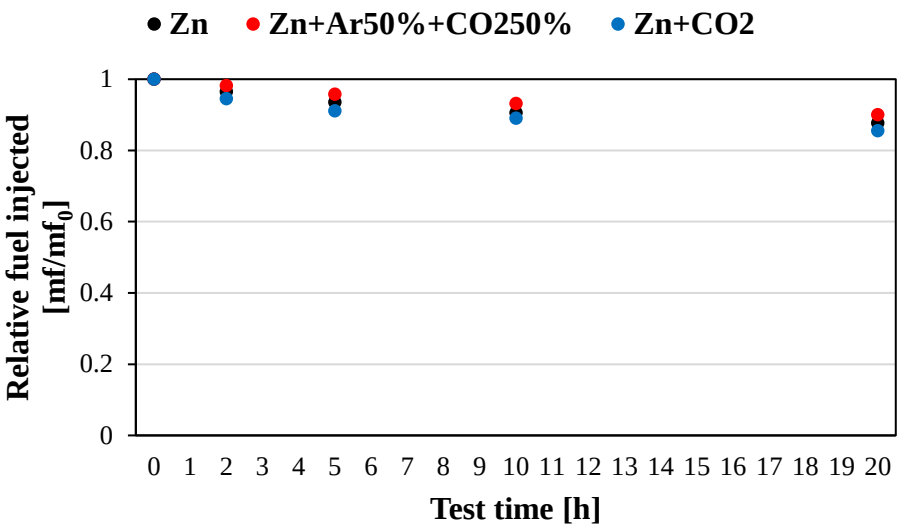

Fig. 4.31 Relative fuel injected amount at 1,000 μs.

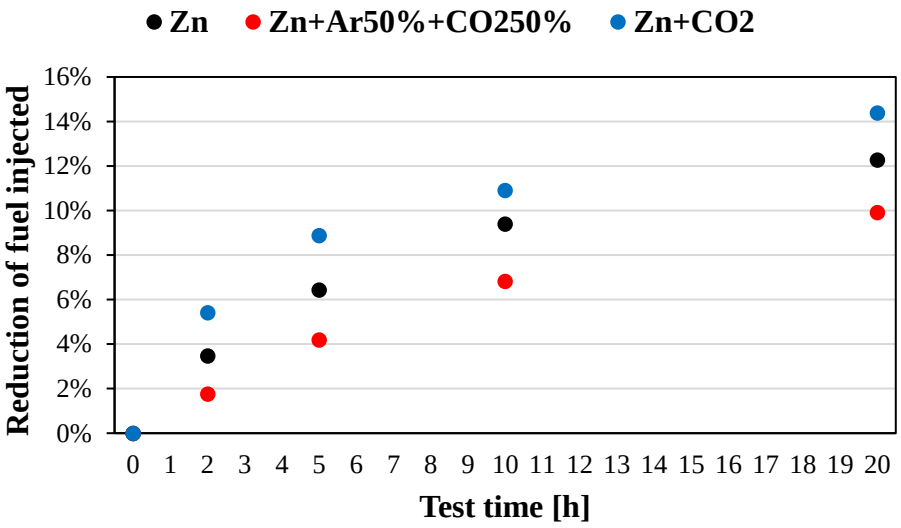

Fig. 4.32 Fuel injected difference at 1,000 μs.

Fig 4.30-4.32 show the reduction of fuel injected with time in all cases. The most strongly drop in fuel injected is pure CO_2 condition as 14% of fuel injected. The effect of injection duration at 1,000 μs bringing of the different results from 480 μs. It is found that the reduction of fuel injected in pure argon condition is larger than 50% of CO_2 condition. This could be assumed as the effect of flow characteristics inside the nozzle hole is bigger than inside injector in fully open of the needle lift condition.

4.3.2 Deposit Analysis by Means of the EDS Technique

Fig. 4.33-4.44 show characteristics EDS-spectra of the deposits at nozzle hole of each test conditions, as shown in Table 4.6. The nozzle hole deposits are observed at three different area as inlet, middle and outlet of the nozzle hole.

Table 4.6 List of tested injectors.

Injector No.	Seat temperature (°C)	Ambient gas	Fuel additive	Test duration (h)
No. 1	350	Argon	None	20
No. 2			Zinc	
No. 3		*Argon + CO_2	None	
No. 4		CO_2		

*Ar 50% + CO_2 50%

[Nozzle no.1: 01P21216: inlet / middle / outlet]

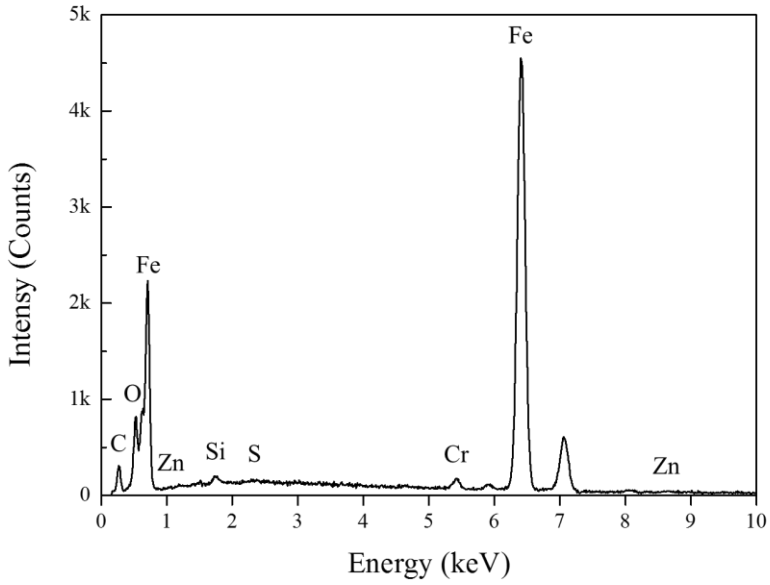

Fig. 4.33 Characteristic EDS-spectra of injector no.1 at the inlet of hole.

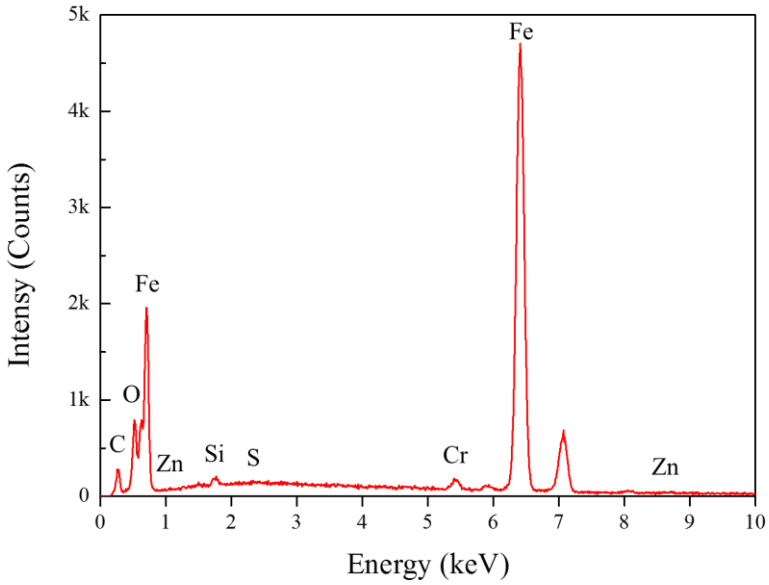

Fig. 4.34 Characteristic EDS-spectra of injector no.1 at the middle of hole.

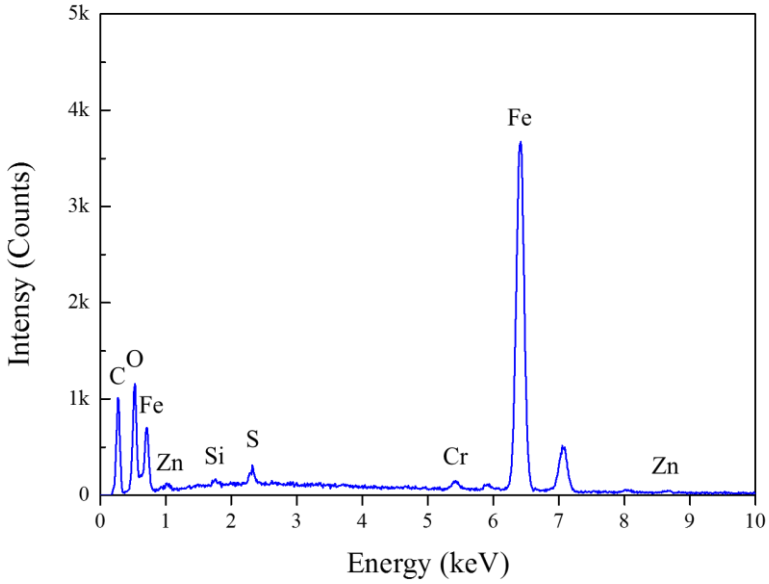

Fig. 4.35 Characteristic EDS-spectra of Injector no.1 at the outlet of hole.

[Nozzle no.2: 01P23447: inlet / middle / outlet]

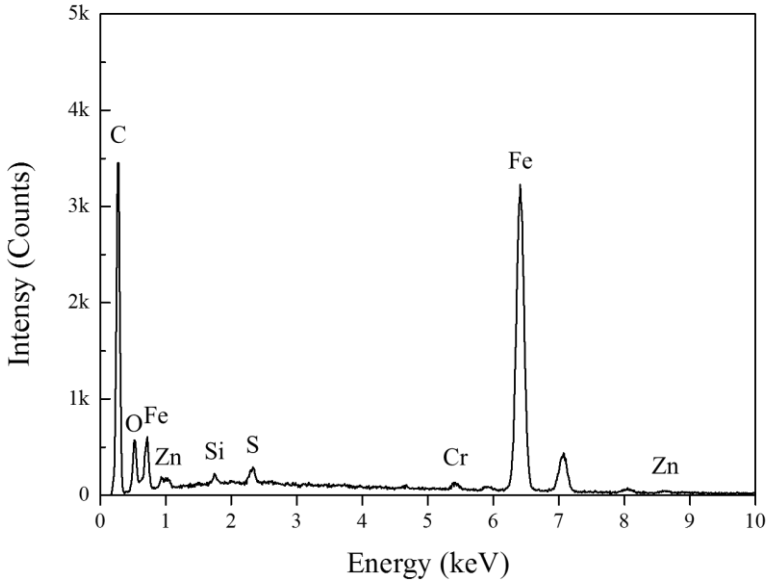

Fig. 4.36 Characteristic EDS-spectra of injector no.2 at the inlet of hole.

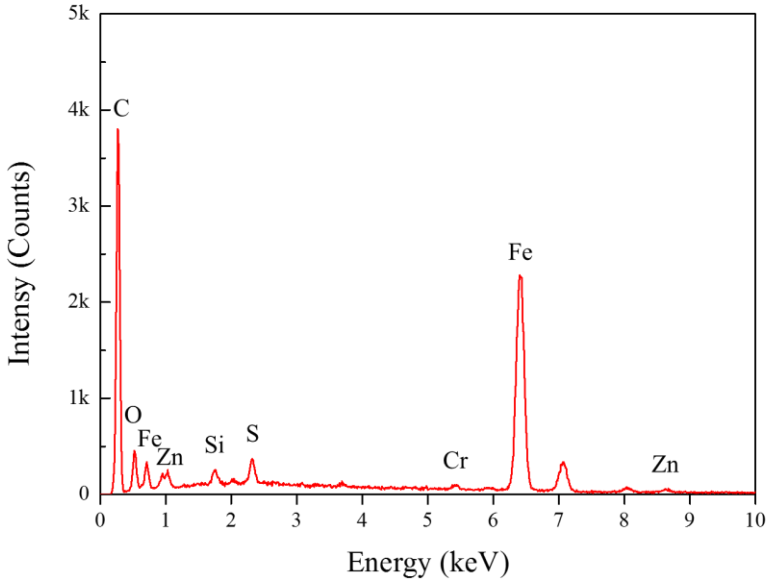

Fig. 4.37 Characteristic EDS-spectra of injector no.2 at the middle of hole.

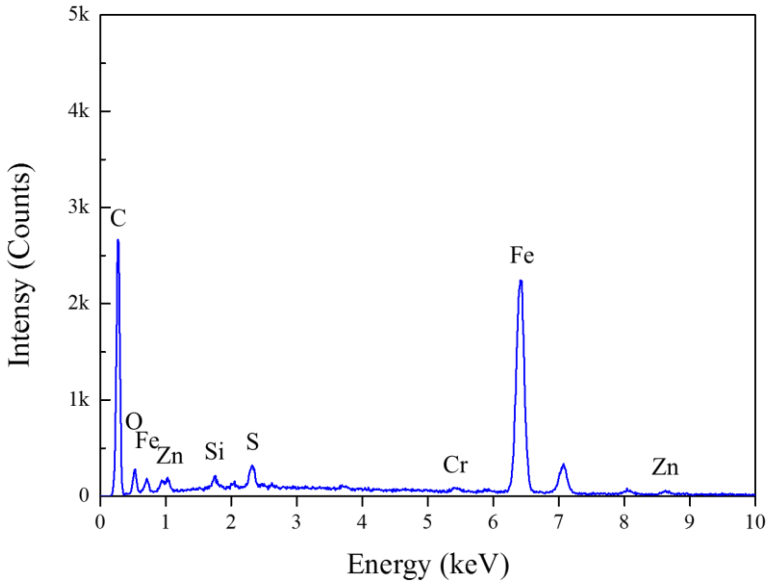

Fig. 4.38 Characteristic EDS-spectra of injector no.2 at the outlet of hole.

[Nozzle no.3: 10N00725: inlet / middle / outlet]

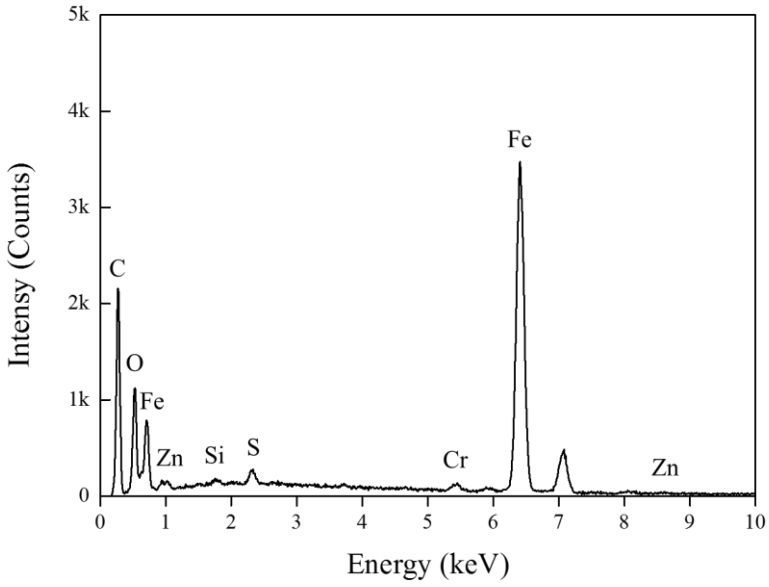

Fig. 4.39 Characteristic EDS-spectra of injector no.3 at the inlet of hole.

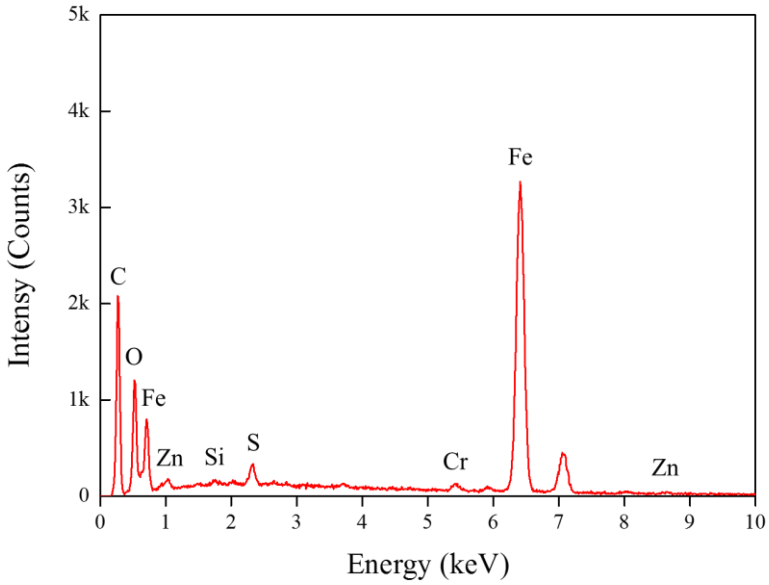

Fig. 4.40 Characteristic EDS-spectra of injector no.3 at the middle of hole.

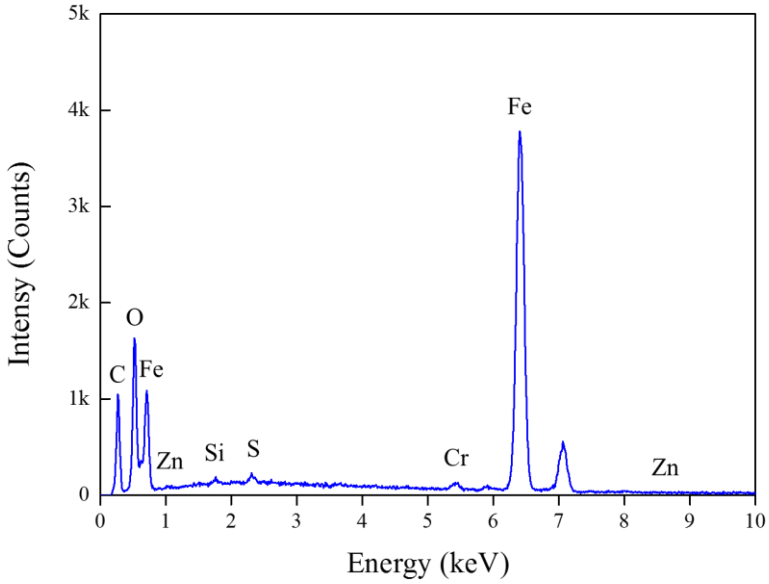

Fig. 4.41 Characteristic EDS-spectra of injector no.3 at the outlet of hole.

[Nozzle no.4: 01P23462: inlet / middle / outlet]

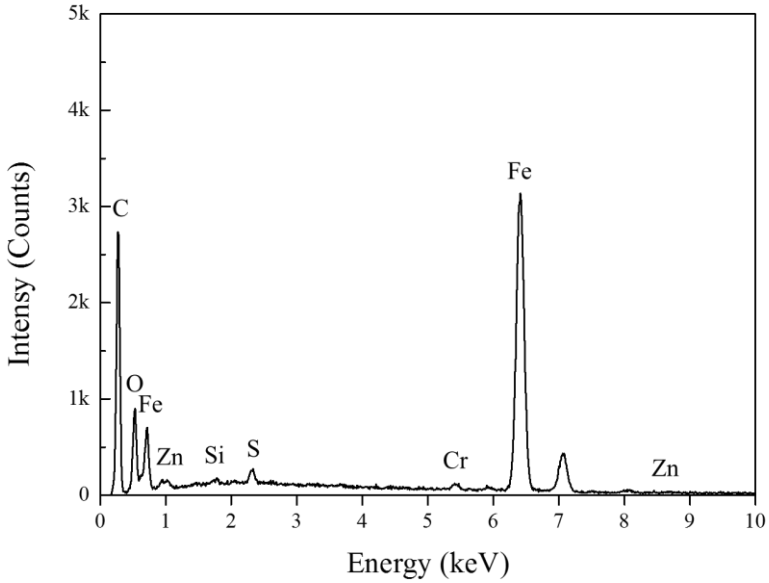

Fig. 4.42 Characteristic EDS-spectra of injector no.4 at the inlet of hole.

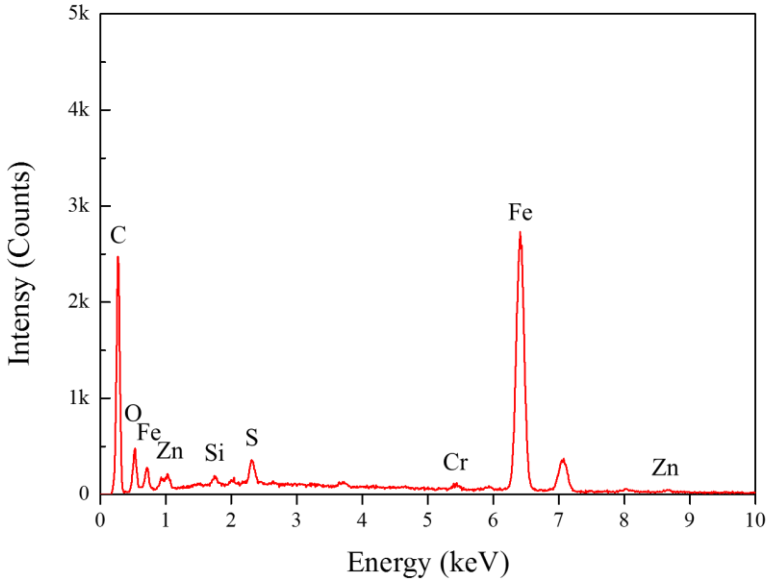

Fig. 4.43 Characteristic EDS-spectra of injector no.4 at the middle of hole.

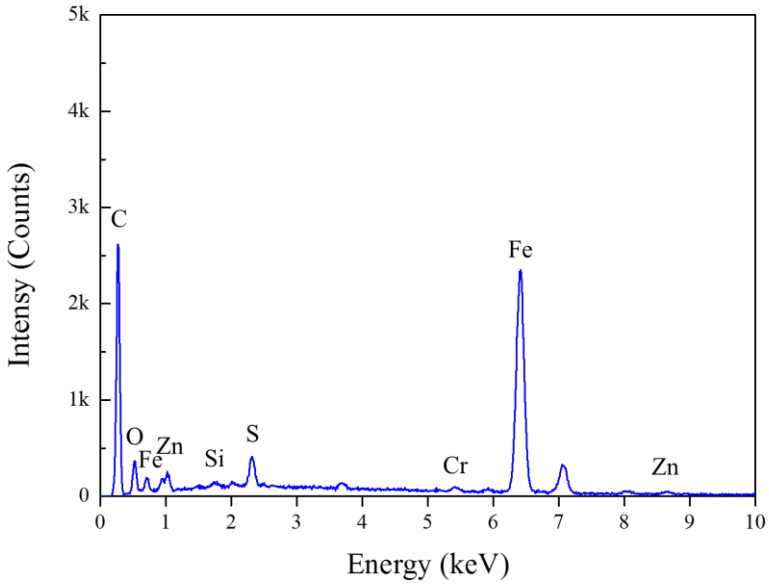

Fig. 4.44 Characteristic EDS-spectra of injector no.4 at the outlet of hole.

The EDS-spectra of deposits on the nozzle hole are realized in order to obtain quantitative information on the elemental constituents. The tests are performed 4 injectors with the different test conditions. The refracted wave intensity, which is reported on the ordinate, depends on the specific response of the element to the electron beam and is proportional to the concentration of such an element in the area under observation.

Experiment with increased concentrations of CO_2 as an ambient gas are carried out. The results concerning the deposits composition are shown in Fig. 4.33-4.44. Significant quantities of carbon have been determined. The carbon originated from the decomposition of fuel hydrocarbon and from base material of the nozzle can be seen in the results of injector no.1 (01P21216). In fact, the analysis of the EDS in the flow direction inside the nozzle hole from inlet towards outlet revealed a slightly different due to the inhomogeneous compounds of deposits.

The increment of CO_2 concentrations shows obvious results using EDS observation. The peaks of carbon increase corresponding to CO_2 concentrations. This can be concluded that CO_2 concentration promotes the formation of nozzle hole deposits.

Finally, the experiments carried out on the non-combustion test machine have shown a significant formation of nozzle hole deposits. This resulted in a reduced efficiency of diesel injector.

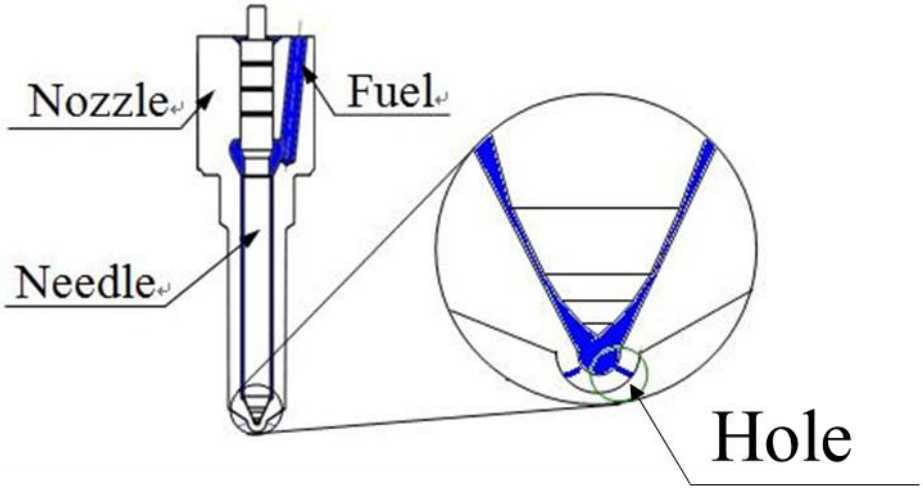

Fig. 4.45 Schematic diagram of fuel flow in injector nozzle.

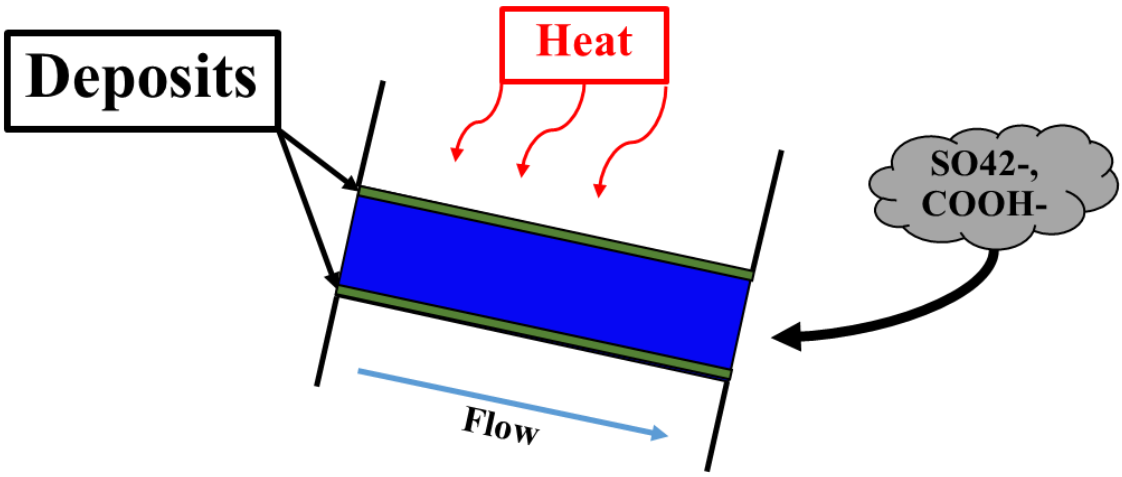

Fig. 4.46 Schematic diagram of deposit formation in injector nozzle hole.

The deposits formation which has been investigated in chapter 4.2 and 4.3 can be explained as shown the following mechanism, in Fig.4.45-4.46. The use of Zn additive on actual engine for preventing wear and deformation are applied to be the deposit accelerator in this research. The increasing injection pressure of new generation fuel injection system causes the increment of temperature in the system as well. These make the fuel easy to deteriorate, decompose and vaporize. At the end of injection stage, residual fuel in the nozzle hole absorbs heat from the combustion stroke and starts to vaporize. Heavy and sticky molecules from the fuel such as carbon, zinc, and sulfur adhere to the nozzle hole surface by physical force and become deposits. In addition, the deteriorated and decomposed fuel interact with combustion gases containing CO_2, SO_4^{2-}, and $COOH^-$ then result in mineral salts and carboxylate compounds, in particular $ZnCO_3$.

4.4 Effect of Time Between Injection on Deposit Formation

Although many dominant factors were proposed in previous research, the time between injections has never been investigated and studied yet. In this study, the effects of time between injections and number of injections on the deposit inside the nozzle hole and the effects of the deposition on injection and spray characteristics were investigated with an injector testing device, which was constructed based on a commercial common-rail injection system.

4.4.1 Methodology and Results

To investigate the effect of the time interval between injections on injection rate and spray characteristics, the body seat temperature was set to 350 ºC by electric heaters around the nozzle. The fuel tank temperature was controlled at 75 ºC, while injection pressure and duration were 180 MPa and 480 μs, respectively. Thus, we tried to put as much thermal stress on the fuel as possible. In order to prevent unwanted ignition and degradation of the fuel, argon gas was purged into the chamber under 1.5 bar at 1 liter/min. A list of controlled parameters is shown in Table 4.7. Commercial diesel fuel was used in the experiment with the addition of zinc in the form of zinc neodecanoate (zinc salt) as an additive. For all test conditions, zinc was added into the fuel at a concentration of 15 ppm as it functions to accelerate the formation of deposits in the fuel injection system [18-19].

Table 4.7 Test conditions.

Fuel	Additives	HFRR
	Acid	400 μm
Injector model	G3S	
Nozzle	0.11 mm diameter x 8 holes	
Nozzle seat temperature	350 °C	
Injection pressure	180 MPa	
Injection duration	480 μs	
Pump speed	1,400 rpm	
Purge gas	1 L/min of Argon	
Test time	20 hours	
Interval	At 2, 3, 5 and 10 hours	

Table 4.8 Test conditions for effect of time between injection.

Condition	Rotational speed of fuel supply pump (rpm)	Test duration (h)	Number of injection (Times)
A	700	0	0
B		10	210,000
C		20	420,000
D	1,400	0	0
E		5	210,000
F		10	420,000

The study in this part focuses on deposits inside the nozzle hole of a diesel injector. The deposit which occurs at the fuel injection equipment, particularly inside the nozzle hole, directly affects the injection characteristics of the injector and leads to power loss during long term operation in the actual engine. The intended investigation on the fuel additive parameter is desired to blend zinc into the fuel tank at a 15 ppm concentration to precipitate the formation of deposits. The cut nozzle will be observed by SEM technique to understand the morphology of the deposits in the nozzle hole, as shown in Fig. 4.47. Also, the cut nozzle will be observed with EDS and ATR-FTIR to investigate the chemical properties of the deposits in the nozzle hole.

The injector is operated at the F condition as shown in Table 4.8. The rotational speed of the fuel supply pump is controlled at 1,400 rpm. The injection pressure and duration are 180 MPa and 480 μs, respectively. Argon gas is purged into the injection chamber to prevent the degradation and ignition of diesel fuel. The total time for this test is 10 hours.

The results of SEM images of the cross-sectional nozzle clearly show a black region of the nozzle hole surface, which could be confirmed as the presence of deposits covering the nozzle hole surface. It is considered that the fuel has been deteriorated by the heat from the body seat to form deposits on the nozzle hole surface.

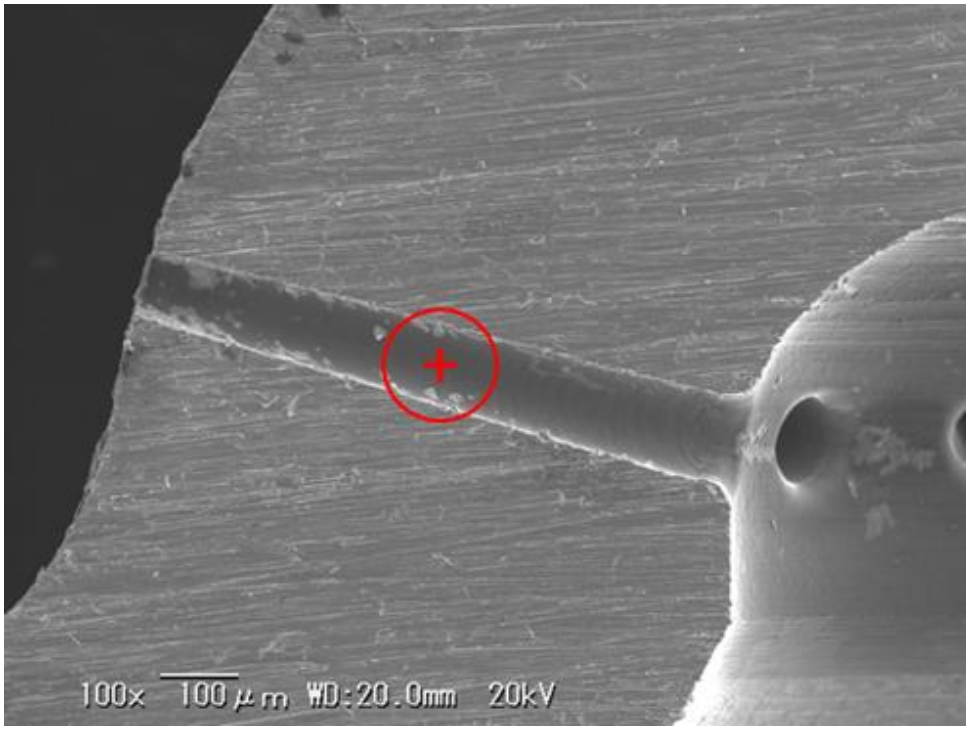

Fig. 4.47 Observed location of nozzle hole deposit.

The cross-sectional cuts of the new (before test) and tested (after 10 h of heated injection test under 1,400 rpm, F condition) nozzles were observed by the EDS technique to compare the presence of Zn element on the nozzle hole surface, as shown in Fig. 4.48(a) and Fig. 4.48(b), respectively. The received EDS-spectra displays qualitative information about the nozzle hole deposits. The values of the y-axis correlation are a function of the element-specific response to the primary electron beam and the concentration of the element in the area under observation. The peak of zinc in EDS-spectra can be used to ensure that the use of zinc as the fuel additive causes the fouling of the injector and reduction of the fuel injected. Metallic elements such as iron (Fe), silicon (Si), and chromium (Cr) are reported as the main components of the nozzle when compared to the EDS results in Fig. 4.48(a) and Fig. 4.48(b) of the peaks of Zn and Fe, the peak of Zn in Fig. 4.48(b) increases with the significant value. The peak of Zn is rarely observed, in contrast to the result in Fig. 4.48(a), which refers to the previously tested nozzle. Therefore, this can imply deposits formed in the presence of zinc at 15 ppm within the doped fuel.

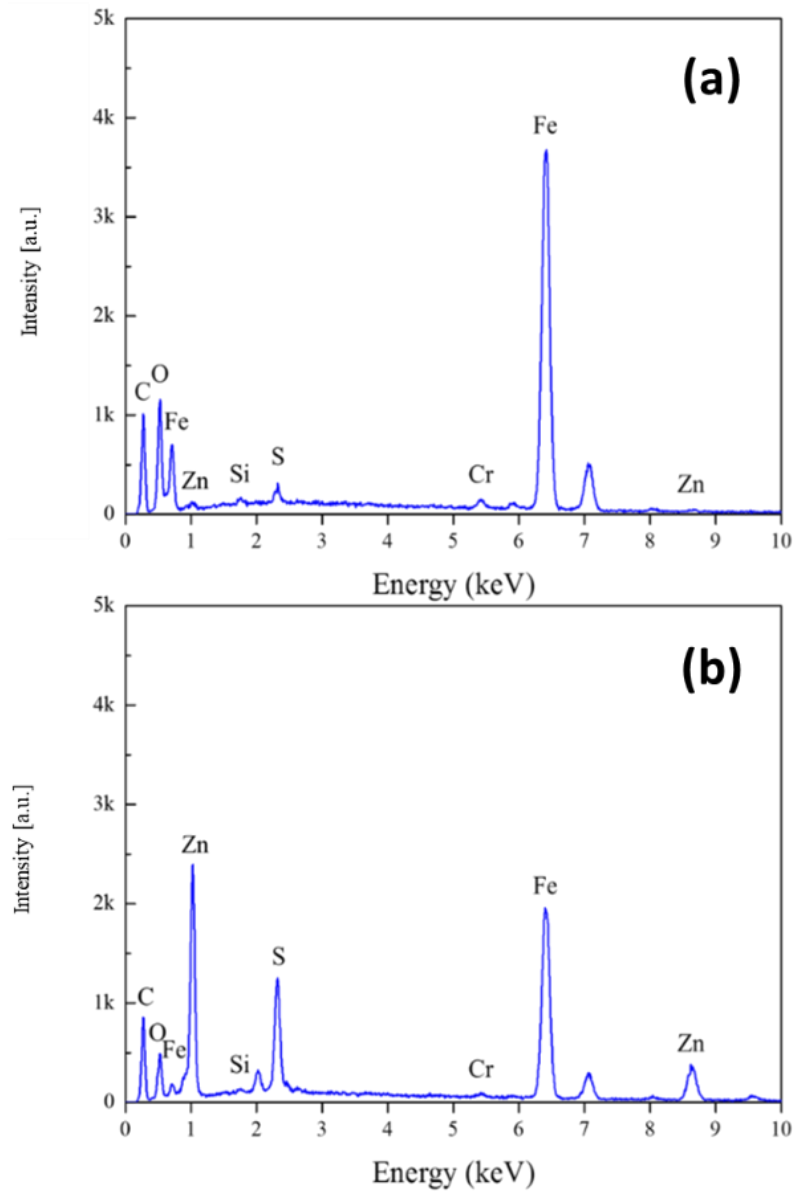

Fig. 4.48 EDS Spectra of nozzle hole deposits: (a) Before and (b) After test.

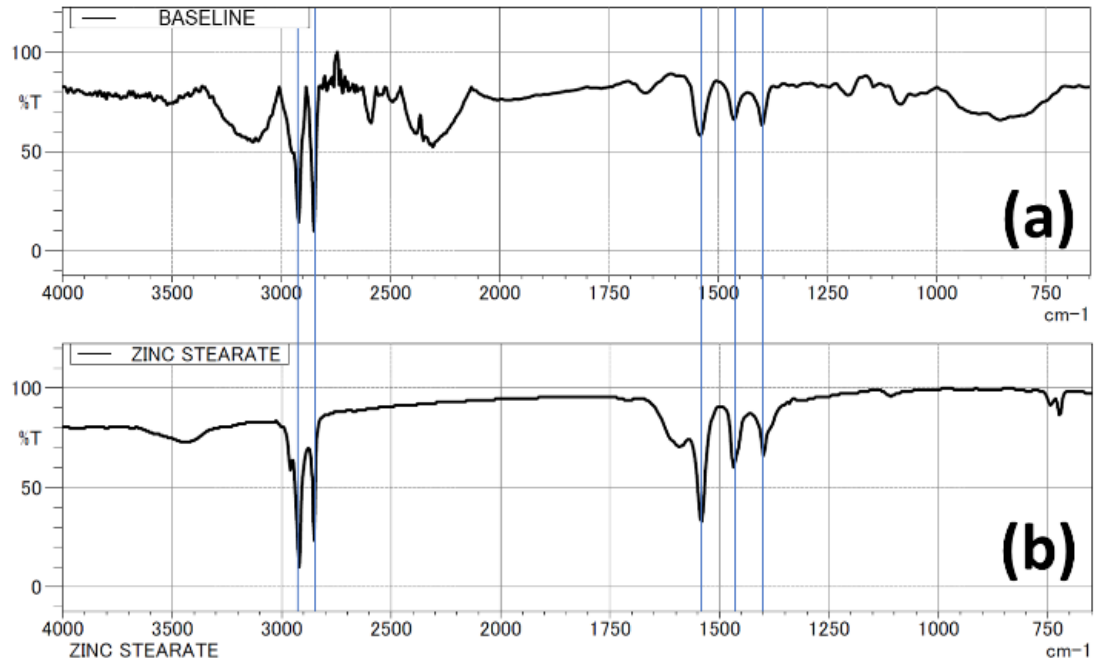

Fig. 4.49 FITR spectra of nozzle hole deposits: (a) Tested nozzle and (b) Zinc stearate.

The FTIR was introduced to investigate and confirm the formation of the deposit inside the nozzle hole. The zinc which was used as the additive in this research is in the form of zinc salt, neodecanoate. Fig. 4.49(a) shows the FTIR spectra of the nozzle hole deposits of the tested nozzle (after 10 h of the heated injection test under 1,400 rpm, F condition). The FTIR spectra of zinc stearate is shown in Fig. 4.49(b) as a reference. In the details of the FTIR spectra of the nozzle hole deposits, bands connected with structures typical for the deposited surface are observed. That is: a band at approximately 2,917 cm^{-1}, connected with vibrations of associated alkyl groups; a band at approximately 2,849 cm^{-1} connected with vibrations of C-H bonds in alkyl groups; a band at approximately 1,536 cm^{-1} connected with the presence of carboxylate salts; a band at approximately 1,462 cm^{-1} connected with vibrations of methyl and methylene groups; a band at approximately 1,400 cm^{-1} connected with the presence of complex salts. According to the FTIR results in Fig. 4.49(a), zinc stearate or zinc octadecanoate, $Zn(C_{18}H_{35}O_2)_2$, formed at the nozzle hole surface.

4.4.2 Temporal Change of Fuel Injection During Heating Injection Test

From the results in the previous section, it was found that the deposit, as zinc stearate, was found on the surface of the tested nozzle hole. Therefore, the study on the effect of the deposit inside the nozzle hole on the change of the fuel injection characteristics is designed to be conducted.

The influence of a deposit inside the nozzle hole of a diesel injector on injection parameters is the topic of this section. The deposit that forms at the fuel injection equipment, particularly inside the nozzle hole, has a direct impact on the injector's fuel injection properties and results in power loss over time in the actual engine. Since the experiment is run in a non-combustion environment, the measurements of fuel injection rate and discharge coefficient (Cd) of the injector are employed to be the indicators of the appearance of deposit in the injector instead of the measurement of power loss of the actual engine. The rotational speed of the fuel supply pump is controlled at 1,000 rpm for the injection rate measurements. The injection pressure and duration are 180 MPa and 1,000 μs, respectively. The reduction of injected fuel can lead to the conclusion of deposit formation.

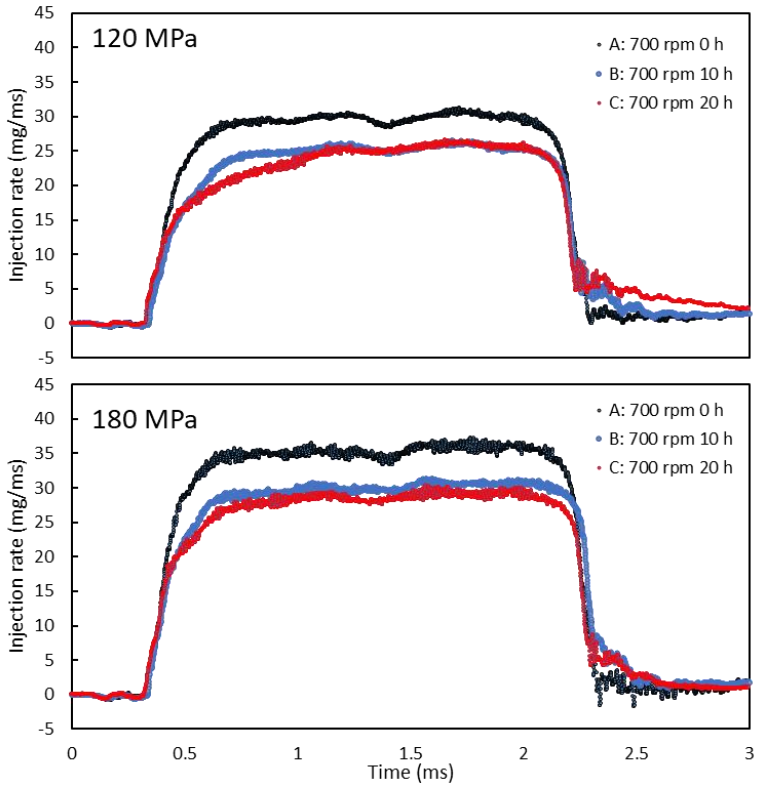

Fig. 4.50 Injection rate of 700 rpm tested nozzle.

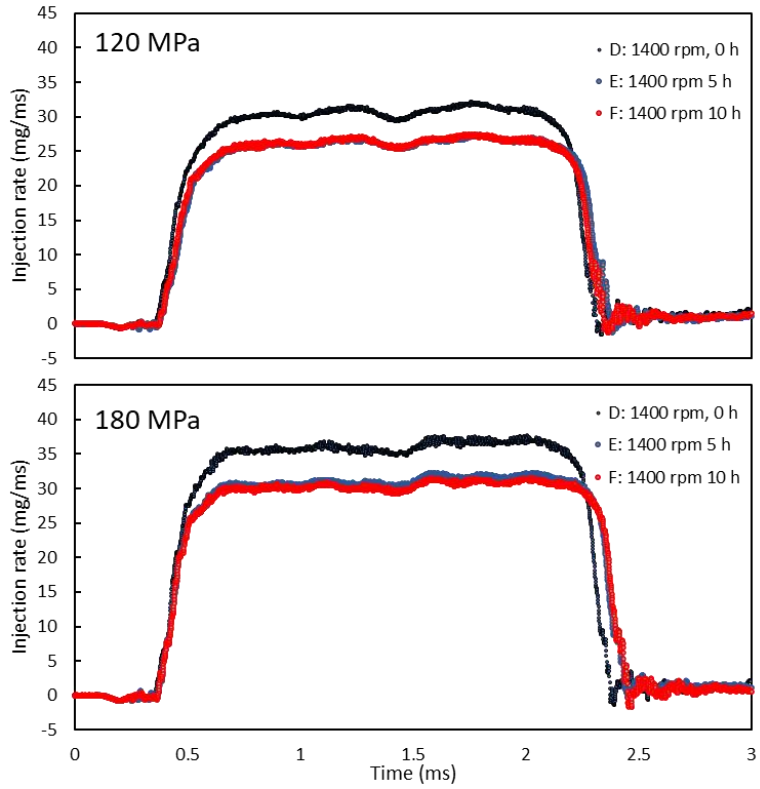

Fig. 4.51 Injection rate of 1,400 rpm tested nozzle.

The injection pressure is concerned because the different injection pressures cause different injector needle-lifts, which strongly affect the flow inside the injector. Therefore, the injected fuel measurement results are shown in two injection pressure conditions at 120 and 180 MPa. To investigate with the same number of injections, the injection rates are observed at 0, 10, and 20 hours for 700 rpm conditions and at 0, 5, and 10 hours for 1,400 rpm conditions. The list of the tested nozzle conditions is shown in Table 4.8. The injection rate results at the test condition of 700 rpm are shown in Fig. 4.50. The injection rate results of the tested nozzle at condition A (the initial condition of the nozzle before the heated injection test) are the highest of all injection pressure conditions. The injection rate results of condition B (at the time of 10 h after the start of the heated injection test) decrease in all cases when compared with the clean nozzle, condition A. The reductions in the injection rate under condition B are 14.72% and 14.95%, at injection pressures of 120 and 180 MPa, respectively. The injection rate results of condition C (at the time of 20 h after the start of the heated injection test) are the lowest of all the injection pressure conditions. At injection pressures of 120 MPa and 180 MPa, the injection rate drops by

16.84% and 19.04%, respectively, under test condition C.

At the test condition of 1,400 rpm, the reductions of injection rate at condition E (at the time of 5 h after the start of the heated injection test) are 14.31% and 15.93% at injection pressures of 120 and 180 MPa, respectively. The reductions in injection rate at condition F (at the time of 10 h after the start of the heated injection test) are 10.39% and 11.06% at injection pressures of 120 and 180 MPa, respectively, as shown in Fig. 4.51. The differences in rise/fall time and shape can be seen in all injection pressure conditions, especially at condition F (at the time of 10 h after the start of the heated injection test), which also has the lowest injection rate.

These results can be addressed as the effect of the deposit formation inside the nozzle, which increases with test duration. The formation of deposits inside the nozzle hole reduces the nozzle hole diameter. Therefore, the effective hole diameter and effective flow area are reduced. This leads to a lower injection flow rate at the steady flow of the injection. The longer injection duration in this test was caused by the partial obstruction of the nozzle. When the deposit forms inside the nozzle hole, it reduces the effective flow area of the fuel. With the same boundary conditions (injection pressure and energized duration), the less flow area blocks the fuel flow in the fuel passage. It results in the increase of the back pressure inside the sac chamber and affects the nozzle closure phase. Therefore, the prolonged effect of the injection duration is found in the injection rate results of the tested nozzles [33-34].

The study by Yabe et al. [35] can support the explanation of the phenomenon of the fuel flow inside the nozzle. This work explains modifications in fuel injection characteristics brought on by heating tests. Following that, a more thorough analysis of the phenomenon that occurred in both nozzles will be done after both nozzles' performance changes and the appearance of deposit accumulation on the needle part as a result of the heating test are taken into account.

The body seat wears and deforms as a result of the needle being pressed against it at high speed while the nozzle is heated for an extended period of time while spraying. Additionally, as fuel is injected under high heat, deposits build up inside the nozzle, and internal erosion from cavitation occurs. Surface erosion has been found to have a significant impact on large engines, such as ships, and deposit accumulation to have a significant impact on small diesel engines [27]. This is due to the fact that a large diesel

engine rotates at a slower speed than a small one and injects more fuel per injection. Since both the atmospheric pressure and the injection pressure may be low, erosion and cavitation may both take place in such circumstances. On the other hand, small diesel engines use high-pressure fuel injection and need high-speed fuel atomization because of their high-speed rotation. Because of this, even though less cavitation is produced, the temperature inside the nozzle increases, which makes it simpler for the fuel to go through thermal denaturation. Large diesel engines have started using high-pressure injection as a preventative measure, and the issue of surface erosion and high heat has been solved by implementing a nitriding nozzle and an oil cooling structure. As mention in the previous chapter, it has been demonstrated that the deposit accumulation can be prevented by coating the nozzle with DLC as well.

The results for low lift (42 μm), medium lift (170 μm), and high lift (300μ m) are presented as a represent of deposit formation inside the nozzle. These results include the pressure distribution, turbulence, gas phase distribution, and an examination of the fuel flow. Following that, the flow rate coefficient and porosity for the entire opening and closing operation are displayed, and the flow direction vector diagram at the conclusion of injection and the porosity distribution are used to further the analysis. Based on these findings and the behavior at injection pressure of 180 MPa), it will be discussed why the fuel fluidity change and flow rate coefficient behavior that accompanied the heating test.

The pressure distribution of the outcomes of the numerical analysis under various circumstances is shown in Fig. 4.52. In this analysis, the analysis display primarily spans from the sack to the nozzle hole's center.

According to these findings, a low needle lift has the effect of bending the fuel flow, sending the fuel into the injection hole, and creating a pressure difference on the side of the sack. At high lift, this effect is diminished. The distance of the needle lift, which symbolizes the deformation and deposit formation on the nozzle surface, determines the phenomenon of the various fuel pressures. Additionally, a change in pressure inside the sack was noticed. This is thought to be the result of a decrease in speed when the fuel flow direction is bent inside the sack.

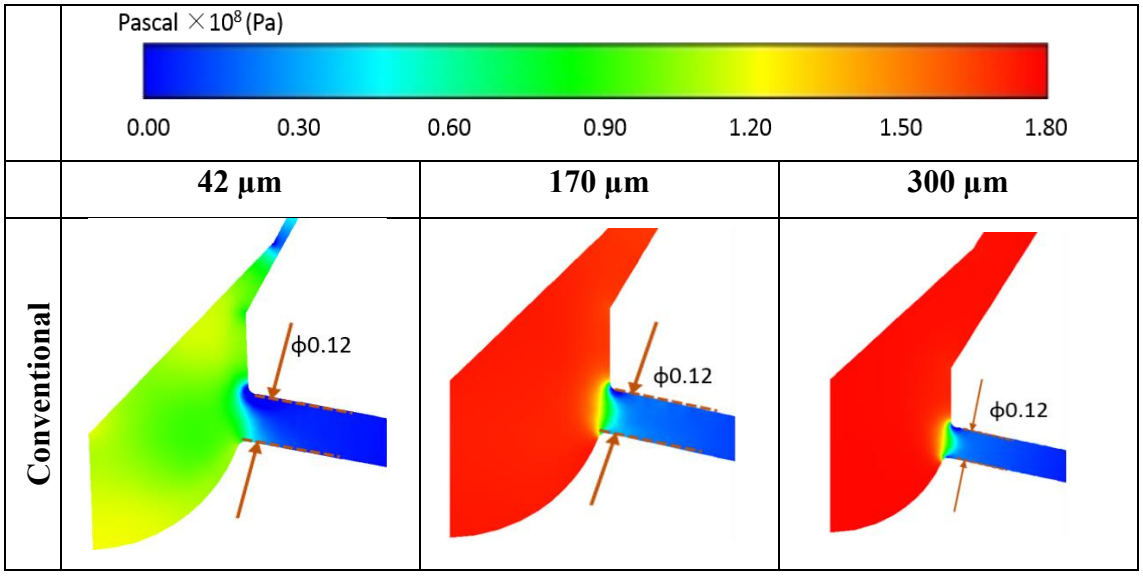

Fig. 4.52 Results of pressure analysis under 180 MPa.

The results of the turbulent flow analysis are shown in Fig. 4.53 (left). As a result, under all circumstances, the lower part of the injection hole inlet had a higher likelihood of experiencing turbulence than the upper part, and at low opening, the turbulent flow formation area grew and the maximum value tended to rise. At the bottom of the injection hole at low opening, the turbulent flow from above collides with the turbulent flow from the bottom of the bag. When the needle moves upward, this tendency vanishes.

The analysis of the fuel flow direction and velocity is shown in Fig. 4.53 (right). Depending on the opening, the flow's separation position from the needle's side to the injection hole's side changed. With the increase in needle lift, the separation position moved to the bottom of the sack. The results of the formation region and the degree of the gas phase region are shown in Fig. 4.54. To maintain the viewpoints, the generation of cavitation above and below the injection hole is seen here on the plane of symmetry. Even if the gas phase region in the figure from the symmetrical plane is only generated on the upper surface or only on the lower surface, cavitation is still visible on the side, but the situation is unbalanced. Here, cavitation can be generated on the side if it occurs above and below the injection hole inlet, and the difference in the amount of formation inside is minimal. Therefore, if cavitation occurs above and below the nozzle hole, deposits can be removed effectively.

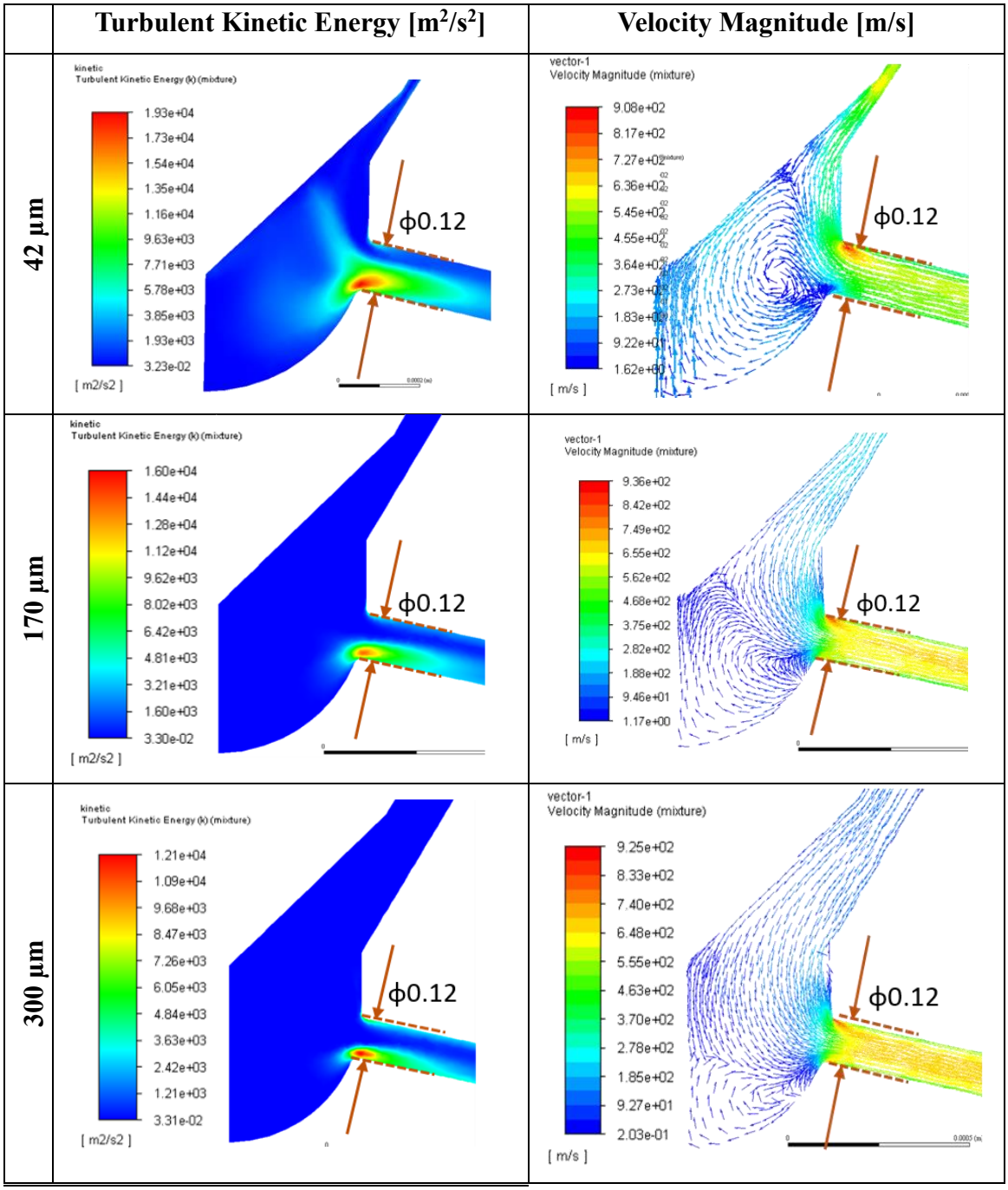

Fig. 4.53 Results of turbulent energy analysis (left), flow direction and speed analysis under 180 MPa (right).

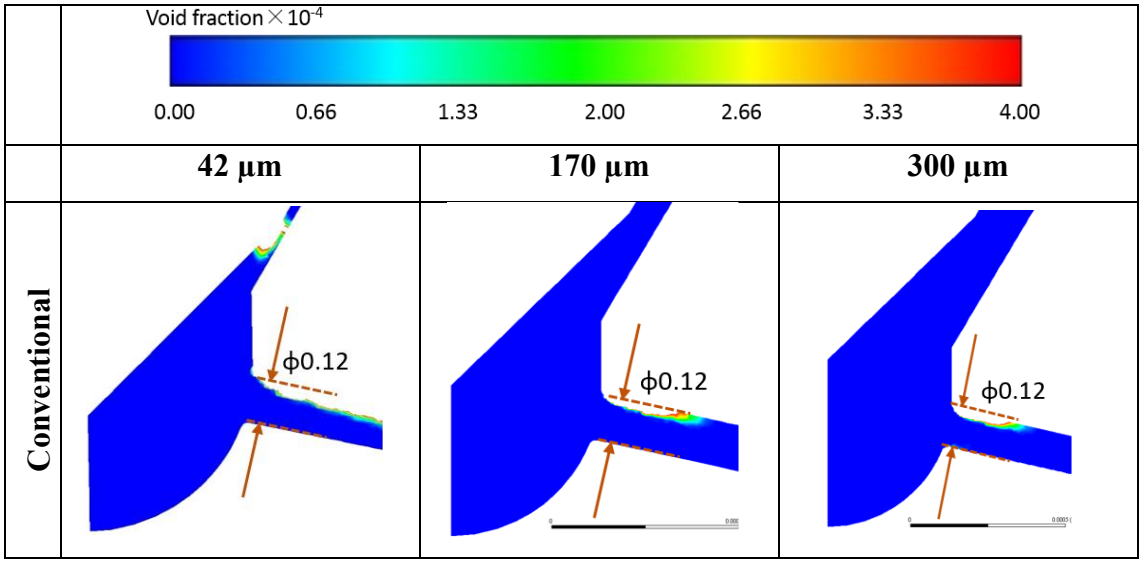

Fig. 4.54 Results of void fraction area analysis under 180 MPa.

In Fig. 4.54, similar to the chamfer radius, the areas where the gas phase may exist are highlighted in red, and the areas with the most cavitation are those with white spots. A significant amount of gas phase area was seen in the conventional nozzle at the upper portion of the injection hole entrance at the start of opening. As a result, it is believed that a significant amount of cavitation is produced at the start of injection. In Fig. 4.53 (right), at the start of injection, the flow from the center of the sack merges with the one on the injector side, suppressing the bending of the flow around the injection hole and facilitating cavitation on the injection hole side. Additionally, even as the degree of opening increased, the tendency that there were more gas phase regions on the upper surface of the nozzle hole than on the lower surface remained unchanged

From the entire explanation, it can be inferred that the change of the inside shape of the nozzle, by wear/deformation and deposit, affects the flow inside the nozzle and leads to the worst injection characteristics of the nozzle.

4.4.3 Effect of Elapsed Time and Accumulated Injection Number During Heating Injection Test on Deposit Formation

In order to compare the effects of different times between injections on diesel injector nozzle deposits, the discharge coefficient, Cd, has been introduced as an injection efficiency indicator. Fig. 4.55 shows a comparison of normalized Cd by the initial value before test of all test conditions under the injection pressure and the injection duration at 180 MPa and 1,000 μs, respectively. The Cd of the unused nozzles, before the accelerated deposit formation test, are at the same highest values, above 0.85. The Cd of both the 700 and 1,400 rpm conditions decreases by 17.7% and 14.0%, respectively, after 210,000 injections. case of the number of injections at 420,000 times, the Cd of 1,400 rpm condition decreases by 15% while the Cd of 700 rpm condition further decreases by 19%.

Fig. 4.56. shows the comparison of normalized Cd and test duration. It can be seen that there is the same tendency for both Cd values of 700 and 1,400 rpm. During the first 5 hours of testing, the CD of both the 700 and 1,400 rpm conditions rapidly decreases. From the test duration of 5 to 20 h, the Cd of the 1,400-rpm condition slightly decreases until 10 h of test duration. Then it remains constant until 20 h of test duration. In the case of the 700-rpm condition, the Cd constantly decreases until the end of the test. From the Cd results, this can be described as the longer interval between injections promoting more deposit formation inside the injector nozzle hole and leading to the reduction of injection efficiency.

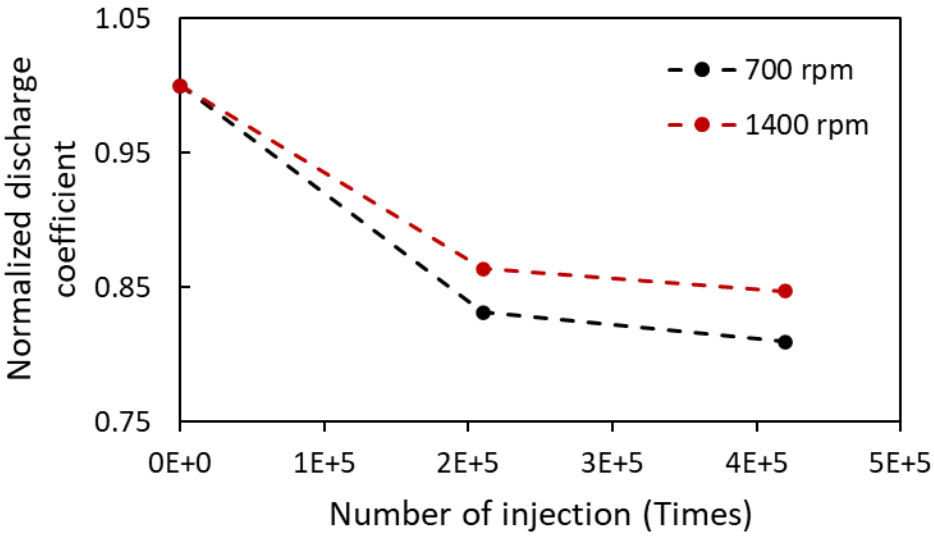

Fig. 4.55 Discharge coefficient at different number of injections.

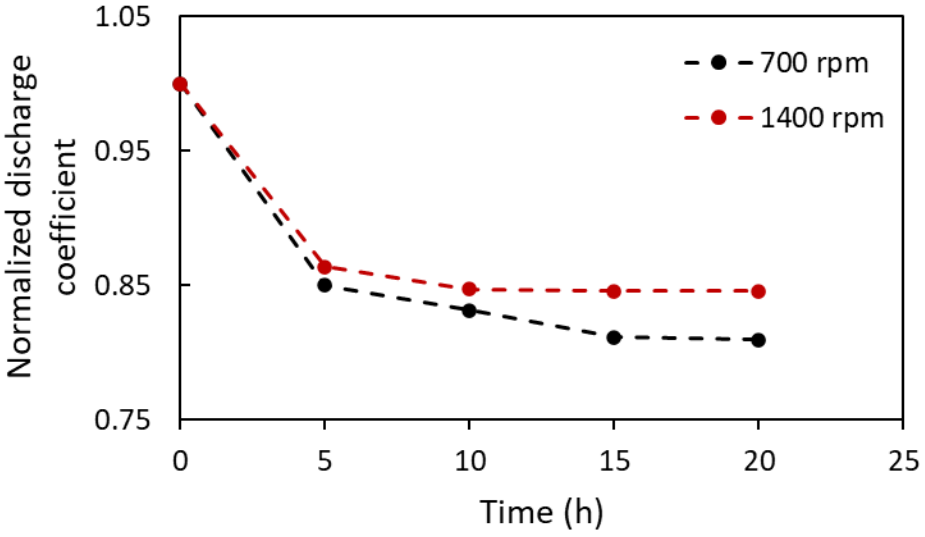

Fig. 4.56 Normalized discharge coefficient at different test duration.

4.4.4 Mechanism of Deposit Formation inside Nozzle Hole

As shown in Fig. 4.57 (a), deposit formation mechanism in the nozzle hole is a complicated process involving physical mechanisms, chemical mechanisms, and mechanical mechanisms. The hypothesis for deposit formation mechanism in nozzle hole is described as a time function.

At the end of injection, the large molecules of the fuel components accumulate and form a deposit precursor with the remaining fuel on the nozzle hole surface. Deposits have formed as a result of the evaporation of liquid components. The surface temperature and the temperature of the fuel close to the surface have a significant impact on this process. The higher density of the fuel components increases their propensity to condense and adhere to the surface of the nozzle hole. These substances serve as precursors to deposit formation [36].

The particle density near the nozzle hole surface increases as evaporation occurs. Strong bonds can be formed between particles. The cohesion effect is caused by the force between the surface of particles and the nozzle hole surface. The deposits continue to grow because of the bonding and accumulation of extra particles from injections [21]. Chemical reactions (pyrolysis, polymerization, carbonization, etc.) may occur when deposits attach to the nozzle hole surface [37, 38]. The chemical reactions are affected by the temperature and the length of time the substances are retained in the reaction. By using electric heaters or high-temperature combustion within the engine, the fuel can evaporate at the nozzle hole's surface. Finally, the deposit forms on the nozzle hole's surface [35].

When the injection signal is energized, the lifting of the needle allows the pressurized fuel to flow through the nozzle passage [39]. The fuel, itself, consists of a deposit precursor. When the injection event stops, the residual fuel and deposit precursor remain in the nozzle hole and cover the nozzle hole surface as a thin layer. The residual fuel requires sufficient time to evaporate and form a deposit. Fig. 4.57 (b) and Fig. 4.57 (c) show the deposit formation mechanism for shorter and longer time intervals between injection conditions, respectively. Compared to the same amount of time, the longer time between injections allows the residual fuel on the nozzle surface to have sufficient time to evaporate and develop to be the deposit precursor [40-41]. This results in more deposit formation than the shorter time between injections.

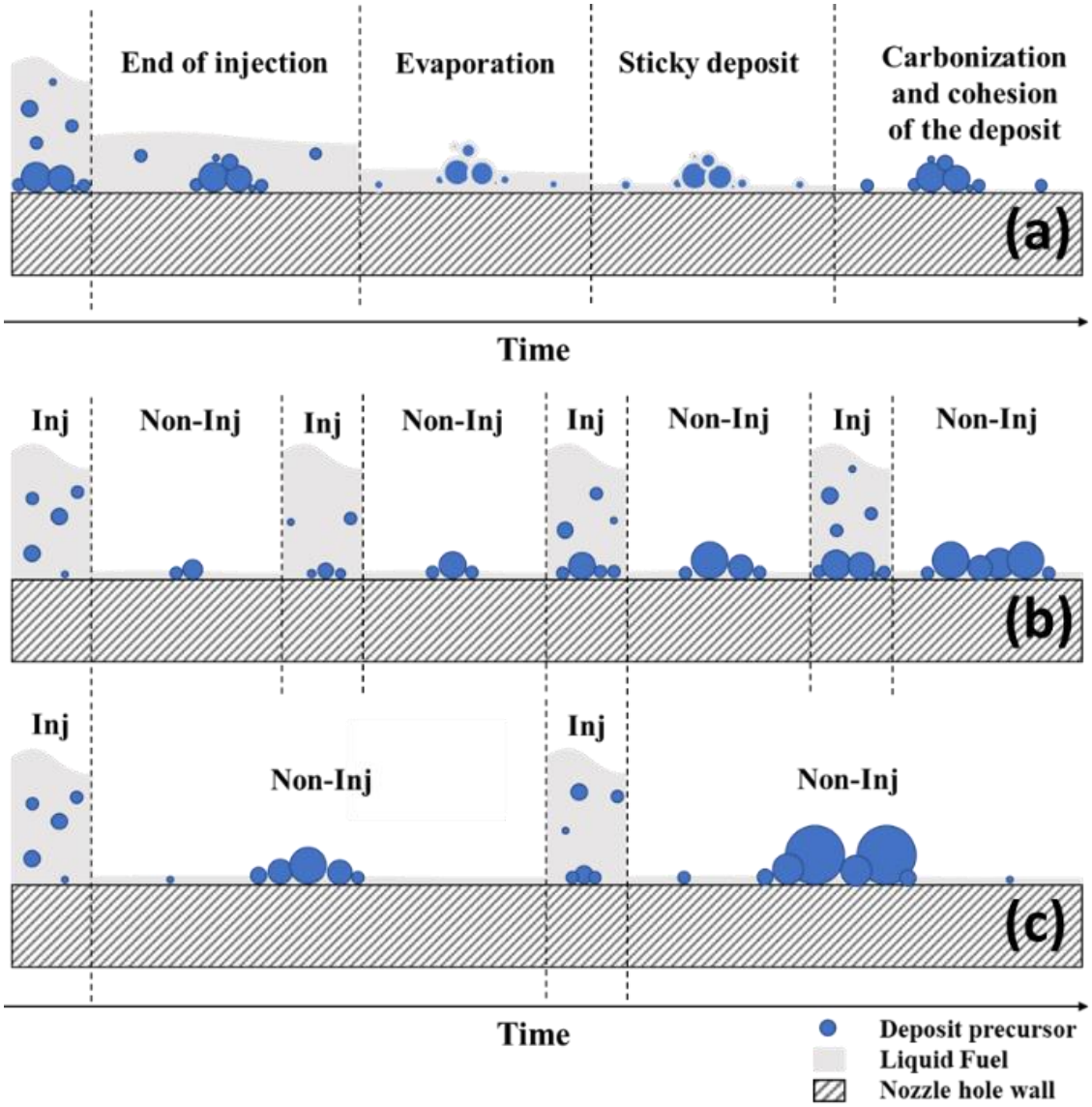

Fig. 4.57 Deposit formation mechanism: (a) Deposit formation hypothesis (b) Short-time and (c) Long-time between injection.

The removal of the nozzle hole deposit can occur due to the cavitation in the nozzle hole. The cavitation inside the nozzle hole also promotes erosion on the nozzle hole surface [42-43]. Although the new design nozzle was introduced to reduce the cavitation inside the nozzle, the cavitation still occurs at the opening and closing periods of the needle [43-44]. From this phenomenon, the formation of nozzle hole deposits is inhibited by cavitation.

4.4.5 Spray Image Analysis

In this section, the effects of nozzle hole deposit on the spray characteristics were investigated in terms of spray penetration, spray cone angle, and spray volume. The experiment was conducted for the nozzles which were used in the heated injection tests at different times between injections with the rotational speed of the pump at 700 and 1,400 rpm. The controlled conditions are 180 MPa of injection pressure, 1,000 μs of injection duration, and 2 MPa of ambient pressure. Fig. 4.58 shows a sequence of spray images of the new and tested injectors at different times after SOI under 700 and 1,400 rpm. At the early stage of the injection, there is an asymmetric distribution of the spray up to 0.2 ms after SOI at all the injection events. This can be the effect of the eccentrical movement of the needle. In addition, the liquid phase of the emerging spray also causes the variation of the spray shape at the early stage of the injection. The spray penetration and cone angle are determined in order to compare the spray development of each test duration. Fig. 4.59 shows the temporal change in spray penetration at different test durations under 700 and 1,400 rpm test conditions. In both 700 and 1,400 rpm conditions, the longer test duration nozzles report a reduction in spray penetration compared with the nozzle before the heated injection test. When the test duration is increased, the penetration decreases in all cases. Finally, the longest test durations (20 h test of 700 rpm and 10 h test of 1,400 rpm) express the greatest reduction of penetration due to the nozzle hole deposit formation.

The results of the spray cone angle are shown in Fig. 4.60. At 700 rpm, the fluctuations are found in the transient phase of the injection at the early injection event. The spray cone angle profiles of 0 and 10 h of test duration show the overlap along the injection event from 0.2 ms, while the profiles of 20 h of test duration are higher than the profiles of 0 and 10 h cases from 0.3 ms to 0.6 ms. As well as the profiles of the 700-rpm test condition, the spray cone angle profiles of the test duration at 1,400 rpm also overlap along the injection event from 0.3 ms in 0 and 5 h cases. The spray cone angle profile of a 10-hour test shows the highest spray cone angle between 0.3 and 0.6 ms.

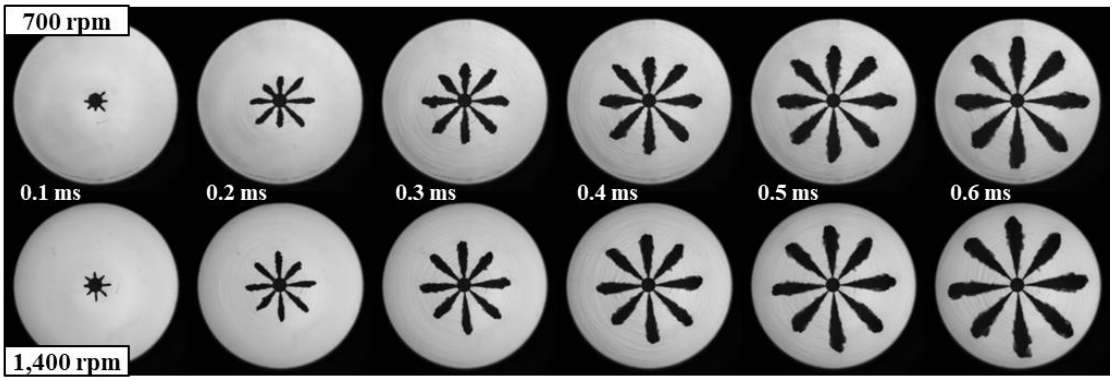

Fig. 4.58 Spray images of 700 (above) and 1,400 rpm (below) test conditions.

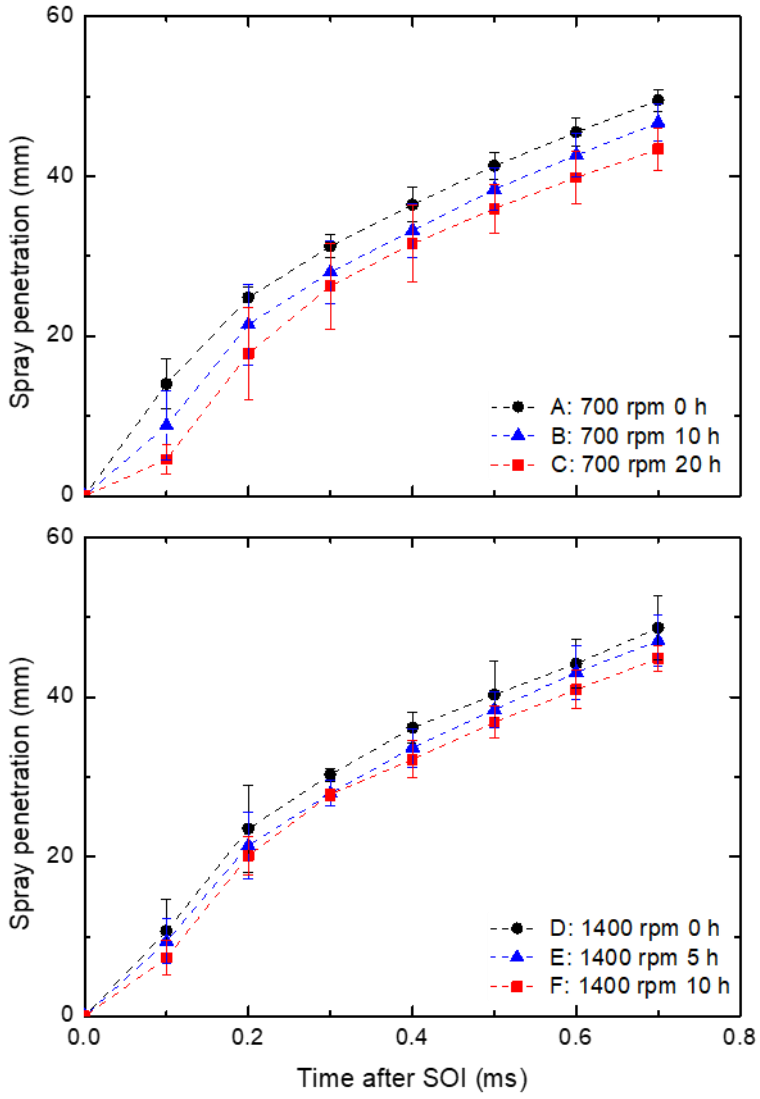

Fig. 4.59 Comparison of spray penetration.

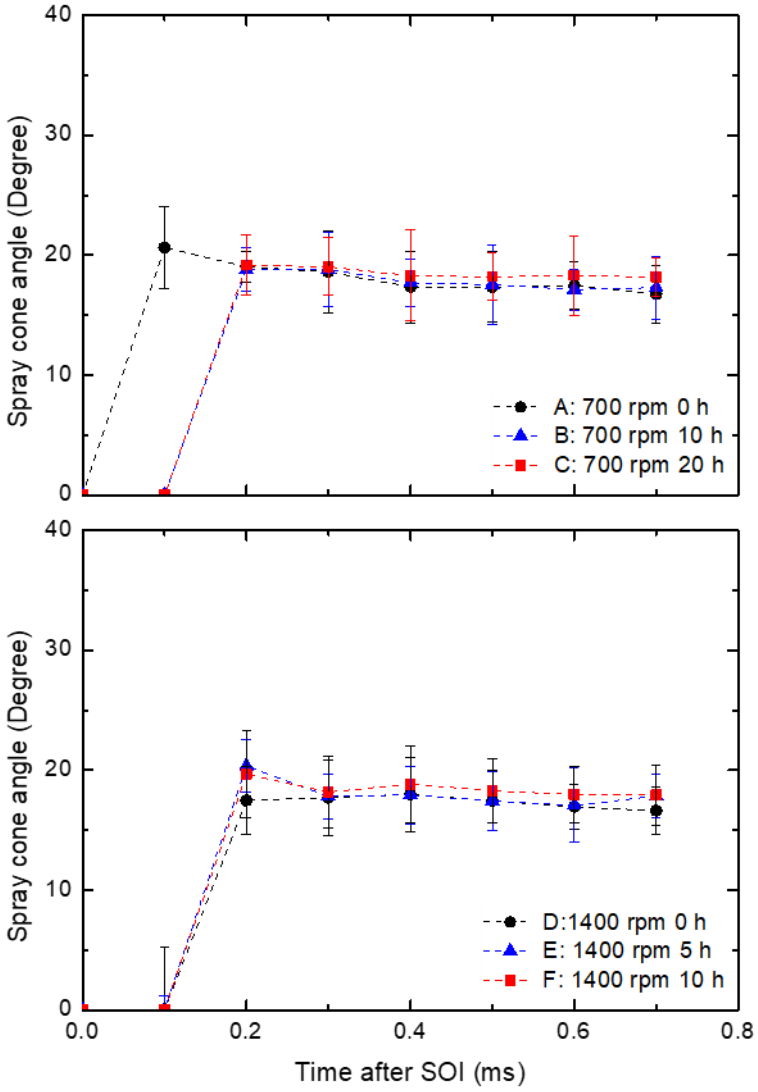

Fig. 4.60 Comparison of spray cone angle.

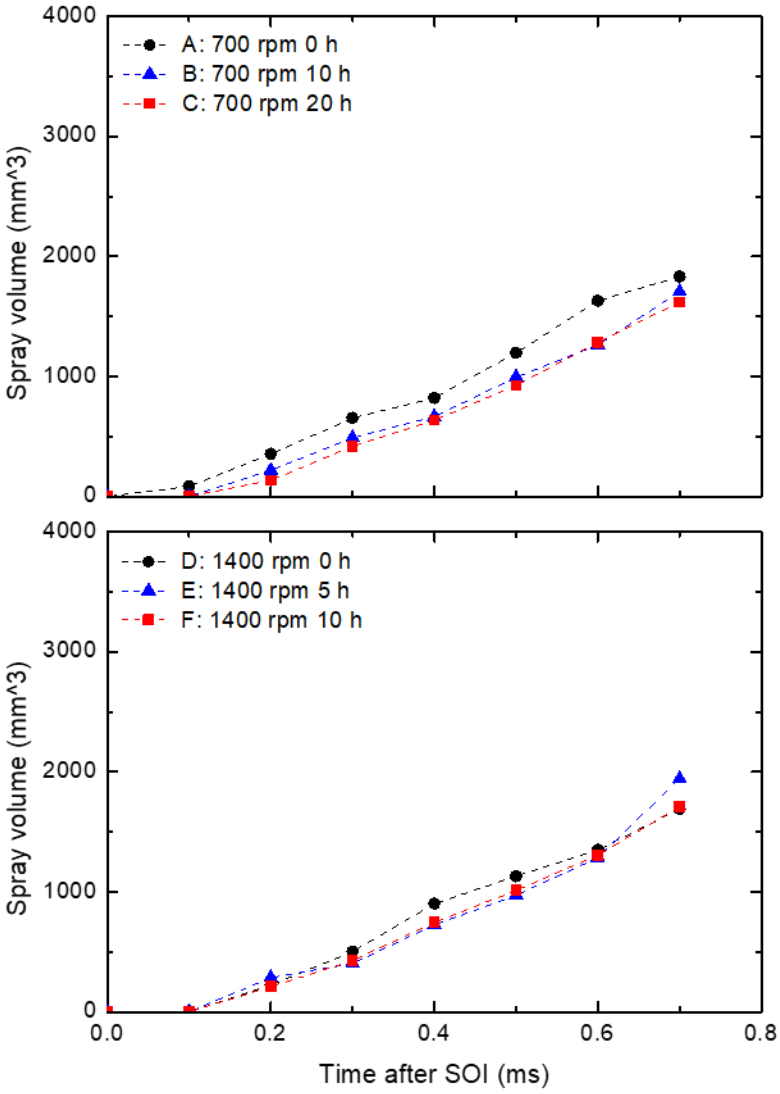

Fig. 4.61 Comparison of spray volume.

The formation of the nozzle hole deposit directly affects both the spray penetration and spray cone angle. When a deposit forms inside the nozzle hole, it reduces the injection hole cross section. The smaller effective hole diameter strongly affects the reduction of the fuel flow rate. Then the momentum of the fuel spray consequently reduces. Therefore, the spray penetration is shorter and the spray cone angle is wider [45-49]. Moreover, the decreased injection hole cross section by the deposit formation also escalates the effect of cavitation inside the nozzle hole [50-51]. Therefore, the spray cone angle is widened as well. From these reasons, the spray volume decreases with the deposit formation, as shown in Fig. 4.61.

4.5 Conclusions

This study focused on the deposit formation and the effects of the deposits on fuel injection together with the spray characteristics under the different additive, ambient gas, and times between injections. The experiments were run on the testing machine, which was designed based on the commercially used common-rail system. The injection pressure was controlled at the maximum, which was 180 MPa, and the injection duration was controlled at 480 μs. The electric motor was employed to control the injection time at 700 and 1,400 rpm. The nozzle seat temperature was controlled at 350 °C. The observations were designed to study the effects of additive, ambient gas, time between injections, and number of injections on the deposit inside the nozzle hole and the effects of the deposition on injection and spray characteristics. The following lists are the conclusions of this study.

-In the conditions of the body seat temperature are greater than 300 °C or equal, the generating of deposits was found in the injector nozzle hole.

-The results of the amount of injected fuel measurement were found that the use of zinc as the additive to precipitate the deposits promoted the formation of deposits inside the injector nozzle hole.

-Use of CO_2 as the ambient gas promotes deposits formation in all concentrations of CO_2 gas.

-The chemical observation of the deposit at the nozzle hole surface shows the trace of Zn as the additive to accelerate the deposit formation process.

-Along with the increment of test duration, which allows the occurrence of the deposit formation, the decrease of the fuel injection rate can be obtained.

-The longer the time between injections results in the greater reduction of fuel injection rate. It also affects the reduction of Cd at the same number of injections. The longer time between injections promotes the deposit formation process.

-The reduction of Cd shows that the accumulation of deposits inside the injector nozzle hole is a function of test duration.

-The reduction of spray penetration is affected by the longer time between injection and the increased test duration.

-The longer time between injections shows a negligible change in spray cone angle.

-As the reduction of spray penetration by the longer time between injections, the spray volume is also decreased as well.

-The accumulation of deposits inside the injector nozzle is promoted by the increment of time between injections. It affects not only the fuel injection as the loss of fuel flow, the lower injection rate, and injection efficiency, but also the spray characteristics as the reduction of spray penetration and volume. These effects may be the source of engine performance and emission issues.

Bibliography

[1] Heywood, J. E., Internal Combustion Engine Fundamentals, 1989.

[2] Klaua, T., 2006, "Diesel Injector Deposits Potential in Future Fueling Systems," SAE Paper No. 2006-01-3359.

[3] Barker, J., Richards, P., Snape, C., and Meredith, W., "A Novel Technique for Investigating the Nature and Origins of Deposits Formed in High Pressure Fuel Injector Equipment," SAE 2009-01-2637.

[4] Quigley, R., Barbour, R., Fahey, E., Arters, D., Wetzel, W. and Ray, J., "A Study of Internal Diesel Injector Deposit Phenomenon," in: Bartz, W.J.: Fuels: Conventional and Future Energy for Automobiles; 8th International Colloquium on fuels, January 19 - 20, 2011; TAE, Ostfildern, Germany, 2011, p. 565-578, ISBN 3-924813-86-8.

[5] Lacey, P., Gail, S., Kientz, J., Milovanovic, N. et al., "Internal Fuel Injector Deposits," SAE Int. J. Fuels Lubr. 5(1):132-145, 2012, https://doi.org/10.4271/2011-01-1925.

[6] Schwab, S., Bennett, J., Dell, S., Galante-Fox, J. et al., "Internal Injector Deposits in High-Pressure Common Rail Diesel Engines," SAE Int. J. Fuels Lubr. 3(2):865-878, 2010, https://doi.org/10.4271/2010-01-2242.

[7] Kumagai, S., Takahashi, A., Nagato, H., and Stradling, R., "Development of an Injector Deposit Formation Test Method for a Medium-Duty Diesel Engine," SAE Technical Paper 2015-01-1914, 2015, https://doi.org/10.4271/2015-01-1914.

[8] Behrendt, C. and Smith, A., "A Study of Diesel Fuel Injector Deposit Effects on Power and Fuel Economy Performance," SAE Technical Paper 2017-01-0803, 2017, https://doi.org/10.4271/2017-01-0803.

[9] Ikemoto, M., Omae, K., Nakai, K., Ueda, R. et al., “Injection Nozzle Coking Mechanism in Common-rail Diesel Engine,” SAE Int. J. Fuels Lubr. 5(1):78-87, 2012, https://doi.org/10.4271/2011-01-1818.

[10] Smith, A. and Williams, R., “Linking the Physical Manifestation and Performance Effects of Injector Nozzle Deposits in Modern Diesel Engines,” SAE Int. J. Fuels Lubr. 8(2):344-357, 2015, https://doi.org/10.4271/2015-01-0892.

[11] Caprotti, R., Breakspear, A., Graupner, O., Klaua, T., Schik, A., and Rouff, C., 2005, “Injector Deposit Test for Modern Diesel Engines,” Proceedings of the TAE Symposium 2005, Esslingen, Germany.

[12] Liaquat, A.M., Masjuki, H.H., Kalam, M.A., Fazal, M.A., Khan, A.F., Fayaz, H., and Varman, M., “Impact of Palm Biodiesel Blend on Injector Deposit Formation”, Applied Energy 111 (2013) 882–893.

[13] Aradi, A., Imoehl, B., Avery, N., Wells, P. et al., “The Effect of Fuel Composition and Engine Operating Parameters on Injector Deposits in a High-Pressure Direct Injection Gasoline (DIG) Research Engine,” SAE Technical Paper 1999-01-3690, 1999, https://doi.org/10.4271/1999-01-3690.

[14] Venkataraman, R., and Eser, S., “Characterization of Deposits Formed on Diesel Injectors in Field Test and From Thermal Oxidative Degradation of n-hexadecane in a Laboratory Reactor,”. Chemistry Central journal vol. 2 25. 17 Dec. 2008, doi:10.1186/1752-153X-2-25.

[15] Caprotti, R., Bhatti, N., and Balfour, G., 2010, “Deposit Control in Modern Diesel Fuel Injection Systems,” SAE Paper No. 2010-01-2250.

[16] Caprotti, R., Breakspear, A., Graupner, O., and Klaua, T., 2005, “Detergency Requirements of Future Diesel Injection Systems,” SAE Paper No. 2005-01-3901.

[17] Hoang, A.T., and Le, A.T., 2019. “A Review on Deposit Formation in the Injector of Diesel Engines Running on Biodiesel,” Energy Sources, Part A Recover. Util. Environ. Eff., vol. 41, no. 5, pp. 584–599.

[18] Risberg, P. and Alfredsson, S., “The Effect of Zinc and Other Metal Carboxylates on Nozzle Fouling,” SAE Technical Paper 2016-01-0837, 2016, https://doi.org/10.4271/2016-01-0837.

[19] Caprotti, R., Leedham, A., Graupner, O., and Klaua, T., 2004, “Impact of Fuel Additives on Diesel Injector Deposits,” SAE Paper No. 2004-01-2935.

[20] Dearn, K., Xu, J., Ding, H., Xu, H. et al., "An Investigation into the Characteristics of DISI Injector Deposits Using Advanced Analytical Methods," SAE Int. J. Fuels Lubr. 7(3):771-782, 2014, https://doi.org/10.4271/2014-01-2722.

[21] Birgel, A., Ladommatos, N., Aleiferis, P., Zülch, S. et al., "Deposit Formation in the Holes of Diesel Injector Nozzles: A Critical Review," SAE Technical Paper 2008-01-2383, 2008, https://doi.org/10.4271/2008-01-2383.

[22] Caprotti, R., Graham, B., Ullmann, J., Geduldig, M., and Stutzenberger, H. A., 2008, "Investigation on the Formation and Prevention of Internal Diesel Injector Deposits," SAE Paper No. 2008-01-0926.

[23] Hoffmann, H., Koch, W., and Lucka, K. (2015). "A Novel Injector Deposit Fuel Test Method: ENIAK," Proceedings of the European Combustion Meeting 2015.

[24] Stahl, M., Damaschke, C., and Tropea, C., 2006, "Experimental Investigation of Turbulence and Cavitation Inside a Pressure Atomizer and Optical Characterization of the Generated Spray," ICLASS, Kyoto.

[25] Cao, T., He, Z., Zhou, H., Guan, W., Zhang, L., amd Wang, Q., "Experimental study on the effect of vortex cavitation in scaled-up diesel injector nozzles and spray characteristics," Experimental Thermal and Fluid Science 113: 2020, 110016 doi: 10.1016/j.expthermflusci.2019.110016.

[26] Mancaruso, E., Sequino, L., Vaglieco, B., and Ciaravino, C., "Coking Effect of Different FN Nozzles on Injection and Combustion in an Optically Accessible Diesel Engine," SAE Technical Paper 2013-24-0039, 2013, https://doi.org/10.4271/2013-24-0039.

[27] Tang, J., Pischinger, S., Lamping, M., Korfer, T., Tatur, M., and Tomazic, D., 2009, "Coking Phenomena in Nozzle Orifices of DI-Diesel Engines," SAE Paper No. 2009-01-0837.

[28] Som, S., Ramirez, A. I., Longman, D. E., and Aggarwal, D. E., "Effect of Nozzle Orifice Geometry on Spray, Combustion, and Emission Characteristics under Diesel Engine Conditions," Fuel 90 (2011) 1267–1276. doi: 10.1016/j.fuel.2010.10.048.

[29] D'Ambrosio, S., and Ferrari, A. (April 12, 2012). "Diesel Injector Coking: Optical-Chemical Analysis of Deposits and Influence on Injected Flow-Rate, Fuel Spray and Engine Performance," ASME. J. Eng. Gas Turbines Power. June 2012; 134(6): 062801. https://doi.org/10.1115/1.4005991.

[30] Bosch, W., “The Fuel Rate Indicator: A New Measuring Instrument for Display of the Characteristics of Individual Injection,” SAE Technical Paper 660749, 1966, doi:10.4271/660749.

[31] Dernotte, J., Hespel, C., Foucher, F., Houillé, S., and Rousselle, C.M., “Influence of Fuel Properties on the Diesel Injection Process in Non-Vaporizing Conditions,” Atomization and Spray 22(6): 461-492, 2012, doi: 10.1615/AtomizSpr.2012004401.

[32] Xu, Q., Xu, M., Hung, D., Wu, S. et al., “Diesel Spray Characterization at Ultra-High Injection Pressure of DENSO 250 MPa Common Rail Fuel Injection System,” SAE Technical Paper 2017-01-0821, 2017, https://doi.org/10.4271/2017-01-0821.

[33] Payri, R., Martí-Aldavarí, P., Montiel, T., and Viera, A., (2020). “Influence of Aging of a Diesel Injector on Multiple Injection Strategies,” Applied Thermal Engineering. 181. 115891. 10.1016/j.applthermaleng.2020.115891.

[34] Zhou, X., Li, T., Yi, P., Zhang, Z., Wang, N., and Wei, Y., “On the Fuel Injection Rate Profile as Boundary Conditions for Diesel Spray Combustion Simulations,” Fuel, Volume 276, 2020, 118026, ISSN 0016-2361, https://doi.org/10.1016/j.fuel.2020.118026.

[35] Yabe, M., Butmarasri, A., Nagasawa, T., Sato, S., and Kosaka, H., “Effect of Inner Geometry of Nozzle on Internal Fuel Flow and Diesel Spray Characteristics”, 2020 JSAE Annual Congress (Autumn) Proceedings, October 2020.

[36] Pham, V., V., and Nguyen, D., (2020). “A Brief Review of Formation Mechanisms, Properties and Affecting Factors of Combustion Chamber Deposits in Diesel Engines using Biodiesel,” AIP Conference Proceedings. 2292. 040011. 10.1063/5.0030964.

[37] Lepperhoff, G., and Houben, M., 1993, “Mechanisms of Deposit Formation in Internal Combustion Engines and Heat Exchangers,” SAE Paper No. 931032.

[38] Tang, J., Pischinger, S., Grutering, U., and Keck, J., “Influences on the Formation of Deposits on Injection Nozzles in Direct-Injection Diesel Engines,” MTZ 0912008 Volume 69.

[39] Catania, A. E., Ferrari, A., and Spessa, E., 2009, “Numerical-Experimental Study and Solutions to Reduce the Dwell Time Threshold for Fusion-Free Consecutive Injections in a Multijet Solenoid-Type C.R. System,” J. Eng. Gas Turbines Power 131(1), p. 022804.

[40] Leuthel, R., Pfitzner, M., and Frobenius, M., “Numerical Study of Thermal-Fluid-Interaction in a Diesel Fuel Injector,” SAE Technical Paper 2008-01-2760, 2008, https://doi.org/10.4271/2008-01-2760.

[41] Watkinson, A. P., and Wilson, D. I., 1997, “Chemical Reaction Fouling: A Review,” Exp. Therm. Fluid Sci., 14, pp. 361–374.

[42] Payri, F., Bermudez, V., Payri, R., and Salvador, F. S., 2004, “The Influence of Cavitation on the Internal Flow and Spray Characteristics in Diesel Injector Nozzles,” Fuel, 83, pp. 419–431.

[43] Caprotti, R., Fowler, W., Lepperhoff, G., and Houben, M., “Diesel Additive Technology Effects on Injector Hole Erosion/Corrosion, Injector Fouling and Particulate Traps,” SAE Technical Paper 932739, 1993, https://doi.org/10.4271/932739.

[44] Blessing, M., König, G., Krüger, C., Michels, U. et al., “Analysis of Flow and Cavitation Phenomena in Diesel Injection Nozzles and Its Effects on Spray and Mixture Formation,” SAE Technical Paper 2003-01-1358, 2003, https://doi.org/10.4271/2003-01-1358.

[45] Montanaro, A. and Allocca, L., “Impact of the Nozzle Coking on Spray Formation for Diesel Injectors,” SAE Technical Paper 2013-01-2546, 2013, https://doi.org/10.4271/2013-01-2546.

[46] Hoang, A.T., Le, V.V., Pham, V.V., and Tham, B.C., 2019. “An Investigation of Deposit Formation in the Injector, Spray Characteristics, and Performance of a Diesel Engine Fueled with Preheated Vegetable Oil and Diesel Fuel,” Energy Sources, Part A Recover. Util. Environ. Eff., pp. 1–13. https://doi.org/10.1080/15567036.2019.1582731.

[47] Song, H., Xiao, J., Chen, Y., and Huang, Z., “The Effects of Deposits on Spray Behaviors of a Gasoline Direct Injector,” Fuel, Volume 180, 2016, Pages 506-513, ISSN 0016-2361, https://doi.org/10.1016/j.fuel.2016.04.067.

[48] Pos, R., Cracknell, R., and Ganippa, L., “Transient characteristics of diesel sprays from a deposit rich injector,” Fuel, Volume 153, 2015, Pages 183-191, ISSN 0016-2361, https://doi.org/10.1016/j.fuel.2015.02.114.

[49] Cracknell, R., Wardle, R., Pos, R., and Ganippa, L., (2016). “Effect of diesel injector tip deposits on transient spray behavior,” https://doi.org/10.1007/978-3-658-12918-7_13.

[50] Wang, L., Lowrie, J., Ngaile, G., and Fang, T. “High injection pressure diesel sprays from a piezoelectric fuel injector,” Applied Thermal Engineering 152, 807-824, 2019, doi: 10.1016/j.applthermaleng.2019.02.095.
[51] Payri, F., Arrègle, J., López, J., and Hermens, S., “Effect of Cavitation on the Nozzle Outlet Flow, Spray and Flame Formation in a Diesel Engine,” SAE Technical Paper 2006-01-1391, 2006, doi:10.4271/2006-01-1391.

CHAPTER 5
CONCLUSIONS AND FUTURE WORKS

5.1 Conclusions

This chapter is the final conclusion of this dissertation.

-Temperature influences deformation of the nozzle body seat significantly, especially at high temperatures. It causes the material of the nozzle to soften, thereby increasing deformation. Test duration governs the plastic deformation of the body seat, particularly under long test durations due to the release of dislocations in the nozzle material, which decreases hardness.

-Tempering is an effective technique for preventing body seat deformation. The strong structure “cementite” advances precipitation as the tempering temperature rises. During the heated injection test, when the nozzle material is heated above the tempering temperature, however, the tempering process eliminates the isotropic dislocations, resulting in a low density of dislocations and structural changes and the deformation is promoted.

-Zinc, a fuel additive, is significant in the formation of nozzle hole deposits. Fuel injection is reduced as a result of the deposit that forms inside the nozzle hole due to the combination of zinc-doped fuel and high temperature. This demonstrates that nozzle hole deposit can form under non-combustion test conditions.

-The test duration and time between injections facilitate the formation of nozzle hole deposit. The process of deposit formation itself evolves as test duration and time between injections increase. This reduces the maximum injection flow rate and the discharge coefficient. When a deposit forms inside the nozzle hole, the spray characteristics degrade, including a decrease in spray penetration, an increase in spray cone angle, and a decrease in spray volume.

5.2 Future Works

There are other efforts which can be made in the following study.

-In this study, a small constant volume chamber was used for achieving the spray observation at 2 MPa of back pressure, so that spray would be impinged on the wall. Therefore, it is recommended to consider the higher back pressure to consider the effect on spray characteristics.

-According to the small size of the nozzle hole and the small amount of the deposit inside the nozzle, the effective solution to access and observe the deposit inside the nozzle hole with non-destructive method should be considered.

-The nozzle hole deposit can affect both performance and emissions of the actual engine. Therefore, the test of coking nozzle on the actual engine test bench is recommended to investigate the effects on the performance and emissions.